

**Using Molecular, Isotopic, and Spectroscopic Analysis to Assess Natural
Organic Matter Sources and Petroleum Contaminants in Water and Sediment
of the St. Lawrence Waterway (Quebec, Canada)**

Anic Imfeld

A Thesis
In the Department
of
Chemistry and Biochemistry

Presented in Partial Fulfillment of the Requirements
for the Degree of
Doctor of Philosophy (Chemistry) at
Concordia University
Montreal, Quebec, Canada

July 2022

© Anic Imfeld, 2022

CONCORDIA UNIVERSITY

School of Graduate Studies

This is to certify that the thesis prepared

By: Anic Imfeld

Entitled: Using molecular, isotopic, and spectroscopic analysis to assess natural organic matter sources and petroleum contaminants in water and sediment of the St. Lawrence Waterway (Quebec, Canada)

and submitted in partial fulfillment of the requirements for the degree of

Doctor of Philosophy (Chemistry)

complies with the regulations of the University and meets the accepted standards with respect to originality and quality.

Signed by the final Examining Committee

Chair
Dr. Elena Kuzmin

External Examiner
Dr. Violaine Ponsin

External to the Program
Dr. Xianming Zhang

Examiner
Dr. Cameron Skinner

Examiner
Dr. Christine DeWolf

Supervisor
Dr. Yves G elinas

Approved by _____
Dr. Louis Cuccia, Graduate Program Director

August 30th, 2022 Dr. Pascale Sicotte, Dean, Faculty of Arts and Science

Abstract

Using Molecular, Isotopic, and Spectroscopic Analysis to Assess Natural Organic Matter Sources and Petroleum Contaminants in Water and Sediment of the St. Lawrence Waterway (Quebec, Canada)

Anic Imfeld, Ph.D.

Concordia University, 2022

The St. Lawrence waterway is a dynamic aquatic system with inputs of organic matter (OM) originating from various terrestrial and marine sources, and a freshwater to saltwater gradient from the St. Lawrence River to the Gulf. The OM along this waterway is highly reworked in the water column, with a small fraction making its way into the sediments which acts as a long-term sink for organic matter. This waterway is also an important transportation route for numerous commodities, including petroleum and petroleum products. Our research involved the comprehensive mapping of the OM in the sediments and water column of the St. Lawrence River, Estuary, Gulf and the Saguenay Fjord. Water samples were collected along the River, Estuary, Gulf and Saguenay Fjord and parallel factor analysis was used to tease out various groups of fluorophores. In addition to the natural water samples collected along the St. Lawrence waterway, water samples containing UV irradiated petroleum products were included in the PARAFAC model to determine its efficiency at teasing out the components originating from natural OM from those linked to oil contamination. The PARAFAC analysis resulted in the identification of 6 components in our data set, with 4 components indicative of natural organic matter (3 terrestrial OM and one marine OM) and 2 representing oil components. With these findings, we were able to characterize groups of fluorophores along this transect and develop a ratio using 2 components (C4/C1) to differentiate oil contributions from natural OM in the water column. Similarly, surface sediments along the St. Lawrence Estuary, Gulf and Saguenay Fjord were collected and extracted to isolate the straight-chain *n*-alkanes to map the current abundances and sources of hydrocarbons in sediments of the Estuary and Gulf using molecular (diagnostic ratios) and isotopic fingerprinting ($\delta^{13}\text{C}$, $\delta^2\text{H}$). Variations in the carbon isotope signatures of odd-to-even straight chain alkanes allows for the differentiation of naturally occurring hydrocarbons

from those of petroleum source, and the addition of hydrogen isotope signatures further increases our power of discrimination. Based on the diagnostic ratios alone, the OM sources were misrepresented and inaccurate when there was more than one input of OM. However, with the addition of the compound specific carbon and hydrogen isotope analysis, it was determined that *n*-alkanes were derived predominantly from natural sources. Additionally, we found that even numbered *n*-alkanes, which are less frequently analyzed due to their lower abundances in natural samples, would allow for the identification and tracking of petroleum-derived contaminants in sediments to a greater degree than molecular data alone. Analyzing both the possibility of oil contamination in the water column and sediments allows for the tracking of recent and long term impacts an oil spill would have along the St. Lawrence River, Estuary Gulf and Saguenay Fjord.

Acknowledgements

I would first like to thank my research advisor, Yves Gélinas for putting up with me these past 7 years, especially when we disagreed on the number of replicates that should be run (the right answer (and mine) is 4). Thank you for the opportunities and experiences I've gotten to enjoy, including travelling to conferences and the amazing experience of the sampling cruise along the St. Lawrence. I could not have finished this PhD without your constant support, encouragement and understanding. These opportunities have shaped me to be a better researcher as well as a better person. I am a better version of myself than I was when I first started all those years ago, and for that I thank you.

There are then the technical and support staff at Concordia University that have been great throughout my time there, specifically Alain Tessier, who made long days in CBAMS more bearable and who was always willing to teach me something new and offer help with a smile whenever I wanted to give up on my instruments.

I would like to thank my friends and family for their constant support throughout this endeavor, as well as all past and present lab members who are too many to name. I was not expecting to make lifelong friends along this journey, but I am so thankful for them. Specifically, Fred. Thank you for being such a great friend through the ups and downs during the past few years. Thank you for listening to my rants and for picking me up when I was down. I'm so glad we got to go through some of this process together. Thank you to Gabi and John for their helpful conversations, whether about research or commiserating about PhD life. I'm thankful to have met you during this experience and grateful for the friendships that will last past it.

Finally, to my amazing husband Jeremy, thank you for being my rock through this whole process. Thank you for agreeing to move to Montreal with me to pursue grad school and for the constant support through the tears and many times I wanted to give up. I could not have done this without you, so thank you for believing in me and I can't wait to see what the future holds for us.

Contribution of Authors

Chapter 2 was written by Anic Imfeld and reviewed by Alexandre Ouellet, Peter Douglas, Gregor Kos and Yves Gélinas. All sample workup, instrument measurements and data analysis were done by Anic Imfeld. Peter Douglas provided use of a GC-IRMS set up for hydrogen measurements. Gregor Kos aided with the statistical analysis, to ensure proper interpretation of the PCA results. Alexandre Ouellet and Yves Gélinas initial idea for the study morphed into the manuscript that has been published in *Organic Geochemistry* in February 2022.

Chapter 3 was written by Anic Imfeld and reviewed by Yves Gélinas. Samples were analyzed by Anic Imfeld and all EEMs and PARAFAC analysis were done by Anic Imfeld as well. Lindsay Hounjet provided the expertise for the solar irradiation simulator set-up. Céline Guéguen and Gwénaëlle Chaillou provided aid in the interpretation of our results.

Financial support for this study was provided by a grant from the Centre d'expertise en analyse environnementale du Québec of the Québec Ministère de l'Environnement et de la Lutte contre les changements climatiques to Alexandre Ouellet and Yves Gélinas, as well as by operation and instrument grants to Yves Gélinas (Geotop Regroupements stratégiques, Fonds de Recherche du Québec Nature et Technologies; Discovery and Research Tools and Instruments, Natural Sciences and Engineering Research Council of Canada; Canadian Foundation for Innovation).

Table of Contents

List of Figures	ix
List of Tables	xii
List of Abbreviations	xiii
Chapter 1: General Introduction	1
1.1 Natural Organic Matter in the St. Lawrence Waterways	4
1.2 The Use of Biomarkers to Track and Characterize Organic Matter	5
1.3 Application of Stable Isotope Analysis for Organic Matter Source Identification	7
1.4 Using Optical Properties to Determine Organic Matter Sources	9
1.5 Molecular, Isotopic and Spectroscopic Differences Between Natural and Petroleum Derived Hydrocarbons	11
1.6 Objectives.....	13
1.7 Arrangement of Thesis	14
Chapter 2: Molecular and stable isotope analysis ($\delta^{13}\text{C}$, $\delta^2\text{H}$) of sedimentary <i>n</i>-alkanes in the St. Lawrence Estuary and Gulf, Quebec, Canada: importance of even numbered <i>n</i>- alkanes in coastal systems	16
2.1 Abstract	17
2.2 Introduction	17
2.3 Materials and methods	19
2.3.1 Sampling locations and collection.....	19
2.3.2 Elemental and bulk sediment isotope analysis.....	21
2.3.3 Extraction and quantitation of <i>n</i> -alkanes.....	22
2.3.4 <i>n</i> -Alkane molecular proxies	23
2.3.5 Compound-specific carbon and hydrogen isotope analysis	24
2.3.6 Statistical analyses.....	24
2.4 Results	24
2.4.1 Bulk sediment isotope analysis ($\delta^{13}\text{C}$, $\delta^{15}\text{N}$) and C/N ratio	24
2.4.2 <i>n</i> -Alkane abundances and diagnostic ratios	26
2.4.3 $\delta^{13}\text{C}$ and $\delta^2\text{H}$ of individual <i>n</i> -alkanes in surface sediments	30
2.5 Discussion	32
2.5.1 Variations in bulk sediment $\delta^{13}\text{C}$, $\delta^{15}\text{N}$ values and C/N ratios	32
2.5.2 Changes in <i>n</i> -alkane abundances along the St. Lawrence Estuary and Gulf	34
2.5.3 Changes in <i>n</i> -alkane diagnostic ratios along the St. Lawrence Estuary and Gulf.....	36
2.5.4 $\delta^{13}\text{C}$ and $\delta^2\text{H}$ of individual <i>n</i> -alkanes in surface sediments	40

2.6 Conclusions	45
2.7 Acknowledgments	46
Chapter 3: Tracking changes in dissolved organic matter along the St. Lawrence River, Estuary and Gulf using PARAFAC analysis, and distinguishing natural organic matter from oil-derived compounds	47
3.1 Abstract	48
3.2 Introduction	49
3.3 Materials and methods	51
3.3.1 Sampling location and collection	51
3.3.2 Photooxidation set-up.....	52
3.3.3 DOC measurements.....	53
3.3.4 Absorption and fluorescence spectroscopy	53
3.3.5 Indices	53
3.3.6 PARAFAC analysis.....	54
3.4 Results	54
3.4.1 DOC and indices of surface waters along the St. Lawrence River, Estuary, and Gulf, as well as the Saguenay Fjord.....	54
3.4.2 Photooxidation effects on DOC and EEMs of oil	57
3.4.3 PARAFAC model results	59
3.5 Discussion	61
3.5.1 DOC and indices along the St. Lawrence River, Estuary, and Gulf, as well as the Saguenay Fjord.....	61
3.5.2 Photooxidation effects on DOC and EEMs of oil	64
3.5.3 Component interpretation and variations along the freshwater-seawater continuum ..	65
3.5.4 Proposed ratio for distinguishing natural OM from petroleum OM	70
3.6 Conclusion.....	71
Chapter 4: Conclusions, Perspectives and Future Work	74
References:	78
Appendix A	90
Appendix B.....	95
Appendix C	102

List of Figures

Figure 1.1 Map of the sampling area, showing the three main sections of the St. Lawrence Waterway; the River, Estuary and Gulf.	3
Figure 1.2 GC-FID trace of various oil types modified from Bayton et al. 2015.	12
Figure 2.1 Map showing study sites across the St. Lawrence Estuary and Gulf in Quebec, Canada.	20
Figure 2.2 $\delta^{13}\text{C}$ values and C/N ratios of bulk sediments at all stations with typical ranges of OM inputs.	26
Figure 2.3 <i>n</i> -Alkane concentrations in the top 10 cm of sediments at each station. The same scale was used for the y-axis.	27
Figure 2.4 Compound-specific $\delta^{13}\text{C}$ (a) and $\delta^2\text{H}$ (b) values of <i>n</i> -alkanes (nC23 to nC36) in the sediments at the various sampling stations. Error bars correspond to the standard deviation (n=3).	31
Figure 2.5 a) Sum of odd and even LMW (C17-C22) <i>n</i> -alkanes at all stations, b) sum of odd and even HMW (C23-C36) <i>n</i> -alkanes at all stations. Error bars show standard deviations.	35
Figure 2.6 Relationship of odd and even <i>n</i> -alkane abundances and the bulk sediment $\delta^{13}\text{C}$ values. Station Sag05 (not shown on the graph) was omitted from the regression of the odd <i>n</i> -alkanes. Error bars show standard deviations.	36
Figure 2.7 TAR values and standard deviations at each station when using the traditional equation with the odd <i>n</i> -alkanes in the dominator (traditional) and when using even <i>n</i> -alkanes in the denominator (modified).	36
Figure 2.8 Relationship between bulk sediment $\delta^{13}\text{C}$ values and a) weighted average $\delta^{13}\text{C}$ values of odd and even <i>n</i> -alkanes and b) weighted average $\delta^2\text{H}$ values of odd and even <i>n</i> -alkanes.	41
Figure 2.9 Principal component analysis of all stations: a) scores with 95% confidence ellipses. Individual data points are individual <i>n</i> -alkanes at each station, and the larger symbol within each group represents the average for all the individual <i>n</i> -alkanes; b) loadings. Note that the TAR variable used in the PCA is the modified TAR index as presented in the discussion.	44
Figure 3.1 Map showing study sites across the St. Lawrence River, Estuary and Gulf, as well as the Saguenay Fjord in Quebec, Canada.	52
Figure 3.2 DOC concentrations in the surface waters of A) the Saguenay Fjord and B) the St. Lawrence River, Estuary and Gulf for both 2017 and 2018 samples	55

Figure 3.3 SUVA₂₅₄ and SR values for surface waters along the Saguenay Fjord (A and C) and the St. Lawrence River, Estuary and Gulf (B and D) for both 2017 and 2018 samples. 56

Figure 3.4 BIX, HIX and FI values calculated in surface waters of the Saguenay Fjord (A, C, E) and the freshwater stations along the St. Lawrence River and Estuary until the maximum turbidity zone at station E4 (B, D, F) for both 2017 and 2018 samples. 57

Figure 3.5 DOC concentrations in the water subphase for both irradiated and control samples at varying timepoints..... 57

Figure 3.6 SUVA₂₅₄ and SR values, A and B respectively, for both the irradiated and control samples as irradiation time progressed..... 59

Figure 3.7 Excitation and emission wavelengths of the 6 components (A) and contour plots describing the intensities as a function of their spectral characteristics (B) identified by the PARAFAC model. 60

Figure 3.8 DOC concentrations (A) and SUVA₂₅₄ (B) trends along the St. Lawrence waterway from the river to the gulf. 62

Figure 3.9 BIX and HIX trends along the freshwaters of the St. Lawrence River and Estuary, from station R1 to station E4. 63

Figure 3.10 Relative contribution of each component to total fluorescence for the control (A) and irradiated (B) samples at all time points..... 66

Figure 3.11 Relative contribution of C1 and C3 to total fluorescence for all surface samples along the St. Lawrence River, Estuary, Gulf and Saguenay Fjord, for both 2017 and 2018..... 67

Figure 3.12 Relationship between C4 and C5 with C3 in all samples in contact with oil (control and irradiated samples)..... 68

Figure 3.13 Relative contribution of each component to total fluorescence for surface waters collected along the Saguenay Fjord in 2017 (A) and 2018 (C) and along the St. Lawrence River, Estuary and Gulf in 2017 (B) and 2018 (D). The stations labelled P (2017 only) correspond to water sampled in the plume of north shore rivers. 69

Figure 3.14 Relative contribution of each component to total fluorescence for waters at all depths collected along the Saguenay Fjord in 2017 (A) and 2018 (C) and along the St. Lawrence River, Estuary and Gulf in 2017 (B) and 2018 (D)..... 69

Figure 3.15 Comparison of the absolute fluorescence value of C4 (A) and C5 (B) between the irradiated and control samples at all time points..... 70

Figure 3.16 Ratio of C4 to C1 for all waterway samples at all depth (2017 and 2018), alongside the samples exposed to oil..... 71

Figure A.1 Regression of TAR values vs bulk carbon isotope values, R² values shown for TAR values calculated with odd *n*-alkanes compared to even *n*-alkanes in the denominator. Error bars represent standard deviations. 94

Figure A.2 Relationship between bulk nitrogen and carbon isotope values with regression not including stations DE and G. Error bars represent standard deviations..... 94

Figure B.1 Relationship between DOC concentration and total fluorescence for surface waters along the St. Lawrence River, Estuary and Gulf as well as the Saguenay Fjord 101

List of Tables

Table 1.1 Commonly identified fluorophore groups (adapted from Coble 2007 and references within).	10
Table 2.1 Description of sampling sites in the St. Lawrence Estuary and Gulf.	21
Table 2.2 <i>n</i> -Alkane molecular proxies used in this study ('→' indicates range).	23
Table 2.3 Percentages (\pm standard deviations) of organic carbon (OC), total nitrogen (TN), atomic C/N.	25
Table 2.4 Concentrations and standard deviations of total, low molecular weight (LMW) and high molecular weight (HMW) <i>n</i> -alkanes, as well as calculated C_{\max} , CPI, ACL, TAR, NAR and P_{aq} molecular ratios at each station.	29
Table 2.5 Weighted average $\delta^{13}C$ and δ^2H values of odd and even chain length <i>n</i> -alkanes, and independent student t-test p-values to determine significant difference between WA odd and even <i>n</i> -alkanes.....	32
Table 3.1 Excitation and emission wavelengths for the major and minor peaks determined from the EMMs of the control and irradiated samples	58
Table 3.2 Classification of the six components identified by PARAFAC analysis based on previous literature results.	61
Table A.1 Concentration ($\mu g/gOC$) and standard deviation of individual <i>n</i> -alkanes at each station (n=3).....	91
Table A.2 $\delta^{13}C$ value (‰) and standard deviation of individual <i>n</i> -alkanes at each station (n=3) 92	
Table A.3 δ^2H value (‰) and standard deviation of individual <i>n</i> -alkanes at each station (n=3). 93	
Table B.1 Traditional nomenclature for stations samples, along with the name assigned for the purpose of this paper, as well as longitude, latitude, depth, bottom depth, salinity, DOC, temperature, dissolved oxygen transmissivity and density for each sample collected	96
Table B.2 BIX, HIX and FI values calculated at the various time points for both control and irradiated samples.....	101
Table C.1 Carbon isotope values (‰) of <i>n</i> -alkanes for various oil samples analyzed in triplicate with their standard deviations	103
Table C.2 PAH concentrations (ppm) of mixed hydrocarbon samples.....	104
Table C.3 Alkane concentrations (ppm) of mixed hydrocarbon samples	105
Table C.4 Carbon isotope values (‰) of <i>n</i> -alkanes of mixed hydrocarbon samples.....	106

List of Abbreviations

OM : Organic Matter
CDOM : Chromophoric Dissolved Organic Matter
CPI : Carbon Preference Index
ACL : Average Chain Length
NAR : Natural Alkane Ratio
TAR : Terrigenous Aquatic Ratio
P_{aq} : Emergent Submerged/Floating Aquatic Ratio
NADPH : Nicotinamide Adenine Dinucleotide Phosphate
IRMS : Isotope Ratio Mass Spectrometry
VPDB : Vienna Pee Dee Belemnite
VSMOW : Vienna Standard Mean Ocean Water
CSIA: Compound Specific Isotope Analysis
EA : Elemental Analysis
EEM : Excitation Emission Matrix
PARAFAC : Parallel Factor
FI : Fluorescence Index
HIX : Humification Index
BIX : Biological Index
GC-FID : Gas Chromatography-Flame Ionization Detector
PAH : Polycyclic Aromatic Hydrocarbons
OC : Organic Carbon
TN : Total Nitrogen
GC-MS : Gas Chromatography-Mass Spectrometry
LMW : Low Molecular Weight
HMW : High Molecular Weight
PCA : Principal Component Analysis
C/N : Carbon/Nitrogen Ratio
WA : Weighted Average
DOC : Dissolved Organic Carbon
TAR_(mod) : Terrigenous Aquatic Ratio Modified

MSW : Mixed Sweet Blend

SUVA₂₅₄ : Specific Ultraviolet Absorbance at 254 nm

SR : Spectral Slope

MW : Molecular Weight

BTEX : Benzene, Toluene, Ethylbenzene And Xylene

UV : Ultraviolet

Chapter 1: General Introduction

The St. Lawrence Waterway is a major stretch of water spanning 2000 km in length in the eastern North America. It is an important and dynamic system for both animal life and mankind. The St. Lawrence Waterway is split into 3 main sections, namely, the St. Lawrence River, Estuary and Gulf, as shown in Fig. 1.1. The river finds its source at the outflow of Lake Ontario and drains a populated and industrialized watershed with various large cities found along its banks. East from Quebec City, the river widens and feeds into the Estuary, which is further divided into the shallower (30-140 m) Upper Estuary between Quebec City and the Saguenay Fjord, and the deep (>300 m) Lower Estuary east of the Saguenay Fjord. The Upper Estuary, where the maximum turbidity zone is located at the junction between fresh water from the river and salt waters from the gulf, receives organic matter (OM) inputs primarily from the St. Lawrence River and freshwater runoff. The stratified Lower Estuary marks the beginning of the Laurentian Channel, where the water reaches maximum salinity, and receives inputs from the Upper Estuary, various rivers on the north shore, as well as from the 90 km long submerged valley of the Saguenay Fjord which is located at roughly the meeting point of the Upper and Lower Estuary. It is this meeting point of the Upper and Lower Estuary that contributes to the oceanic like salinity levels as there is upwelling from the deep salty waters of the Lower Estuary and mixing with the surface waters. The Pointe-des-Monts village on the northern shore of the estuary marks the eastern limit of the Lower Estuary, where it opens into the Gulf of the St. Lawrence, which extends to the Cabot Strait between the Newfoundland and Nova Scotia provinces. The Lower Estuary therefore has a stratified region with mixing of estuarine surface waters and marine bottom waters from the Gulf and the North Atlantic Ocean. With a gradient of freshwater in the river to salt waters in the Gulf, and inputs of both terrestrial and marine OM, this diverse ecosystem is home to a variety of flora, vegetation, and species. These unique characteristics allow for the study of OM in the water column and sediments at the two endmembers and regions containing varying proportions of the two types of OM along the freshwater - seawater continuum.

This waterway is also an important route for the transportation of goods between Canada and the United States. The St. Lawrence River, Estuary and Gulf are a part of this 3700-km marine highway, containing a network of over 40 ports connecting the Great lakes to the Atlantic Ocean, allowing for the distribution of goods from both international and domestic vessels (The St. Lawrence Seaway Management Corporation, 2021). While this connecting of people and

ports via the waterways is essential for international and domestic commerce, it does come with risks to the environment. In Canadian waters alone, 24 million tonnes of crude oil are transported through the Great Lakes along the St. Lawrence Seaway and 67 million tonnes in the St. Lawrence Estuary and Gulf (Clear Seas, 2022). Tankers not only carry unrefined crude oil and refined petroleum products which society relies on everyday, they also carry the potential for oil spills. Oil spills can occur when a vessel is involved in an accident or through discharge of the oil the vessel uses for propulsion. While the number of yearly spills over the past few decades have decreased due to improved measures to prevent oil spills, such as requiring tankers to have double hulls and routine inspections, there are still incidences resulting in large volumes of oil being lost to the environment (ITOPF, 2018). Due to these still occurring spills, it is imperative to continue to address the impact oil spills can have on the environment as well as continue the development of methods and techniques to detect and analyze the components found in oil in the waters and sediments along the marine highway passing through the St. Lawrence River, Estuary and Gulf.

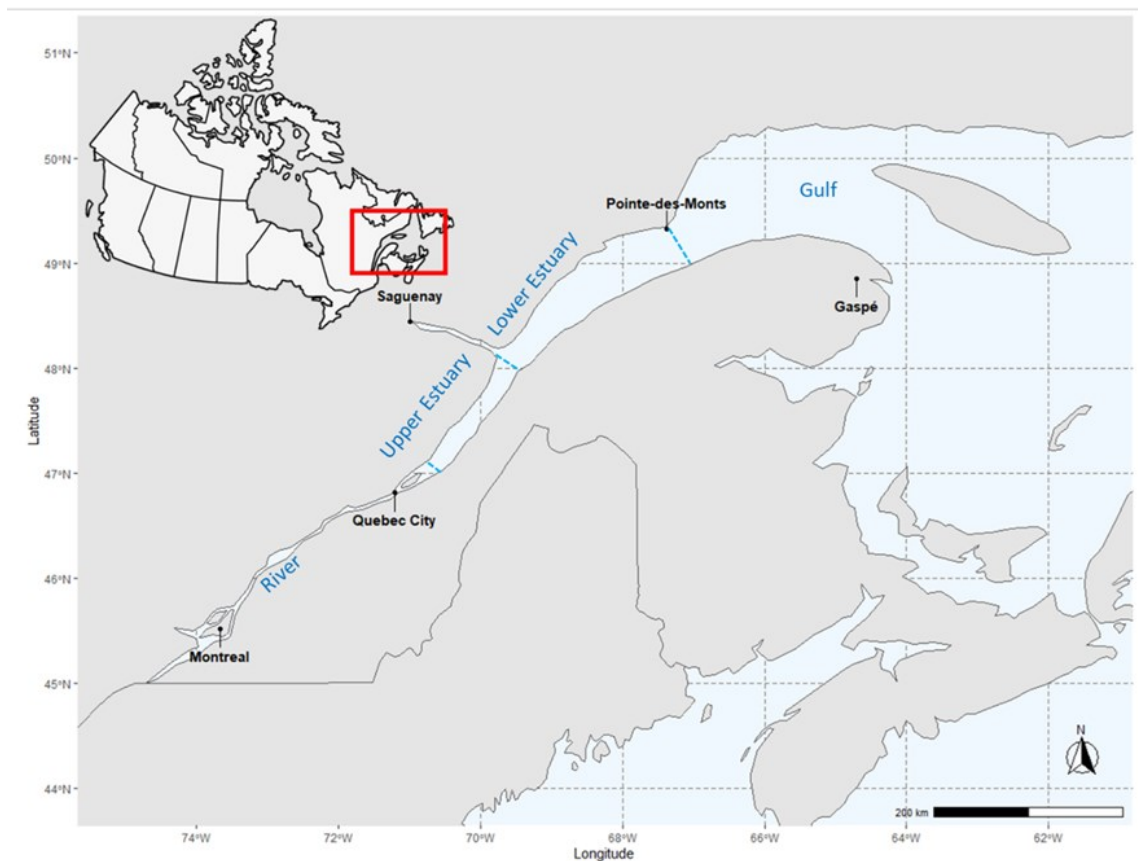


Figure 1.1 Map of the sampling area, showing the three main sections of the St. Lawrence Waterway; the River, Estuary and Gulf.

1.1 Natural Organic Matter in the St. Lawrence Waterways

The St. Lawrence receives OM input from various sources due to its gradient from freshwaters coming from Lake Ontario to salt waters in the Gulf originating from the Atlantic Ocean. Terrestrial OM is described as OM originating from sources external to the aquatic environment, as well as its degradation products. Many different watersheds are responsible for delivering this terrestrial OM to the large bodies of water surrounding them, and for the St. Lawrence Waterways, these watersheds include the boreal forest north of the St. Lawrence River and Estuary, as well as a temperate forest on the south side of the River, Estuary and lining the Saguenay Fjord. In addition to the forested areas, watersheds from cultivated land also introduce terrestrial OM into the St. Lawrence (Hedges et al., 1997). Compositionally, terrestrial OM consists primarily of biological and chemically recalcitrant compounds originating mainly from vascular plants, as well as their alteration and degradation products. Vascular plants are almost exclusively found in terrestrial ecosystems and thus contribute unique compounds to this source of OM such as lignins, cellulose, tannins, resins, and cuticular waxes (Hedges et al., 1997). While terrestrial OM contributes to a greater extent to the overall OM pool at the more terrestrial locations in the River, Upper Estuary and Saguenay Fjord, there is also the input of marine OM originating from the Gulf and Lower Estuary. Contrary to terrestrial-derived OM, marine OM is more labile and is composed of smaller molecules such as simple lipids, proteins, peptides, and carbohydrates derived mostly from autotrophic phytoplankton and bacteria (Wakeham et al., 1997). This OM is either produced by phytoplankton and algae through photosynthesis using dissolved carbon dioxide and bicarbonate, which are the most available inorganic carbon source in the ocean, or by bacterial activity and growth. The proportion of marine and terrestrial OM inputs along the St. Lawrence continuum varies depending on the distance from the St. Lawrence River mouth. The majority of the OM discharged in this system is reworked in the water column and only a small fraction makes its way into the sediment. Bacterial degradation is the main driver for the altering of particulate and/or dissolved OM in the water column and surface sediments (Packard et al., 2000). This results in high molecular weight organic compounds being hydrolyzed into smaller compounds. Additionally, in the surface waters, OM can be degraded via irradiation from the sun, known as photodegradation. During this process, chromophoric dissolved organic matter (CDOM) is transformed into smaller, more oxygenated compounds compared to their parent molecules.

1.2 The Use of Biomarkers to Track and Characterize Organic Matter

Biomarkers are an important tool in biogeochemistry as they can be used to trace the origins of OM as well as biogeochemical processes that influence its composition and fate. Biomarkers can be defined as “a complex organic compound having little to no changes in its chemical structure from the precursor molecules that once existed in living organisms” (Derrien et al., 2017 and references within). If the biomarkers are source specific and their original structure is mostly preserved, they present a direct link to their original source (Killops and Killops, 2013). The most commonly used biomarkers for OM source identification include lignin-phenol, plant pigments, carbohydrates, proteins and simple lipids, with lipids being the most advantageous biomarkers in marine, terrestrial and estuarine systems as they are ubiquitous in these environments, highly diverse, and chemically stable (Derrien et al., 2017 and references within). The most useful lipid biomarkers for OM source characterization include straight chain alkanes (referred to as *n*-alkanes and abbreviated in this thesis to nC_x where *x* is the chain length), fatty acids, and sterols and stanols. For the work presented in this thesis, the focus will be on *n*-alkanes as they lack any reactive functional groups and are thus especially stable and long-lived compounds in natural environments.

n-Alkanes are the most abundant hydrocarbons found in sediments as they are biosynthesized by terrestrial plants, aquatic plants, and plankton. Terrestrial plant derived *n*-alkanes are characterized by a strong predominance of odd numbered carbon chain lengths in the C_{25} to C_{35} carbon range, whereas shorter chain length alkanes in the range C_{15} to C_{19} are attributed to aquatic algae and bacteria (Han and Calvin, 1969; Ficken et al., 2000; Silva et al., 2012). Mid-length alkanes (C_{20} to C_{25}) have been found to be most dominant in submerged or floating aquatic macrophytes (Cranwell, 1984; Ficken et al., 2000). *n*-Alkanes can also originate from anthropogenic sources such as oil and oil products. Contrary to these natural sources of *n*-alkanes, those derived from petroleum sources show no preference of odd over even chain lengths (Marzi et al., 1993). The most abundant *n*-alkane in terrestrial OM tends to be in the nC_{25} to nC_{35} carbon range, whereas for petroleum or anthropogenic sources, it tends to fall in the short to mid-length alkanes (Chen et al., 2014). While naturally occurring *n*-alkanes found in the environment originate mostly from epicuticular leaf waxes and phytoplankton production, anthropogenic *n*-alkanes can originate from transportation, production, consumption, or storage

of petroleum products. Petroleum is formed through the diagenesis and subsequent catagenesis of biomatter (Tissot and Welte, 1984), therefore petroleum OM is naturally occurring OM that has undergone physicochemical transformation altering the relative abundances of the *n*-alkanes present.

These variations in relative *n*-alkane abundances based on their origins have allowed for the calculation of various indices used for source tracing. A few of the most commonly used indices for OM source identification in sediments, and those used in this thesis include the carbon preference index (CPI), average chain length (ACL), natural *n*-alkane ratio (NAR), terrigenous aquatic ratio (TAR) and the terrestrial, emergent submerged/floating aquatic ratio (P_{aq}) which can be found in Table 2.2 (Poynter and Eglinton, 1990; Marzi et al., 1993; Bourbonniere and Meyers, 1996; Ficken et al., 2000; Mille et al., 2007). CPI is determined using the ratios of the concentrations of odd to even numbered chain length *n*-alkanes between nC_{16} and nC_{36} . This ratio represents the degree of preservation of the original *n*-alkane relative distribution. Fresh, terrestrially-derived higher plants typically have CPI values of > 3 reflecting the predominance of odd *n*-alkanes in vascular plants, whereas petroleum OM or inputs from marine sources exhibit values close to 1 due to their lack of preference of odd or even carbon numbers (Marzi et al., 1993; Chen et al., 2014). The ACL ratio refers to the weight-average number of carbon atoms in higher plant *n*-alkanes (nC_{25} to nC_{33}), and it is also used to distinguish higher plants from marine and petrogenic OM (Poynter and Eglinton, 1990). NAR is calculated based on the relationship of even *n*-alkanes to total *n*-alkanes in a sample and is used to assess the proportion of natural *n*-alkanes versus those derived from petroleum-derived *n*-alkanes (Mille et al., 2007). Finally, TAR and P_{aq} are ratios designed to differentiate between terrestrial and aquatic OM, with TAR evaluating the relative proportions of terrigenous OM to marine OM and P_{aq} distinguishing between terrestrial and aquatic plants (Bourbonniere and Meyers, 1996; Ficken et al., 2000). Both ratios rely solely on odd numbered *n*-alkanes, with TAR calculated as the ratio of the sum of nC_{27} , nC_{29} , and nC_{31} to that of nC_{15} , nC_{17} , and nC_{19} , and P_{aq} similarly calculated as the ratio of the sum of nC_{25} , nC_{27} , and nC_{29} to that of nC_{23} , nC_{25} , nC_{27} , and nC_{29} . It is important to note that while these ratios depend on the relative abundances to infer the sources of OM found in sediments, other methods utilizing stable isotope values can complement and further our understanding of OM cycling in the St. Lawrence system.

1.3 Application of Stable Isotope Analysis for Organic Matter Source Identification

The stable isotopes of OM can be exploited to further track the fate of OM and add a greater degree of differentiation of source input. While radioactive isotopes such as ^{14}C have been used to date samples in general, and sediments in particular, in this research we looked at the variations in the stable isotopes of carbon (^{12}C and ^{13}C) and hydrogen (^1H and ^2H). About 98.89% and 99.98% of all carbon and hydrogen respectively is found naturally as the lighter isotopes (^{12}C and ^1H), with the remaining 1.11% and 0.02% consisting of ^{13}C and ^2H respectively. These percentages are approximate with the natural abundances varying at the fourth and fifth decimal place, depending on the source material and biosynthetic precursors and reactions (Hayes, 1993; Sessions et al., 1999). For carbon, the proportion of ^{13}C to ^{12}C in OM is set during the carbon fixation process. Different source materials and different fixation pathways lead to variations in the ^{13}C proportions. Terrestrial plants using the C3 Calvin carbon fixation pathway fix carbon directly from atmospheric CO_2 , whereas C4 plants utilize the Hatch-Slack pathway resulting in C4 plants being enriched in ^{13}C compared to C3 plants (Peters et al., 2005). Phytoplankton utilizes inorganic bicarbonate as the carbon source during synthesis and therefore have a very different ratio of ^{13}C to ^{12}C in the resulting OM. The conditions that determine the proportion of ^2H and ^1H in OM again has to do with source material, but for hydrogen isotope values it is the source water used during photosynthesis. Other factors which contribute to variations in hydrogen isotope ratios include differing biosynthetic pathways (e.g., mevalonate vs. non-mevalonate), differences in carbon chain length, and degree of saturation, as well as the source of nicotinamide adenine dinucleotide phosphate (NADPH), with different pools of NADPH have different isotope ratios (Sessions et al., 1999, 2002; Chikaraishi and Naraoka, 2003; Zhang and Sachs, 2007; Zhang et al., 2009). These differences in ratios are measured using isotope ratio mass spectrometry (IRMS) and are reported using the delta notation using the following equation:

$$\text{Eq. (1.1)} \quad \delta(\text{‰}) = \left(\frac{R_{\text{sample}}}{R_{\text{reference}}} - 1 \right) \times 1000$$

Where R is the ratio of the heavy isotope over the light isotope of either the sample or the reference material. For the research presented in this thesis, these ratios would thus be $^{13}\text{C}/^{12}\text{C}$ or $^2\text{H}/^1\text{H}$ for carbon and hydrogen isotope analysis respectively. By convention, the reference material for

carbon analysis is a carbonate mineral, Vienna Pee Dee Belemnite (VPDB) and is a universal reference given a $^{13}\text{C}/^{12}\text{C}$ value of zero. The same is true for the Vienna Standard Mean Ocean Water (VSMOW) for hydrogen, again this reference material is given a $^2\text{H}/^1\text{H}$ value of zero.

The isotope ratio mass spectrometer (IRMS) does not measure the isotope values of the sample directly, but rather the sample is first combusted to CO_2 or pyrolyzed to H_2 for carbon and hydrogen analysis, respectively. A series of Faraday cups are used to simultaneously measure the specific abundance of ions of different masses for carbon and hydrogen isotopologues. For carbon, masses 44, 45 and 46 are measured, which correspond to $^{12}\text{C}^{16}\text{O}_2$ for mass 44, $^{13}\text{C}^{16}\text{O}_2$, and $^{12}\text{C}^{17}\text{O}^{16}\text{O}$ for mass 45, and finally $^{12}\text{C}^{18}\text{O}^{16}\text{O}$, $^{13}\text{C}^{17}\text{O}^{16}\text{O}$, and $^{12}\text{C}^{17}\text{O}_2$ for mass 46. For hydrogen isotope analysis, there are only two isotopologues of interest, e.g., mass 2, $^1\text{H}^1\text{H}$, and mass 3, $^2\text{H}^1\text{H}$. Nitrogen isotope analysis ($^{15}\text{N}/^{14}\text{N}$) is also possible by collecting masses 28 (^{14}N , ^{14}N), 29 ($^{14}\text{N}^{15}\text{N}$) and 30 ($^{15}\text{N}^{15}\text{N}$). Other isotopic analyses are also possible, but these are the ones used in the research presented in this thesis.

In this thesis, both bulk and compound specific isotope analysis (CSIA) were used to acquire isotopic data. For bulk isotope analysis, an elemental analyzer (EA) is coupled to the IRMS and a small amount of the sample (e.g., sediment) is introduced directly into a combustion tube. This method results in an average isotopic value for the entire sample. Contrarily, CSIA uses gas chromatography to initially separate the compounds in the sample before they are individually combusted/pyrolyzed and finally analyzed by the IRMS. CSIA thus allows obtaining isotopic values for individual compounds within a sample. These isotopic measurements add additional information about the samples being analyzed. For the research presented in this thesis, compound specific hydrogen and carbon isotope analysis was applied to the straight chain alkanes ranging from $n\text{C}_{23}$ to $n\text{C}_{36}$ extracted from sediments to infer the source of the n -alkanes at various stations along the St. Lawrence Waterway. Bulk carbon and nitrogen isotope analysis was also applied to the sediments to determine the overall input of OM and its sources at each station. These parameters along with the diagnostic ratios allowed us to better understand the sources and processing of OM found in this waterway. This data also provides a baseline level for comparison should an oil spill event occur.

1.4 Using Optical Properties to Determine Organic Matter Sources

Optical properties of CDOM have also become a popular parameter used to trace OM sources, specifically in aquatic environments (Derrien et al., 2017 and references within). Because of the compositional complexity of dissolved OM, it remains largely uncharacterized and identifying individual compounds using traditional analytical techniques becomes extremely difficult (Leenheer and Croué, 2003). The contribution of CDOM to total dissolved organic carbon (DOC) has been estimated to be as low as 20% in the open ocean and as high as 70% in coastal regions with high river inputs (Coble, 2007). Various spectroscopic indices have been developed to aid in the characterization of the chromophoric fraction in dissolved OM. Absorbance spectra and absorbance coefficients at selected wavelengths can be used as indices to elucidate various properties of the measured CDOM. The main absorbance indices which will be discussed in this thesis includes the specific UV absorbance ($SUVA_{254}$) and spectral slope (SR). $SUVA_{254}$ is used to assess the aromatic content and molecular weight of the dissolved OM in a sample by dividing the samples DOC concentration and UV absorption at 254 nm (Weishaar et al., 2003). SR is calculated by dividing the spectral slope between 275 nm and 295 nm by the slope between 350 nm and 400 nm and has also been used to describe the molecular weight of dissolved OM (Helms et al., 2008).

The fluorescence spectroscopic properties of the chromophoric fraction can be used to differentiate between various groups of compounds making up the dissolved OM pool and, more specifically, this can be done using fluorescence excitation emission matrices (EEM) combined with parallel factor analysis (PARAFAC). EEMs are produced by combining emission scans over a range of excitation wavelengths to create a 3D representation of a sample's fluorescence and are more sensitive than absorption spectroscopy (Stedmon and Bro, 2008). EEMs allow for discriminating CDOM sources based on the fluorophores present in the sample. The most common sources or groups of compounds that are identified using EEMs are humic-like, protein-like, and pigment-like fluorescence (Coble, 2007). These can be further broken down into the components shown in Table 1.1. While EEMs are helpful on their own when looking at one sample at a time, analyzing a large dataset of various samples becomes very challenging. This is where PARAFAC has become a popular method in aquatic biogeochemistry, allowing for the decomposition of data into trilinear components (Stedmon et al., 2003). With the addition of

PARAFAC, we can characterize the various groups of fluorophores in a water sample and determine the percentage of each group that contributes to the total fluorescence in the sample, as well as to infer the origin of the dissolved OM (Stedmon et al., 2007). This is possible because PARAFAC allows for the EEMs to be decomposed into 4-8 main components (EEMs), that are correlated to specific OM chromophore groups (Murphy et al., 2013). This method has been used to identify proteins, marine and terrestrial humic substances, anthropogenic humic substances coming from wastewater and agricultural runoff, and naturally occurring humic substance from bacterial degradation of OM (Coble, 2007; Stedmon et al., 2007; Murphy et al., 2008; Tfaily et al., 2015).

Table 1.1 Commonly identified fluorophore groups (adapted from Coble 2007 and references within).

Component	Peak Label	Ex/Em (nm)	Source
Tyrosine-like, protein-like	B	275/305	autochthonous
Tryptophan-like, protein-like	T	275/340	autochthonous
UVC humic-like	A	260/400–460	fulvic acid, autochthonous, terrestrial
UVC humic-like	A	260/400–460	humic, terrestrial, allochthonous
UVA marine humic-like	M	290–310/370–410	anthropogenic from wastewater and agriculture
UVA humic-like	C	320–360/420–460	terrestrial, anthropogenic, agriculture
Pigment-like	P	398/660	

Furthermore, a series of indices base on the fluorescence measurements have been found to be useful in the determination of chemical composition and sources of dissolved OM. The fluorescence index (FI) can be applied to samples to differentiate between terrestrial and microbial dissolved OM using the ratio of fluorescence emitted at 450 nm to that emitted at 500 nm, when the excitation wavelength is 370 nm (McKnight et al., 2001). HIX, the humification index is indicative of the degree of humification in a sample and is based on the ratio of the area under the emission spectra between 435 and 480 nm to that between 300 and 345 nm, at the excitation wavelength of 254 nm (Zsolnay et al., 1999; Ohno, 2002). Finally, the biological index (BIX) is the ratio of fluorescence measured at the emission wavelength of 380 nm to that at the emission wavelength of 430 nm, when excited at 310 nm, and is used to investigate the biological production of dissolved OM (Huguet et al., 2009). These spectral properties allow for further characterization of an OM pool that remains largely uncharacterized, adding another piece of information to the cycling of carbon in aquatic settings. This method to analyze OM in waterways is much simpler, and less time consuming than other typical analytical techniques,

requiring only absorbance and fluorescence measurements. In this thesis, we use EEMs and PARAFAC analysis to assess the origin of the OM in the water column along the St. Lawrence system, to determine if using this more accessible method would allow for the detection of oil contamination in the water column.

1.5 Molecular, Isotopic and Spectroscopic Differences Between Natural and Petroleum Derived Hydrocarbons

While petroleum is a complex mixture of compounds, it is primarily made up of aliphatic and aromatic hydrocarbons with a small percentage of aromatic compounds containing sulfur, nitrogen and oxygen. As mentioned above, oil derived hydrocarbons originate from natural OM that has been heavily degraded, thermally, chemically, and biologically. Oils originating from regions with varying biomatter (e.g., variations in the type of plant matter) can therefore have a different structural makeup and abundances of hydrocarbons from one location to another (Murray et al., 1998). Molecularly, the aliphatic fraction of oil contains straight chain alkanes ranging from nC_6 to nC_{40} . Figure 1.2 shows the gas chromatography-flame ionization detector (GC-FID) trace of a few oils showing the possible variations in n -alkanes relative distribution (Bayona et al., 2015). The similar properties of all these traces is the normal distribution of n -alkanes. Fresh natural OM is characterized by a prominent pattern of odd n -alkanes being more abundant than their neighbouring even n -alkanes owing to their synthetic pathway; indeed, they are produced from the decarboxylation of long chain fatty acids (loss of one carbon atom), which are synthesized from a C_2 molecular building block, acetate. Terrestrial fatty acids thus show a strong preference of even over odd, while terrestrial n -alkanes show a marked odd over even preference. As natural OM is being processed and partially degraded by bacteria, leading to n -alkanes losing one of a few carbon atoms, there is a redistribution in the relative abundances of odd and even n -alkanes, to the point where the most degraded OM samples (oils for example), show a ratio between odd and even n -alkanes equal to unity.

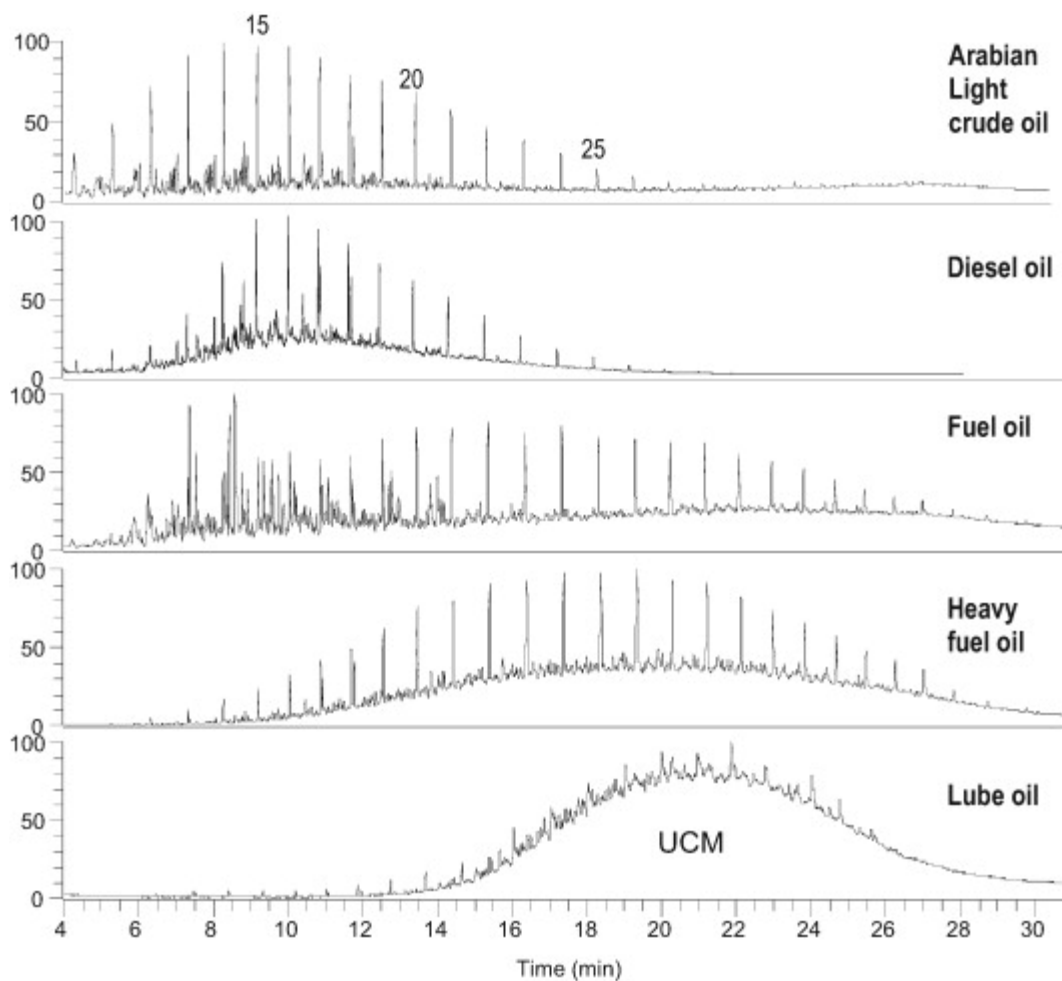


Figure 1.2 GC-FID trace of various oil types modified from Bayton et al. 2015.

Isotopically, natural OM has been shown to vary with carbon isotope values of bulk OM ranging from -12 to -34‰, with C3, C4 and algae having $\delta^{13}\text{C}$ values ranging from -24‰ to -34‰, -6‰ to -19‰, and -12‰ to -23‰ respectively (Smith and Epstein, 1971; Lichtfouse et al., 1994). Compound specific carbon and hydrogen isotope analysis of individual alkanes of higher plants (C3 and C4 plants) have also been shown to vary between plants as well as within a single plant extract (Chikaraishi and Naraoka, 2007), whereas due to the thermal maturation, chemical and biological reworking of the original OM in petroleum, it has been found that oil-derived *n*-alkanes have very similar carbon isotope values across the *n*-alkanes measured (Pedentchouk and Turich, 2018).

While the *n*-alkanes are the most abundant hydrocarbons found in oil, and thus the easiest to measure and analyse, certain aromatic hydrocarbons also are more specific to oils. These

anthropogenic polycyclic aromatic hydrocarbons (PAH) are well-known as being toxic, mutagenic, and carcinogenic. They are therefore important to identify and analyse in aquatic systems where they can cause significant damage to the organisms in those environments (Menzie et al., 1992; Ikenaka et al., 2013). PAHs can occur naturally through biomass burning (e.g., forest fires), volcanic eruptions or diagenesis, but are often linked to anthropogenic origins such as coal and wood burning, petroleum combustion and spills, and industrial processes (Andersson et al., 2014). Their abundance in oils and petroleum products is much lower than *n*-alkanes and can therefore add to the difficulty of proper analysis. Spectroscopically, these PAHs and their photo oxidized products are the compounds that allow us to apply EEMs and PARAFAC analysis on water samples to determine oil input into the water system.

These slight differences in naturally occurring and oil-derived OM can be exploited with molecular, isotopic, and spectroscopic techniques to tease out the origin of OM found in sediments and water samples along the St. Lawrence Waterway.

1.6 Objectives

Using compound specific carbon and hydrogen isotope analysis, coupled with molecular fingerprinting of *n*-alkanes, we characterized the OM currently present in the St. Lawrence Waterway to obtain a molecular and isotopic baseline level for the *n*-alkanes found in the sediments. Having these baseline values allows detection of compositional changes if there were to be an oil spill event along the St. Lawrence system. While natural and petroleum-derived *n*-alkanes are not toxic, the presence of petroleum-derived *n*-alkanes indicates that other, more toxic compounds such as polyaromatic hydrocarbons (PAHs), are also present in the sample. These methods also allow us to determine how efficiently the isotopic and molecular analysis of *n*-alkanes can reflect OM sources. More specifically, we focused on the less abundant even chain length *n*-alkanes that are much less frequently analyzed due to the difficulty to accurately measure their isotopic composition owing to their much lower abundance. This is the first complete data set including molecular finger printing, as well as carbon and hydrogen isotopic analysis of both odd and even chain length *n*-alkanes along a terrestrial-marine continuum. While this method is time consuming, requiring lengthy sample pre-treatment prior to analysis, other characteristics of OM can be exploited to differentiate natural from petroleum-derived OM. Spectroscopic techniques such as EEMs and PARAFAC analysis were also applied to surface

and water column samples collected along the St. Lawrence River, Estuary and Gulf to tease out various components indicative of the source of the dissolved OM pool. In addition to these natural water samples, water samples with photo oxidized oil-derived compounds introduced to the water were included in the data set when running the PARAFAC analysis to determine how well it could tease out the oil components from the natural OM present in the samples. While spectroscopic methods do not allow for identification of individual compounds, it is much more cost and time efficient as it does not require expensive instrumentation and sample work-up. The application of these two methods to the water and sediments samples allows characterization of the OM found along the St. Lawrence Waterway and determination of whether they can be used to discriminate natural OM from OM derived from oil contamination.

1.7 Arrangement of Thesis

This work is comprised of two long manuscripts (one published, and the other to be submitted for publication), followed by a summation of the limitations and future works that should be explored. The manuscripts are presented with figures and tables embedded in the text with supplementary material found in the appendices. The first chapter contains the general introduction, which allows for the contextualisation of the main topics covered in the two manuscripts that follow.

Chapter 2, entitled “Molecular and stable isotope analysis ($\delta^{13}\text{C}$, $\delta^2\text{H}$) of sedimentary *n*-alkanes in the St. Lawrence Estuary and Gulf, Quebec, Canada: Importance of even numbered *n*-alkanes in coastal systems”, was published in *Organic Geochemistry* in February 2022 and presents the advantages of coupling isotopic measurements with molecular diagnostic ratios to characterize sedimentary OM in the St. Lawrence Waterway. It also highlights the importance of using caution when relying solely on molecular data and the importance of even-numbered *n*-alkanes and the information they can provide regarding OM source. This complete isotopic and molecular analysis of the *n*-alkanes along the St. Lawrence system establishes a baseline level to for comparison should there be an oil spill event.

Chapter 3, entitled “Tracking changes in dissolved organic matter along the St. Lawrence River, Estuary and Gulf using PARAFAC analysis and distinguishing natural organic matter from oil-derived compounds”, is to be submitted for publication in *Marine Chemistry*. It reports the findings acquired when PARAFAC analysis was applied to a large set of water samples collected

along the St. Lawrence system at various locations and depths. It also contains samples contaminated with oil that underwent solar irradiation to determine how well this approach could tease out oil derived compounds from natural occurring OM. The applicability of this method to trace OM in the St. Lawrence and its potential for tracking oil spills is also discussed.

Chapter 4 summarizes the main findings of this thesis, as well as perspectives and future work.

Chapter 2: Molecular and stable isotope analysis ($\delta^{13}\text{C}$, $\delta^2\text{H}$) of sedimentary *n*-alkanes in the St. Lawrence Estuary and Gulf, Quebec, Canada: importance of even numbered *n*-alkanes in coastal systems

Anic Imfeld^{1,2}, Alexandre Ouellet³, Peter Douglas^{2,4}, Gregor Kos¹, Yves Gélinas^{1,2}

¹ Department of Chemistry and Biochemistry, Concordia University, 7141 Sherbrooke Street West, Montréal, Québec, Canada, H2B 1R6

² Geotop, Université du Québec à Montréal, C.P. 8888, Succ. Centre-Ville Montréal, Québec, H3C 3P8

³ Centre de contrôle environnemental de l'Outaouais, Ministère de l'Environnement et de la Lutte contre les changements climatiques, 170, rue Hôtel-de-Ville, Gatineau, Québec, J8X 4C2

⁴ Department of Earth and Planetary Sciences, McGill University, 3450 University Street, Montreal, Quebec, Canada, H3A

Corresponding author:

Yves Gélinas

Department of Chemistry and Biochemistry

Concordia University

7141 Sherbrooke Street West,

Montreal, Quebec, Canada, H4B 1R6

Email: yves.gelinas@concordia.ca

Keywords: *n*-Alkanes, Carbon isotopes, $\delta^{13}\text{C}$, Hydrogen isotopes, $\delta^2\text{H}$, Sediments, Diagnostic ratios, Even-numbered

2.1 Abstract

Sediments comprise a multitude of inorganic and organic components, with much of the composition of the organics still not fully characterized. Our research targeted *n*-alkanes, to determine whether compound specific carbon and hydrogen isotope analysis allows for their source identification in coastal sediments. Here, we map the current abundances and sources of straight chain *n*-alkanes in sediments of the St. Lawrence Estuary and Gulf using molecular (diagnostic ratios) and isotopic fingerprinting ($\delta^{13}\text{C}$, $\delta^2\text{H}$). *n*-Alkane abundances (117.11 ± 1.61 to 418.64 ± 70.20 $\mu\text{g/g OC}$), carbon preference index (CPI; 1.95 ± 0.05 to 5.09 ± 0.10), average chain length (ACL; 28.36 ± 0.02 to 28.97 ± 0.01), proportion of aquatic submerged plants and terrestrial plant inputs (P_{aq} ; 0.295 ± 0.003 to 0.377 ± 0.002), terrigenous aquatic ratio (TAR; 3.43 ± 0.16 to 7.99 ± 0.05), and *n*-alkane ratio (NAR; 0.169 ± 0.011 to 0.584 ± 0.011) values varied along the terrestrial-marine continuum. Large differences in the concentration weighted average (WA) $\delta^{13}\text{C}$ and $\delta^2\text{H}$ for odd and even *n*-alkanes were found, with WA $\delta^{13}\text{C}$ ranging from -30.9 ± 0.3 to -33.4 ± 0.09 ‰ and -28.8 ± 0.01 to -32.3 ± 0.2 ‰, respectively, and 165.6 ± 3.6 to -200.8 ± 2.4 ‰ and -96.0 ± 2.8 to -158.7 ± 2.1 ‰ for $\delta^2\text{H}$. The diagnostic ratios were shown to misrepresent the input sources of organic matter (OM) and were inaccurate as source indicators when more than one OM source was present. With the addition of compound specific $\delta^{13}\text{C}$ and $\delta^2\text{H}$ analysis of *n*-alkanes, it was determined that the *n*-alkanes were predominantly derived from natural, rather than anthropogenic sources, with variations being driven by geographic changes in vegetation type and differing ratios of terrestrial and marine OM inputs. Importantly, compound specific isotope analysis of the even numbered *n*-alkanes would permit identification and tracking of petroleum-derived contaminants. Molecular data alone are ineffective for this, owing to the similarity in CPI values for petroleum-derived contaminants and highly degraded OM which is discharged by the St. Lawrence River into the estuary.

2.2 Introduction

Organic matter (OM) deposited in estuarine and coastal sediments is an important part of the global carbon cycle and preserves information about OM source environments. Sedimentary OM contains an abundance of various lipids, including so-called straight chain alkanes (*n*-alkanes), which are derived from terrestrial and aquatic plants and certain algae and are often the most abundant hydrocarbons found in sediments. Vascular plants preferentially synthesize *n*-

alkanes with odd numbered carbon chain lengths compared to even numbered *n*-alkanes in the range of nC_{21} to nC_{35} (Silva et al., 2012), whereas shorter chain alkanes in the range of nC_{15} to nC_{19} are attributed to aquatic algae and bacteria (Han and Calvin, 1969). These hydrocarbons are widely used as biomarkers to trace the origins of the organic matter in a variety of different environments and locations (Pearson and Eglinton, 2000; Pearson et al., 2001; Wakeham et al., 2004; Sachse et al., 2006). Various diagnostic ratios and molecular indices based on the relative abundance of individual compounds have been established for source determination in past studies for *n*-alkanes. Mass ratios, such as carbon preference index (CPI), terrigenous aquatic ratio (TAR), natural *n*-alkane ratio (NAR) and average chain length (ACL), are widely applied to sediment extracts to characterize the origin of OM (Poynter and Eglinton, 1990; Marzi et al., 1993; Bourbonniere and Meyers, 1996; Ficken et al., 2000; Mille et al., 2007). Most studies utilizing hydrocarbons as biomarkers for source apportionment rely heavily on these diagnostic ratios.

However, additional information about the source of these compounds can be elucidated using isotopic measurements of both the bulk sediment and individual compounds. Bulk carbon-to-nitrogen atomic ratios, as well as stable carbon and nitrogen isotope values have the capacity to differentiate the main sources of the OM found in sediments (Peters et al., 1978; Thornton and McManus, 1994; Hou et al., 2007). While bulk analysis can be a useful tool for source identification, compound specific carbon and hydrogen isotope analysis of individual lipids allows for broader application of *n*-alkanes as biomarkers with more precise source identification. This is possible due to characteristic source specific values. *n*-Alkane stable carbon isotope values are mainly driven by the method of CO_2 fixation, as well as the CO_2 source. C_3 plants show $\delta^{13}C$ values ranging from -24‰ to -34‰, C_4 plants have $\delta^{13}C$ values ranging from -6‰ to -19‰, and algae have intermediate values of -12‰ to -23‰ (Smith and Epstein, 1971; Lichtfouse et al., 1994). Hydrogen isotopic variations have been shown to be attributed to variation in the δ^2H of plant source water, which is related to geographic variation in precipitation δ^2H and subsequent evapotranspiration, and to biosynthesis (Sessions et al., 1999; Huang et al., 2004; Sachse et al., 2012).

Applications of $\delta^{13}C$ values, and to a lesser extent δ^2H of individual *n*-alkanes, have been used in plant wax, soil and sediment studies and have been shown to be suitable for identification of OM sources since stable isotope values vary with the type of plants from which

they originate (gymnosperms, angiosperms, aquatic plants) (Chikaraishi and Naraoka, 2007; Hou et al., 2007; Katrantsiotis et al., 2018; He et al., 2020). They have also been used to determine anthropogenic inputs and to identify petroleum derived *n*-alkanes by exploiting the small differences in stable isotope values originating from the initial sources of OC, kinetic fractionation processes, mixing, biodegradation, or $^2\text{H}/^1\text{H}$ exchange with water and minerals (Y. Li et al., 2009; Pedentchouk and Turich, 2018). However, due to the higher abundances, and thus ease of measurement, of odd *n*-alkanes in plants and natural samples, many studies only focus on the $\delta^{13}\text{C}$ and $\delta^2\text{H}$ of odd *n*-alkanes. Compound specific isotope analyses in sediment cores are commonly used as proxies in paleo environmental studies (Ishiwatari et al., 2009; Yamamoto et al., 2010; Katrantsiotis et al., 2018; Aichner et al., 2018; Strobel et al., 2020). These types of studies focus on the temporal variations in sedimentary records, whereas fewer studies examine changes across a water system with changing environmental conditions such as OM source and salinity.

The St. Lawrence waterway has inputs from both marine and terrestrial organic matter, and thus allows for the mapping of the molecular and isotopic changes of individual *n*-alkanes, both odd and even chain lengths, along a terrestrial to marine gradient. This study aims to characterize sedimentary *n*-alkanes to compare well established diagnostic ratios with compound specific $\delta^{13}\text{C}$ and $\delta^2\text{H}$ values to determine the information that can be gained from each method individually and combined. In particular, the information potential of low and high molecular weight even numbered *n*-alkanes, including their stable carbon and hydrogen isotope values, is assessed for the first time over a large (>800 km) transition area between a river mouth and the sea.

2.3 Materials and methods

2.3.1 Sampling locations and collection

The St. Lawrence waterway is a stretch of water spanning 2000 km, split into 3 main sectors, the River, Estuary and Gulf. The Estuary can be further divided into two distinct regions, the shallow (30 – 100 m) turbid Upper Estuary and the deep (>300 m), stratified Lower Estuary, marking the head of the Laurentian Channel. The Saguenay Fjord, an approximately 90 km long submerged valley, connects to the St. Lawrence Estuary at roughly the meeting point of the Upper and Lower Estuary. The Upper Estuary receives inputs primarily from freshwater runoff

and the St. Lawrence River, which drains a populated, industrialized watershed where agricultural activities are important. The Lower Estuary receives inputs from the Upper Estuary, the Saguenay Fjord, as well as a series of rivers on the north shore, and is stratified with mixing of estuarine surface waters and marine bottom water from the deep North Atlantic Ocean through the Laurentian Channel. In June of 2018, nine locations were sampled along the St. Lawrence Estuary, Gulf and Saguenay Fjord for the purposes of this study (Fig. 2.1). Sample locations were selected to cover the gradient of terrestrial to more marine sediments and were collected using a box-core (stations Sag05, 25, 23, 21, 18.5, 18, and 16) and with a Van Veen grab where sediment depth was not deep enough for the box corer (stations DE, G) aboard the *RV Coriolis II*. Locations and descriptive information for these stations can be found in Table 2.1. The top 10 cm of sediment were collected from the box cores and grabs and stored at -20°C until further treatment. Pre-analysis, the sediment samples were thawed, centrifuged to remove excess pore water, freeze-dried, and homogenized using a mortar and pestle in preparation for all subsequent analyses.

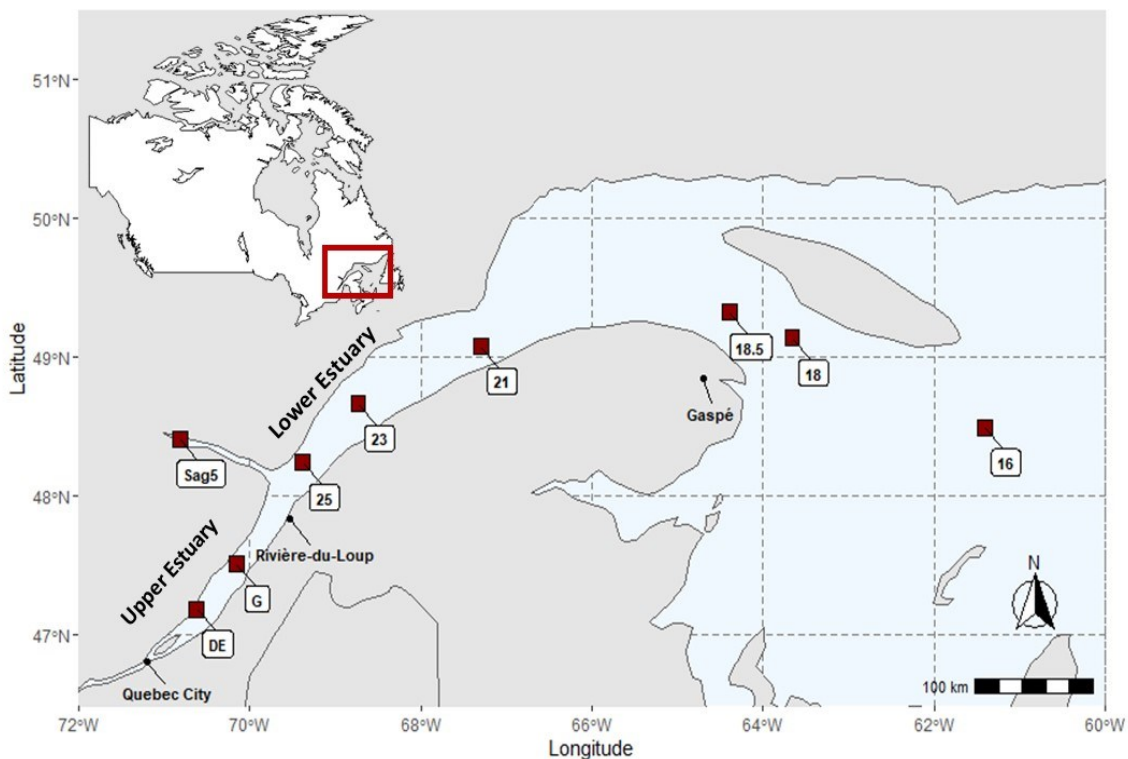


Figure 2.1 Map showing study sites across the St. Lawrence Estuary and Gulf in Quebec, Canada.

Table 2.1 Description of sampling sites in the St. Lawrence Estuary and Gulf.

Station	Latitude	Longitude	Distance from Quebec City (km)	Water column depth (m)	Surface water salinity (psu)	Sedimentation Rate (Smith and Schafer, 1999) (cm/yr)
Sag05	48°24.798'N	70°49.307'W	a	89	0.87	n.a.
DE	47°11.223'N	70°37.419'W	60	17	2.89	b
G	47°30.689'N	70°09.775'W	114	61.8	15.82	b
25	48°14.531'N	69°22.808'W	215	325	25.23	0.545
23	48°40.104'N	68°44.086'W	300	345	25.59	n.a.
21	49°04.750'N	67°18.147'W	400	325	27.32	0.223
18.5	49°19.519'N	64°23.601'W	539	389	28.26	n.a.
18	49°08.428'N	63°39.712'W	600	364	29.01	0.115
16	48°29.664'N	61°24.744'W	780	418	30.89	0.042

^aDistance from Quebec City irrelevant

^bSediments collected with a Van Veen grab

n.a.: Sedimentation rates unavailable

It is important to note the differences in sedimentation rates and thus varying sediment ages along the St. Lawrence Estuary and Gulf (Smith and Schafer, 1999). The average age of the top 10 cm ranged from about 10 years in the lower estuary to up to ~120 years in the Gulf. To allow compound specific isotope analysis to be performed on both odd and even chain length *n*-alkanes (triplicate extractions), it was necessary to start with a large mass of sediment (~100 g dry weight per replicate). Therefore, for the stations which were sampled with a box core, the top 10 cm were used and were thoroughly homogenized before extraction.

2.3.2 Elemental and bulk sediment isotope analysis

The organic carbon (OC) and total nitrogen (TN) contents, as well as the $\delta^{13}\text{C}$ and $\delta^{15}\text{N}$ values, were obtained using an Eurovector elemental analyser (EuroEA3028-HT) coupled to an Isoprime 100 continuous flow isotope ratio mass spectrometer. Concentrations and stable isotope values were obtained from the same calibrations, but carbon and nitrogen were run separately because of the need to remove carbonates in the samples analysed for OC, and the large differences in abundance between the two elements. For OC analysis, 5-level calibration curves were built daily using an in-house β -alanine standard (C = 40.45%, $\delta^{13}\text{C} = -25.98 \pm 0.23\text{‰}$), with intensities spanning the entire range of the instrument. Samples were then run in quadruplicate, with the β -alanine standard and IAEA-C6 certified sucrose standard (C = 42.10%, $\delta^{13}\text{C} = -10.80 \pm 0.47\text{‰}$) inserted between each set of two samples. The in-house β -alanine standard was calibrated independently for carbon using two certified primary standards (IAEA-CH7

polyethylene foil, $\delta^{13}\text{C} = -32.15 \pm 0.10\%$; IAEA-C6 sucrose, $\delta^{13}\text{C} = -10.80 \pm 0.47 \%$. The same approach was used for nitrogen using the in-house β -alanine standard ($\text{N} = 15.72\%$, $\delta^{15}\text{N} = -2.21 \pm 0.24\%$), calibrated using two certified primary standards (IAEA-N-1 ammonium sulfate, $\delta^{15}\text{N} = +0.43 \pm 0.07\%$; IAEA-N-2 ammonium sulfate, $\delta^{15}\text{N} = +20.41 \pm 0.12\%$). For OC and $\delta^{13}\text{C}$ analysis, samples were decarbonated by exposure to HCl fumes for 12 hours followed by a 1 hour heating step at 50°C to remove any remaining water or acid prior to analysis (Hedges and Stern, 1984).

2.3.3 Extraction and quantitation of *n*-alkanes

n-Alkanes were extracted from dry sediments (~ 100 g per replicate, $n=3$) by sonication with a 1:1 acetone:hexane mixture. Following sonication, water was added to the sample and the organic phase was isolated via liquid-liquid extraction. The aliphatic and aromatic fractions were separated on a silica gel column, eluting the aliphatic fraction with hexane and the aromatic fraction with a 25% v/v toluene in hexane mix. Both fractions were passed through a copper powder column to remove any elemental sulfur. At this point an aliquot of the aliphatic fraction was subsampled for quantitation. The *n*-alkanes were further isolated for isotopic analysis using a urea adduction method. In short, a saturated urea/methanol mixture was added to the aliphatic fraction of the extract and left to crystallize at -20°C overnight. The crystals were dried and washed with hexane before dissolving in water and transferring the alkanes to the organic phase with another liquid-liquid extraction using hexane as the organic phase. The final extract was evaporated to $500 \mu\text{L}$ and stored at -20°C until the time of analysis.

n-Alkanes were quantified on an Agilent 6890N gas chromatograph with a flame ionization detector (GC-FID), using an Agilent DB-EUPAH column ($60 \text{ m} \times 0.25 \text{ mm} \times 0.25 \mu\text{m}$) and an alkane calibration mix ($\text{C}_8\text{-C}_{40}$, Supelco ASTM D2887) as external calibration. Samples were run using constant flow with a helium carrier gas. Initial oven temperature was held at 40°C for 10 minutes, then ramped to 230°C at a rate of 6°C per minute, followed by an increase to 320°C at 20°C per minute, which was held for 34 minutes, resulting in a run time of 80.17 minutes per sample. *n*-Alkane identities were confirmed on an Agilent 7890B gas chromatograph coupled to an Agilent 5977B mass spectrometer (GC-MS) with an identical column and temperature program as described above. GC-MS analysis was also used to confirm that there was no co-elution prior to stable isotope analysis.

Due to the extensive sample preparation involving multiple solvent evaporation steps, *n*-alkanes below *n*C₁₇ are not shown, as the recoveries for these alkanes were affected by the cleanup (mainly during the reduction in solvent volume using a gentle N₂ stream) and thus were not an accurate representation of the *n*-alkanes in the sediment. However, these clean up steps are widely used and recoveries for individual *n*-alkanes rarely given; therefore, the values for *n*C₁₅, specifically for terrigenous aquatic ratio (TAR), were still used in respect to the molecular proxies found in the literature. Spiking experiments revealed that the recoveries for *n*-alkanes >C₁₇ were above 90%, with stable isotope values that were not significantly different from the expected values (p<0.05).

2.3.4 *n*-Alkane molecular proxies

The *n*-alkane molecular proxies used in this study can be found in Table 2.2. Total *n*-alkane concentrations were obtained by summing the concentration (in µg/g OC) of each individual *n*-alkane from *n*C₁₇ to *n*C₃₆, and total even and odd *n*-alkanes using even *n*-alkanes from *n*C₁₈ to *n*C₃₆ and odd *n*-alkanes from *n*C₁₇ to *n*C₃₅, respectively. Low molecular weight (LMW) and high molecular weight (HMW) *n*-alkanes are defined as *n*C₁₇ to *n*C₂₂ and *n*C₂₃ to *n*C₃₆, respectively.

Table 2.2 *n*-Alkane molecular proxies used in this study ('→' indicates range).

Ratio	Equation	Reference
Carbon Preference Index (CPI)	$\frac{\sum(nC_{23} \rightarrow nC_{31})_{odd} + \sum(nC_{25} \rightarrow nC_{33})_{odd}}{2 \sum(nC_{24} \rightarrow nC_{32})_{even}}$	Marzi et al., 1993
Average Chain Length (ACL)	$\frac{\sum[25(nC_{25}) \rightarrow 33(nC_{33})]_{odd}}{\sum[(nC_{25}) \rightarrow (nC_{33})]_{odd}}$	Poynter and Eglinton, 1990
Natural <i>n</i> -Alkanes Ratio (NAR)	$\frac{\sum(nC_{19} \rightarrow nC_{32}) - 2 \sum(nC_{20} \rightarrow nC_{32})_{even}}{\sum(nC_{19} \rightarrow nC_{32})}$	Mille et al., 2007
Terrigenous Aquatic Ratio (TAR)	$\frac{nC_{27} + nC_{29} + nC_{31}}{nC_{15} + nC_{17} + nC_{19}}$	Bourbonniere and Meyer, 1996
Terrestrial, emergent submerged /floating aquatic ratio (P _{aq})	$\frac{(nC_{23} + nC_{25})}{(nC_{23} + nC_{25} + nC_{29} + nC_{31})}$	Ficken et al., 2000

2.3.5 Compound-specific carbon and hydrogen isotope analysis

Compound-specific stable carbon isotope analysis was performed on a gas chromatograph-isotope ratio mass spectrometer, using an Agilent 6890 gas chromatograph, with a DB-EUPAH fused silica capillary column (60 m x 0.25 mm x 0.25 μ m), with a Finnigan combustion furnace coupled to a continuous flow Thermo Finnigan Delta Plus XP isotope ratio mass spectrometer. Compound-specific hydrogen isotope values were obtained on a ThermoScientific Trace1310-GCIsolink II system coupled to a ThermoScientific Delta V Plus isotope ratio mass spectrometer with a ThermoFisher TG5-MS fused silica capillary column (60 m x 0.25 mm x 0.25 μ m). Certified alkane and fatty acid standards obtained from Indiana University (A. Schimmelman, A7 Alkanes mix and F8-3 Fatty Acids mix) were run after every set of replicates ($n=3$) to ensure instrument stability and for $\delta^{13}\text{C}$ and $\delta^2\text{H}$ correction purposes. The standards were run at various signal intensities to ensure linearity over the entire range of n -alkane concentrations encountered in this work, thus allowing for the measurement of both odd and even n -alkanes.

2.3.6 Statistical analyses

An independent Student t-test assuming unequal variance was used to compare the weighted average $\delta^{13}\text{C}$ and $\delta^2\text{H}$ values of the odd and even n -alkanes at each station. Principal component analysis (PCA) was completed using R (version 4.0.3) with FactoMineR (version 2.4) and factoextra (version 1.0.7) packages to visualize the data and to determine those parameters attributing the most variation in the dataset.

2.4 Results

2.4.1 Bulk sediment isotope analysis ($\delta^{13}\text{C}$, $\delta^{15}\text{N}$) and C/N ratio

The percentages of organic carbon and total nitrogen and the carbon to nitrogen atomic ratios (C/N) in the surface sediments of the various stations are shown in Table 2.3, along with their respective $\delta^{13}\text{C}$ and $\delta^{15}\text{N}$ values. No apparent trend can be seen in terms of the OC or TN contents at the various stations, with values ranging from 1.29 ± 0.09 to 2.23 ± 0.04 w/w % and 0.116 ± 0.002 to 0.204 ± 0.001 w/w %, respectively. Terrestrial OM typically has $\delta^{13}\text{C}$ values ranging from -25 to -30‰ and -10 to -14‰ for C_3 and C_4 plants, respectively (Smith and Epstein, 1971; Deines, 1980), whereas marine OM ranges from -18 to -24‰ (Gearing et al., 1984). The $\delta^{13}\text{C}$ values shift upwards from stations with higher terrestrial inputs (Sag05 and DE) to stations

which appear to have more marine inputs (stations 18.5, 18 and 16), i.e., from -27.3 ± 0.02 to -22.39 ± 0.09 ‰ (Tan and Strain, 1983). Similar trends have been published showing a ^{13}C enrichment from terrestrial to marine sediments owing to an increased relative proportion of marine sources of OM along the continuum (Tan and Strain, 1979; Hu et al., 2009). Additionally, the $\delta^{15}\text{N}$ values range from 3.78 ± 0.34 to 7.87 ± 0.02 ‰, again with an enrichment trend from the more terrestrial (Sag05 and DE) to the more marine stations (stations 18.5, 18, 16). The carbon to nitrogen ratio (C/N) (ranging from 8.61 ± 0.15 to 16.61 ± 0.42) generally decreases from the Upper Estuary to the lowest C/N value at station 18.5, with an increase again for the two stations furthest in the Gulf. Fig. 2.2 shows the relationship between the bulk sediment carbon isotope values and the C/N ratios for each station along with shaded areas corresponding to various OM source materials (Lamb et al., 2006 and references within).

Table 2.3 Percentages (\pm standard deviations) of organic carbon (OC), total nitrogen (TN), atomic C/N.

Station	%OC	%TN	C/N	$\delta^{13}\text{C}$ (‰)	$\delta^{15}\text{N}$ (‰)
Sag05	2.23 ± 0.04	0.134 ± 0.002	16.61 ± 0.42	-27.3 ± 0.02	3.8 ± 0.3
DE	1.75 ± 0.06	0.168 ± 0.003	10.43 ± 0.40	-26.4 ± 0.3	5.7 ± 0.1
G	1.69 ± 0.14	0.167 ± 0.002	10.11 ± 0.84	-25.7 ± 0.1	5.6 ± 0.07
25	1.36 ± 0.06	0.116 ± 0.002	11.73 ± 0.60	-24.5 ± 0.05	5.9 ± 0.1
23	1.70 ± 0.08	0.175 ± 0.000	9.68 ± 0.47	-23.9 ± 0.08	6.4 ± 0.1
21	1.66 ± 0.09	0.180 ± 0.002	9.23 ± 0.52	-23.3 ± 0.03	7.3 ± 0.1
18.5	1.75 ± 0.03	0.204 ± 0.001	8.61 ± 0.15	-22.6 ± 0.04	7.9 ± 0.02
18	1.29 ± 0.09	0.117 ± 0.004	11.10 ± 0.85	-22.6 ± 0.1	7.8 ± 0.2
16	1.99 ± 0.11	0.168 ± 0.003	11.83 ± 0.70	-22.4 ± 0.09	7.8 ± 0.04

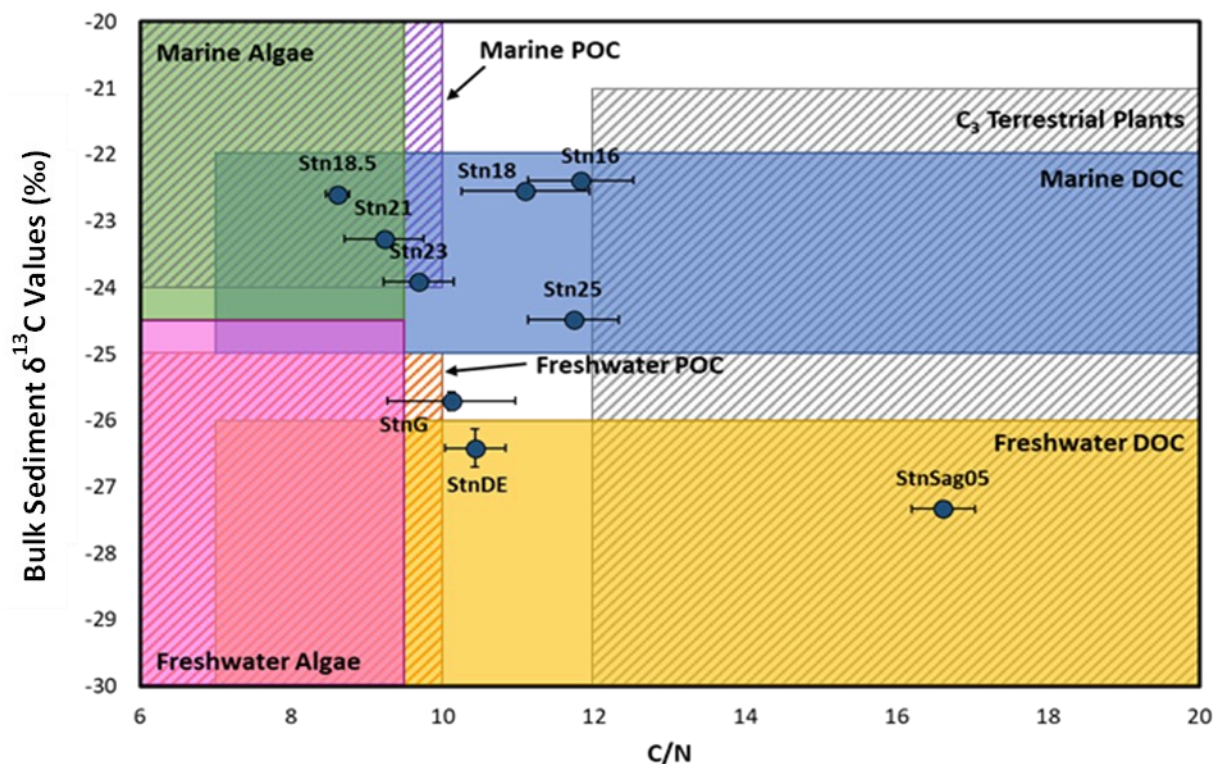


Figure 2.2 $\delta^{13}\text{C}$ values and C/N ratios of bulk sediments at all stations with typical ranges of OM inputs.

2.4.2 *n*-Alkane abundances and diagnostic ratios

Alkanes were characterized at each of the stations along the St. Lawrence Estuary, Gulf and Saguenay Fjord. The concentrations for each individual alkane at all stations normalized to the mass of OC in the sediments can be found in Fig. 2.3. A complete table with all molecular and isotopic data can be found in the Supplementary Material section (Table A.2 and A.3). A clear preference of odd over even numbered straight chain alkanes was found for all stations, with a maximum concentration for $n\text{C}_{29}$ for all stations except Sag05 (C_{max} of $n\text{C}_{27}$). Generally, *n*-alkane maxima at $n\text{C}_{27}$, $n\text{C}_{29}$ or $n\text{C}_{31}$ are indicative of higher plant epicuticular waxes and lower values tend to be attributed to anthropogenic inputs (Chen et al., 2014).

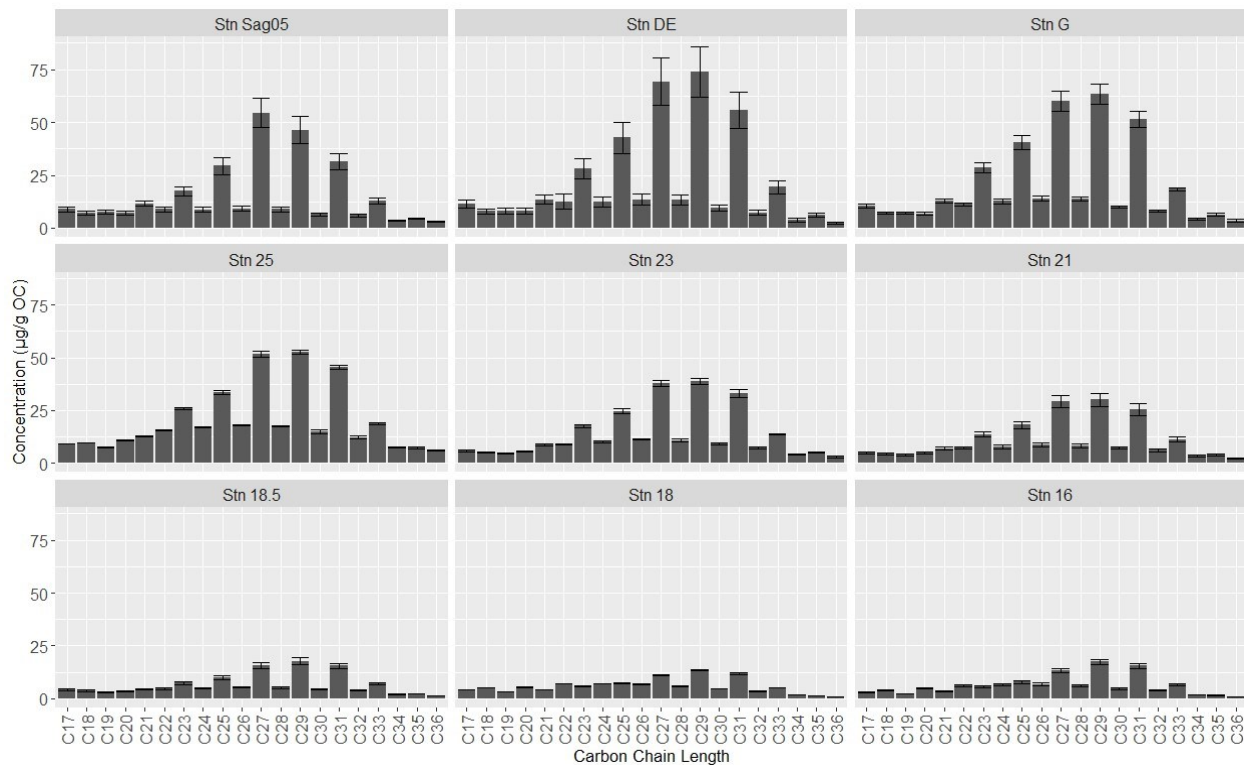


Figure 2.3 *n*-Alkane concentrations in the top 10 cm of sediments at each station. The same scale was used for the y-axis.

Total alkane concentrations (the sum of nC_{17} to nC_{36} , inclusively) in sediments ranged from 117.11 ± 1.61 to 418.64 ± 70.20 $\mu\text{g/g OC}$ with stations DE and 18 having the highest and lowest concentrations of alkanes, respectively. The sum of LMW *n*-alkanes (nC_{17} to nC_{22} inclusive) and the sum of HMW *n*-alkanes (C_{23} to C_{36} inclusive) can be found in Table 2.4 along with the sums separated into odd and even *n*-alkane contributions. The sum of odd *n*-alkane and even *n*-alkane concentrations ranged from 68.35 ± 1.31 to 298.96 ± 22.99 $\mu\text{g/g OC}$, and 40.03 ± 2.57 to 129.82 ± 2.18 $\mu\text{g/g OC}$, respectively. The general trend for these samples showed a decrease in total *n*-alkane concentrations from inland to offshore stations. As expected, the proportion of odd *n*-alkanes contributing to the total *n*-alkanes generally decreases from the terrestrial driven stations towards the Gulf while the percentage of total even *n*-alkanes increased from inland to offshore stations. This trend results in CPI values that decrease from a maximum of 5.09 ± 0.10 (station DE) to a minimum value of 1.95 ± 0.05 (station 18) from inland stations towards the Gulf. One deviation from this trend is the slightly lower than expected value measured at station 25 (2.71 ± 0.05). Alkanes originating from higher terrestrial plant waxes typically yield CPI values of 3 or greater due to their predominant odd over even alkane

distribution. Values closer to 1 indicate anthropogenic inputs from petroleum products and byproducts, due to the lack of preference for either alkane series (Marzi et al., 1993; Chen et al., 2014), but can also indicate inputs from microorganisms or recycled organic matter (Kennicutt et al., 1987). The higher CPI values observed for the stations closest to Quebec City and in the Saguenay Fjord, are typical for sediments with high proportions of OM originating from soils and terrestrial plants.

The contributions of odd- and even-numbered *n*-alkanes to total LMW concentrations (*n*C₁₇ to *n*C₂₂ inclusively) were also compared for each station. The summed concentrations of the odd LMW *n*-alkanes is higher than that of the even alkanes for the terrestrial stations Sag05, DE and G, and both are about equal for stations 23, 21, 18.5. At stations 25, 18 and 16 however, the contribution of even *n*-alkanes is higher than that of the odd. The relative contributions of odd and even HMW alkanes is more uniform, with the sum of odd HMW alkanes consistently higher than the sum of even alkanes, although the proportions of odd HMW alkanes are higher for stations inland compared to the stations near the gulf, as can be seen in Table 2.4.

The ACL and P_{aq} for our samples ranged from 28.36 ± 0.02 to 28.97 ± 0.01 and 0.295 ± 0.003 to 0.377 ± 0.002 respectively, with both parameters being statistically significantly different ($p < 0.05$) for values at the most inland station (station DE) and at the furthest offshore station (station 16). ACL values generally increase from the more terrestrial stations to marine stations with the opposite being true for the P_{aq} values.

The TAR values range between 3.43 ± 0.16 to 7.99 ± 0.05 , with the lowest and highest values at station 18 and station DE, respectively. However, no obvious decreasing trend was found along the terrestrial-marine continuum and in the Gulf of the St. Lawrence, as would be expected with higher relative marine inputs in the gulf (Fig. 2.7). NAR values for stations from the Estuary to the Gulf were found to be less than 0.584 ± 0.011 , with the lowest value of 0.169 ± 0.011 at station 18. NAR values range between zero for petroleum products and one for higher terrestrial plants or marine plants. The NAR values found for sediments along the St. Lawrence Estuary and Gulf would suggest that alkanes originating from petroleum sources are contributing to the total alkanes detected in the sediments

Table 2.4 Concentrations and standard deviations of total, low molecular weight (LMW) and high molecular weight (HMW) *n*-alkanes, as well as calculated C_{max}, CPI, ACL, TAR, NAR and P_{aq} molecular ratios at each station.

Station	Total Alkanes (<i>n</i> C ₁₇ – <i>n</i> C ₃₆) (µg/gOC)			LMW Alkanes (<i>n</i> C ₁₇ – <i>n</i> C ₂₂) (µg/gOC)			HMW Alkanes (<i>n</i> C ₂₂ – <i>n</i> C ₃₆) (µg/gOC)			C _{max}	CPI	ACL	TAR	NAR	P _{aq}
	Σ <i>n</i> C ₁₇₋₃₆	Σ <i>n</i> C ₁₇₋₃₅	Σ <i>n</i> C ₁₈₋₃₆	Σ <i>n</i> C ₁₇₋₂₂	Σ <i>n</i> C ₁₇₋₂₁	Σ <i>n</i> C ₁₈₋₂₂	Σ <i>n</i> C ₂₃₋₃₆	Σ <i>n</i> C ₂₃₋₃₅	Σ <i>n</i> C ₂₄₋₃₆						
		Odd	Even		Odd	Even		Odd	Even						
Sag05	293.03 ± 35.29	224.41 ± 27.89	68.62 ± 8.07	50.62 ± 6.03	27.89 ± 3.22	22.72 ± 2.82	242.42 ± 29.89	196.51 ± 24.67	45.90 ± 5.24	27	4.78 ± 0.13	28.36 ± 0.02	6.70 ± 0.01	0.565 ± 0.008	0.375 ± 0.001
DE	418.64 ± 70.20	327.92 ± 52.96	90.72 ± 17.31	61.27 ± 11.44	32.86 ± 5.38	28.41 ± 6.11	357.37 ± 58.84	295.06 ± 47.58	62.31 ± 11.26	29	5.09 ± 0.10	28.54 ± 0.01	7.99 ± 0.05	0.584 ± 0.011	0.352 ± 0.003
G	390.27 ± 30.30	298.96 ± 22.99	91.31 ± 7.31	55.74 ± 3.97	30.50 ± 2.27	25.24 ± 1.71	334.53 ± 26.34	268.46 ± 20.74	66.07 ± 5.60	29	4.34 ± 0.02	28.55 ± 0.02	7.82 ± 0.07	0.550 ± 0.003	0.376 ± 0.004
25	395.17 ± 7.27	265.36 ± 5.48	129.82 ± 2.18	65.65 ± 1.01	29.46 ± 0.40	36.19 ± 0.61	329.53 ± 6.26	235.89 ± 5.08	93.63 ± 1.70	29	2.71 ± 0.05	28.65 ± 0.01	6.58 ± 0.09	0.367 ± 0.006	0.377 ± 0.002
23	266.54 ± 11.30	190.14 ± 8.00	76.40 ± 3.52	39.50 ± 1.87	19.39 ± 0.99	20.10 ± 0.91	227.04 ± 9.67	170.75 ± 7.31	56.29 ± 2.61	29	3.23 ± 0.08	28.64 ± 0.02	7.68 ± 0.37	0.444 ± 0.008	0.372 ± 0.003
21	208.60 ± 20.68	147.67 ± 14.54	60.92 ± 6.14	32.43 ± 2.80	15.83 ± 1.40	16.60 ± 1.41	176.17 ± 17.88	131.85 ± 13.15	44.32 ± 4.73	29	3.16 ± 0.03	28.69 ± 0.02	7.13 ± 0.13	0.432 ± 0.002	0.365 ± 0.004
18.5	127.67 ± 9.49	87.64 ± 6.92	40.03 ± 2.57	24.02 ± 1.92	11.87 ± 0.98	12.16 ± 0.94	103.65 ± 7.59	75.77 ± 5.97	27.88 ± 1.63	29	2.88 ± 0.07	28.84 ± 0.02	4.82 ± 0.11	0.383 ± 0.007	0.339 ± 0.003
18	117.11 ± 1.61	68.35 ± 1.31	48.76 ± 0.78	29.69 ± 0.33	11.92 ± 0.12	17.77 ± 0.22	87.42 ± 1.51	56.43 ± 1.29	30.99 ± 0.58	29	1.95 ± 0.05	28.86 ± 0.01	3.43 ± 0.16	0.169 ± 0.011	0.340 ± 0.002
16	124.38 ± 9.18	77.33 ± 5.88	47.05 ± 3.33	24.38 ± 1.63	9.02 ± 0.64	15.37 ± 0.99	100.00 ± 7.54	68.34 ± 5.24	31.68 ± 2.34	29	2.33 ± 0.04	28.97 ± 0.01	6.23 ± 0.06	0.248 ± 0.008	0.295 ± 0.003

2.4.3 $\delta^{13}\text{C}$ and $\delta^2\text{H}$ of individual *n*-alkanes in surface sediments

Compound-specific isotope measurements were performed on the *n*-alkanes extracted from the surface sediments of the nine stations to determine their $\delta^{13}\text{C}$ and $\delta^2\text{H}$ values, for both odd and even chain lengths from $n\text{C}_{23}$ to $n\text{C}_{36}$. Both the carbon and hydrogen isotopic values varied in a saw tooth pattern between the odd and even numbered *n*-alkanes for all sediments, as can be seen in Fig. 2.4. In all cases, the odd *n*-alkanes were more depleted in ^{13}C and ^2H than neighbouring even chain length *n*-alkanes. Interestingly, the even numbered *n*-alkanes showed greater variations in the range of isotopic values across the stations than the more abundant odd numbered *n*-alkanes, particularly for $\delta^2\text{H}$, suggesting a greater discrimination potential for even numbered alkane isotope ratios in terms of source identification.

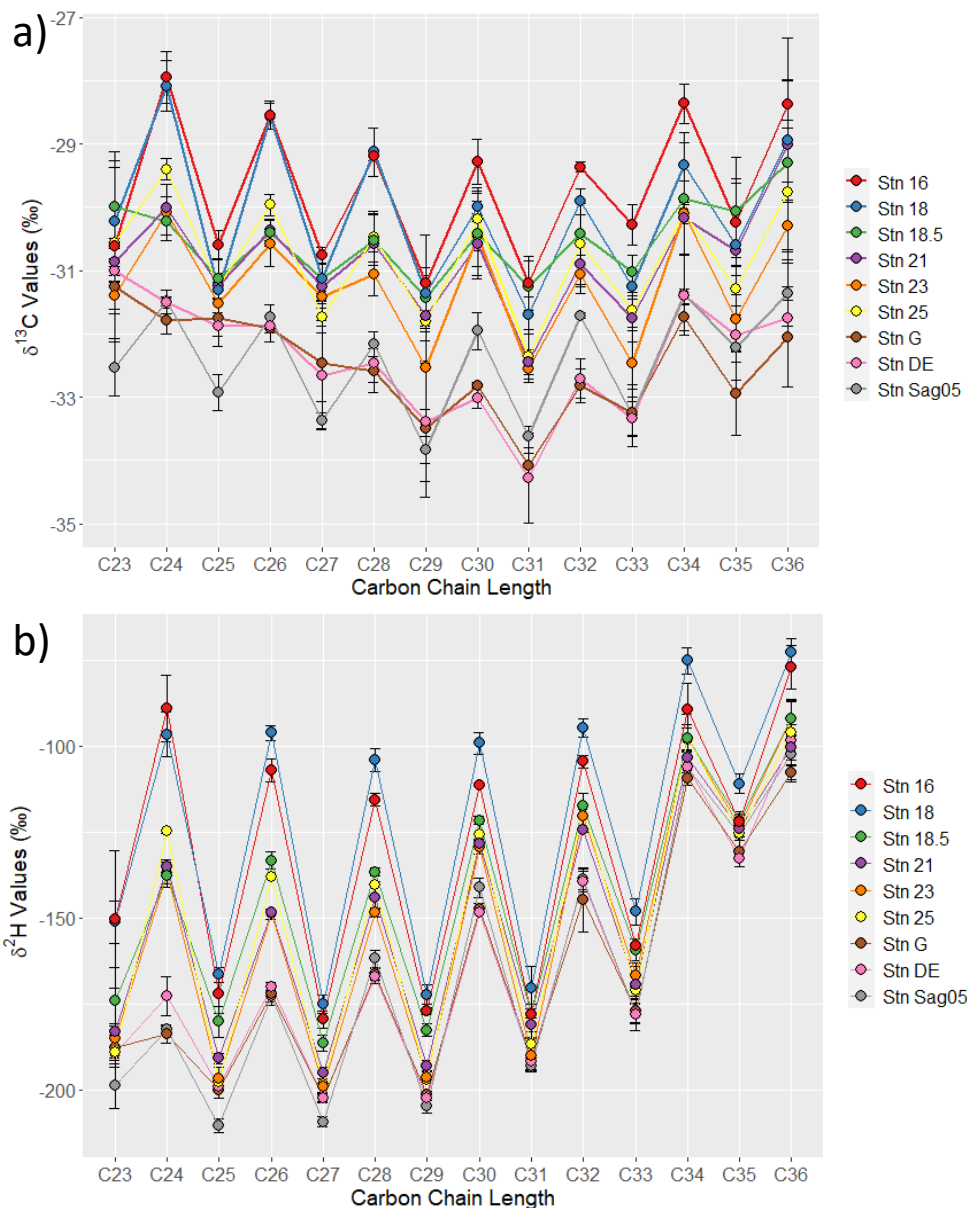


Figure 2.4 Compound-specific $\delta^{13}\text{C}$ (a) and $\delta^2\text{H}$ (b) values of *n*-alkanes ($n\text{C}_{23}$ to $n\text{C}_{36}$) in the sediments at the various sampling stations. Error bars correspond to the standard deviation ($n=3$).

The mass weighted average (WA) $\delta^{13}\text{C}$ and $\delta^2\text{H}$ values for odd and even *n*-alkanes can be found in Table 2.5. The differences in the WA $\delta^{13}\text{C}$ and $\delta^2\text{H}$ values between the odd and even chain length *n*-alkanes are statistically significantly different ($p < 0.05$), except for $\delta^{13}\text{C}$ at stations DE and G. The calculated p -values for independent student-t-test assuming unequal variance are listed in Table 2.5.

Table 2.5 Weighted average $\delta^{13}\text{C}$ and $\delta^2\text{H}$ values of odd and even chain length n -alkanes, and independent student t-test p -values to determine significant difference between WA odd and even n -alkanes.

Station	WA $\delta^{13}\text{C}$ Odd	WA $\delta^{13}\text{C}$ Even	p -value	WA $\delta^2\text{H}$ Odd	WA $\delta^2\text{H}$ Even	p -value
Sag05	-33.4 ± 0.1	-31.8 ± 0.1	1.16E-04*	-200.8 ± 2.4	-153.5 ± 2.1	1.55E-05*
DE	-32.9 ± 0.5	-32.2 ± 0.1	1.12E-01	-195.6 ± 1.5	-156.3 ± 2.6	1.32E-04*
G	-32.8 ± 0.4	-32.3 ± 0.2	1.15E-01	-194.5 ± 1.0	-158.7 ± 2.1	1.91E-04*
25	-31.6 ± 0.1	-30.1 ± 0.2	3.59E-03*	-190.2 ± 0.6	-125.3 ± 0.5	3.06E-08*
23	-32.0 ± 0.1	-30.6 ± 0.2	3.14E-04*	-190.0 ± 1.2	-132.7 ± 1.9	1.07E-05*
21	-31.6 ± 0.2	$-30.4 \pm 0.0_4$	5.06E-03*	-185.6 ± 1.6	-132.4 ± 1.1	4.81E-06*
18.5	-31.1 ± 0.1	-30.3 ± 0.2	6.14E-03*	-177.1 ± 2.7	-125.8 ± 1.8	2.85E-05*
18	-31.2 ± 0.2	-29.0 ± 0.1	1.49E-04*	-165.6 ± 3.6	-96.0 ± 2.8	2.01E-05*
16	-30.9 ± 0.3	$-28.8 \pm 0.0_1$	6.29E-03*	-171.7 ± 4.5	-103.2 ± 3.8	4.36E-05*

Note: Values with an asterisk show p -values <0.05 indicating a significant difference at 95%

The WA $\delta^{13}\text{C}$ for odd and even n -alkanes ranged from -30.88 ± 0.30 to -33.35 ± 0.09 ‰ and -28.75 ± 0.01 to -32.27 ± 0.21 ‰, respectively, and -165.58 ± 3.62 to -200.83 ± 2.39 ‰ and 95.98 ± 2.84 to -158.68 ± 2.14 ‰ for $\delta^2\text{H}$. A clear trend of more enriched values was found for both $\delta^2\text{H}$ and $\delta^{13}\text{C}$ as the stations progressed towards and into the St. Lawrence Gulf. Similarly to the bulk sediment isotope values, the terrestrial driven stations were depleted in ^{13}C relative to the marine stations. However, the bulk sediment carbon isotope values at the more marine stations (stations 18.5, 18, 16) plateaued (-22.59 ± 0.04 to -22.39 ± 0.09 ‰), whereas specific n -alkane (i.e., $n\text{C}_{30}$, $n\text{C}_{32}$, $n\text{C}_{34}$, $n\text{C}_{36}$) $\delta^{13}\text{C}$ values showed more variability at these same stations.

There is also a slight trend of stable carbon isotope values becoming progressively more negative from $n\text{C}_{23}$ to $n\text{C}_{30}$ (even) and $n\text{C}_{31}$ (odd), before becoming progressively more positive from $n\text{C}_{30}$ and $n\text{C}_{31}$ to $n\text{C}_{36}$. A similar trend can be seen for the hydrogen values, though the most negative values in this case are at $n\text{C}_{27}$ (odd) and $n\text{C}_{28}$ (even).

2.5 Discussion

2.5.1 Variations in bulk sediment $\delta^{13}\text{C}$, $\delta^{15}\text{N}$ values and C/N ratios

Bulk sediment $\delta^{13}\text{C}$ and $\delta^{15}\text{N}$ values have been used widely to determine the main source of OM inputs into sediments (e.g., Peters et al., 1978; Thornton and McManus, 1994). The $\delta^{13}\text{C}$ values in the OM in surface sediments of the St. Lawrence Estuary and Gulf are indicative of the proportion of terrestrial and marine OM introduced or produced within the system. At stations

closer to Quebec City, the $\delta^{13}\text{C}$ values are more negative than in the Gulf owing to the input of more ^{13}C -depleted terrestrial OM compared to the predominantly marine OM found in the Gulf (Hélie and Hillaire-Marcel, 2006). It is important to note that the more marine stations (stations 18.5, 18 and 16) also receive terrestrial OM inputs, though to a much lower extent, as the St. Lawrence Gulf is surrounded by land masses. However, the $\delta^{13}\text{C}$ values of the sedimentary OM increase very regularly along the estuary before plateauing in the Gulf at a constant value of about -22.5‰, indicating a change in the proportion of terrestrial and marine OM along the transect up until the Gulf.

Atomic C/N ratios have also been used for OM source identification; values of 5-7 tend to be interpreted as indicative of marine OM and values greater than 15 generally correspond to terrestrial OM (Hu et al., 2009). The stations closer to the St. Lawrence River and Saguenay River outputs are characterized by higher inputs of OM derived from soils or vascular plant tissues and consequently have higher C/N values, while the ratio decreases from stations 25 to 18.5 (11.73 ± 0.60 to 8.61 ± 0.15). This pattern is likely due to inputs from organic matter photosynthesized in the surface estuarine waters, resulting in mixing of different proportions of marine and terrestrial sources (Herman et al., 1999). It would be expected that the more terrestrial driven stations (stations Sag05, DE and G) would have C/N ratios close to 15 or higher, but while Sag05 has a value of 16.61 ± 0.42 , the values at stations DE and G were lower (10.43 ± 0.40 and 10.11 ± 0.84 , respectively). There is likely a source of anthropogenic N from wastewater plants and agricultural runoff, potentially leading to high primary productivity and heterotrophic bacterial biomass, influencing the OM C/N ratios and $\delta^{15}\text{N}$ values at these two stations owing to their proximity to the St. Lawrence River mouth. Indeed, plotting the bulk sediment $\delta^{13}\text{C}$ value for the stations, excluding DE and G, against the respective $\delta^{15}\text{N}$ value shows a linear relationship with an R^2 of 0.990; stations DE and G are clear outliers with $\delta^{15}\text{N}$ values that are more positive by about 1.2 and 0.7 ‰ away from the regression (Fig. A.2).

At the two stations furthest from the St. Lawrence River (stations 18 and 16), the OM C/N ratio increases again to 11.10 ± 0.85 and 11.83 ± 0.70 , respectively. This increase is likely due to the preferential mineralization of nitrogen-rich material during degradation (Twichell et al., 2002; Magid et al., 2004). The more advanced degradation hypothesis also explains the progressive increase in $\delta^{15}\text{N}$ from the upper estuary towards the Gulf, with the more enriched

values caused by the reworking and decomposition of organic matter, resulting in preferential removal of the lighter ^{14}N isotope.

The C/N ratios and bulk sediment $\delta^{13}\text{C}$ scatter plot (Fig. 2.2) shows that station Sag05 is characterized by the highest proportional inputs of terrestrial C_3 plant OM and freshwater DOC, reflecting the fact that the Saguenay River drains a predominantly forested region. The OM from stations G and DE differs slightly from that of the other stations in that it consists of mixed inputs of freshwater algae and coagulated dissolved OC (station DE corresponds to the maximum turbidity zone), with some OM derived from terrestrial plants. As expected, OM from the sampling sites located between the terrestrial driven and marine stations (stations 25, 23, 21 and 18.5) reflects mixed inputs from marine and terrestrial sources, while OM from stations 18 and 16 deviate from this trend with higher-than expected atomic C/N ratios because of the preferential remineralization on N-rich over C-rich components.

2.5.2 Changes in *n*-alkane abundances along the St. Lawrence Estuary and Gulf

The relative and absolute *n*-alkane abundances along the St. Lawrence Estuary and Gulf vary widely between stations, with a general preference of odd over even numbered straight chain alkanes (Fig. 2.3), as is typically found in terrestrially influenced coastal sediments. The change in the proportions of odd and even *n*-alkanes contributing to the sum of LMW and HMW alkanes is shown in Figs. 2.5a and 2.5b. The LMW alkanes show an interesting pattern, with a higher proportion of odd alkanes at the terrestrial driven stations DE, G and Sag05, as typically found for HMW *n*-alkanes from a terrestrial OM dominant source (Fig. 2.5a). The opposite is true for the marine dominated stations in the gulf (stations 18 and 16). This change in relative proportion is likely due to higher contributions of microbial inputs to the sediments, as coastal sediments have been shown to have higher proportions of even LMW *n*-alkanes relative to odd alkanes, which are attributed to marine bacteria (Grimalt et al., 1985; Nishimura and Baker, 1986; Aloulou et al., 2010). OM inputs at stations 23, 21 and 18.5 are thus characterized by almost equal amounts of odd and even *n*-alkanes. Station 25 is an exception to this trend, appearing similar to stations 16 and 18 where the primary input of OM is from marine primary production. The higher levels of even *n*-alkanes is likely due to a combination of increased

surface water primary production and subsequent increase in heterotrophic bacterial activity, resulting from the upwelling of the deep waters in this area (Cyr et al., 2015).

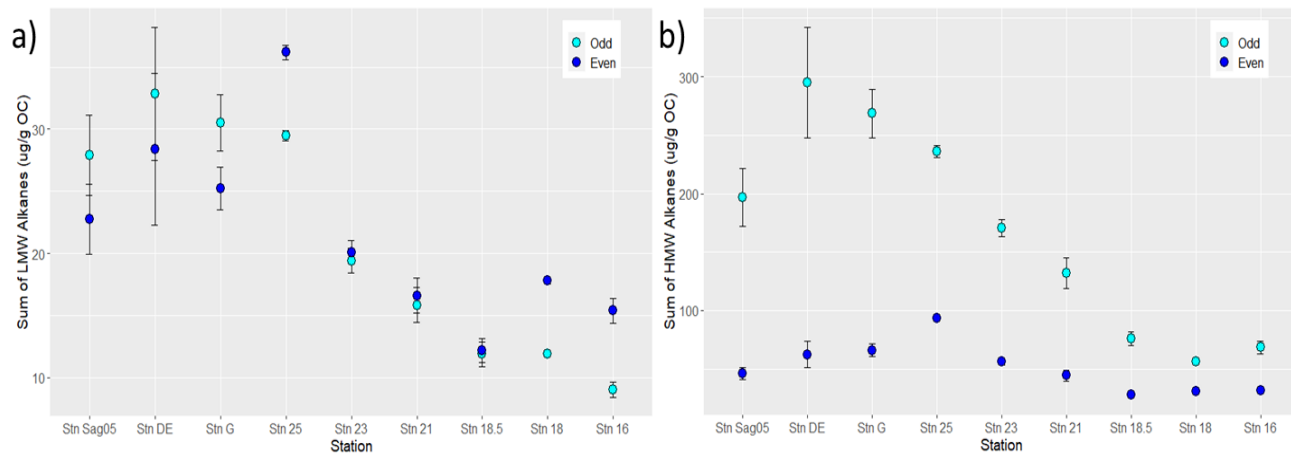


Figure 2.5 a) Sum of odd and even LMW (C_{17} - C_{22}) n -alkanes at all stations, b) sum of odd and even HMW (C_{23} - C_{36}) n -alkanes at all stations. Error bars show standard deviations.

The HMW alkanes exhibit a different trend (Fig. 2.5b). The odd n -alkanes dominate at all stations. However, the difference between the sum of odd and even n -alkanes generally decreases from inland stations towards the Gulf. The relative proportions of odd and even HMW n -alkanes is changing along the terrestrial-marine continuum, likely because of a change in the relative inputs of terrestrial and marine OM. Notably, marine bacteria could be contributing to the even n -alkane pool in the HMW range as well (Grimalt et al., 1985; Nishimura and Baker, 1986), as suggested by the generally higher LMW n -alkane contribution at stations 25, 18 and 16 relative to their closest neighbour. It is these subtle changes in the relative abundances of various n -alkanes that has led to the popularity of diagnostic ratios.

Interestingly, there is a strong negative correlation ($R^2 = 0.95$) between the sum of total odd n -alkane concentrations and the bulk OM $\delta^{13}C$ values, with the exception of station Sag05, whereas the correlation is much weaker ($R^2 = 0.28$) between the bulk OM $\delta^{13}C$ values and the sum of the total even n -alkane concentrations (Fig. 2.6). The strong correlation between the sum of odd n -alkane concentrations and bulk OM $\delta^{13}C$ supports the use of bulk OM $\delta^{13}C$ as a proxy for terrestrial OC as the odd HMW n -alkanes are markers of predominantly plant derived OC. The much lower sum of total terrestrial plant-derived odd n -alkane concentrations compared to the value predicted from the regression in Fig. 2.6 at station Sag05 is likely due to the very different type of vegetation in the Saguenay (mostly gymnosperm trees) and St. Lawrence (mixed angiosperms and gymnosperms) watersheds. While it has been reported that

gymnosperms and angiosperms can produce differing amounts of *n*-alkanes, it does not fully explain the differences seen in this waterway (Diefendorf et al., 2011). This watershed also benefits from less impact by human activity, resulting in less water run-off leading to lower overall OM inputs. Most molecular ratios also indicate a less pronounced terrestrial character for Sag05 compared to station DE (Table 2.4).

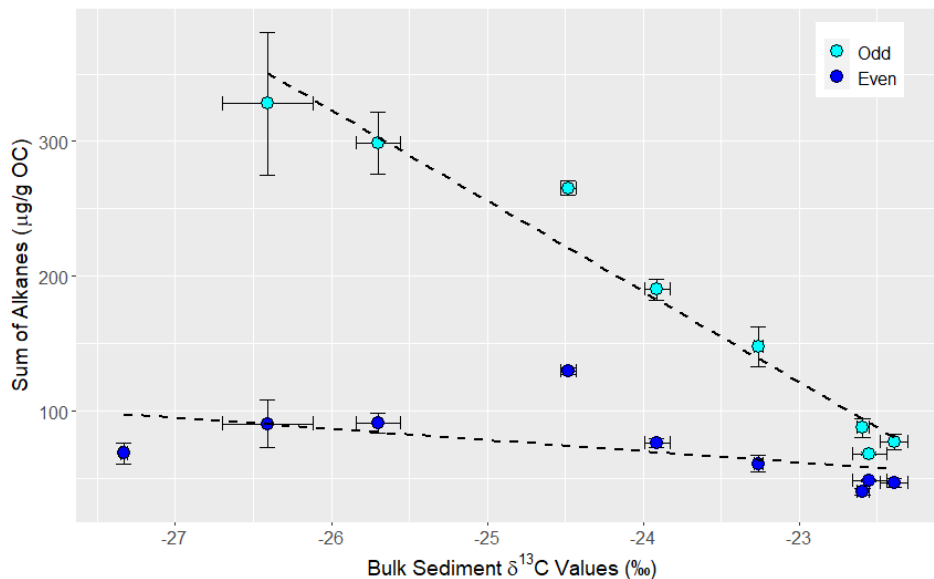


Figure 2.6 Relationship of odd and even *n*-alkane abundances and the bulk sediment $\delta^{13}\text{C}$ values. Station Sag05 (not shown on the graph) was omitted from the regression of the odd *n*-alkanes. Error bars show standard deviations.

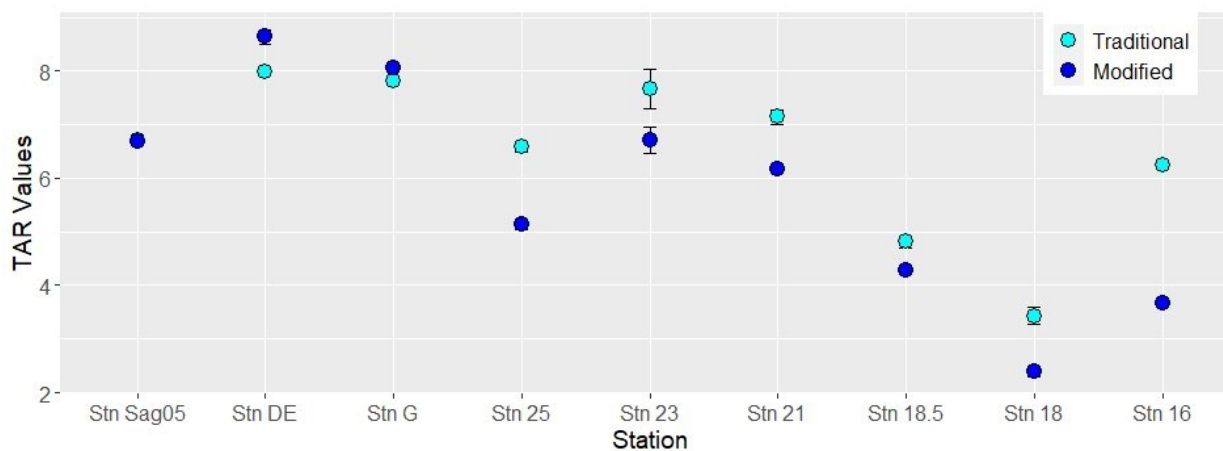


Figure 2.7 TAR values and standard deviations at each station when using the traditional equation with the odd *n*-alkanes in the dominator (traditional) and when using even *n*-alkanes in the denominator (modified).

2.5.3 Changes in *n*-alkane diagnostic ratios along the St. Lawrence Estuary and Gulf

The largest CPI values were observed for the stations closest to Quebec City and in the Saguenay Fjord (4.34 ± 0.02 to 5.09 ± 0.16) are typical for sediments with high proportions of

OM originating from terrestrial plants, while values in the Gulf are closer to 2 (1.95 ± 0.05 to 2.33 ± 0.04). Similarly high CPI values have been found in other estuaries in South India and the UK, with both these studies showing higher CPI values in the upper estuary (Ahad et al., 2011; Ankit et al., 2017). Interestingly, the ACL values in these estuarine settings were highest in the upper estuary, contrary to what we found in the St. Lawrence waterway. The ACL describes the weight-average number of carbon atoms in higher plant alkanes (nC_{25} to nC_{33} , inclusively) (Poynter and Eglinton, 1990). Ankit et al. (2017) reported CPI and ACL values in the Ashtamudi Estuary ranging from 1.1 to 3.9 and 28.5 to 30.5, respectively, with a decreasing trend towards the lower estuary, similar to those reported by Ahad et al. (2011) for the Tyne Estuary (CPI values and ACL values ranging from 1.8 to 6.4 and 28.5 to 29.5, respectively). Although both studies showed relatively lower CPI and ACL values in the lower estuary, Ankit et al. concluded that the lower values were due to heavily recycled OM inputs, supported by the high $\delta^{15}N$ values they measured, whereas Ahad and colleagues attributed the lower CPI and ACL values to a prominent petrogenic inputs, reinforced by ^{14}C -depleted radiocarbon and ^{13}C value with less variation between odd/even n -alkane values closest to the lower estuary (Ahad et al., 2011; Ankit et al., 2017). When only using CPI as an indication of petrogenic inputs, predominantly marine samples could be miscategorized as petrogenic, as the abundance of n -alkanes found in these types of samples approaches the pattern found in petrogenic samples. Notably, both the CPI and the ACL values measured at station 25 support the hypothesis of a more marine character of the organic matter at this site compared to its neighbouring sampling stations due to its elevated primary productivity, further giving credence to a marine origin for the even HMW alkanes.

NAR, as defined by Mille et al., estimates the proportion of natural and petroleum n -alkanes in a sample using the relationship of even n -alkanes to total n -alkanes and has been applied to freshwater systems (Wang et al., 2012) and marine systems (Mille et al., 2007; Sojini et al., 2012; Wang et al., 2018). In our work, NAR values ranged from 0.169 ± 0.011 to 0.584 ± 0.011 with a general decreasing trend from inland stations to those towards the Gulf, with the lowest and highest values at stations 18 and DE, respectively. Again, for the apparently more marine stations, where the difference in abundance between even and odd n -alkanes is smallest, and the NAR values come close to 0, values could indicate predominantly petroleum inputs (Bourbonniere and Meyers, 1996). Based on the NAR values only, all sediment extracts appear

to contain some input of petroleum, again confounding highly degraded sedimentary OM with petroleum inputs, whereas none of the other parameters examined in this study suggest important petroleum inputs. Such inconsistencies in source identification indicate a need for caution when applying and interpreting these molecular ratios. Knowledge of the water systems is imperative, along with consideration of more sensitive parameters (i.e., isotope ratios) to better assign *n*-alkane origins.

The ratio of terrigenous to aquatic (TAR) *n*-alkanes, as described by Bourbonniere and Meyers (1996), is used to probe changes in terrigenous and aquatic *n*-alkane inputs by exploiting differences in the distribution of HMW and LMW *n*-alkanes in these two sources (Table 2.2). In the system studied here, all TAR values were > 1, indicating a prominent input of terrigenous *n*-alkanes (Bourbonniere and Meyers, 1996). As expected, the highest TAR value (7.99 ± 0.05) was found in the upper estuary at station DE, and the lowest in the gulf at station 18 (3.43 ± 0.16), with the values mostly decreasing from the upper estuary towards the gulf. Based on the equation used to determine the TAR values (Table 2.2), the stations that have a higher proportion of LMW *n*-alkanes (i.e., the more marine stations), also have lower TAR values. However, as mentioned by other authors (Silliman et al., 2000; Hu et al., 2009; Chen et al., 2017), the TAR proxy likely overestimates the terrigenous inputs due to preferential preservation of terrestrial over marine OM (Volkman et al., 1987). Another factor not included in this proxy is the possibility of multiple OM sources contributing to the LMW and HMW alkanes. Studies have shown that marine bacteria can contribute to low and high molecular weight *n*-alkanes, specifically even chain length *n*-alkanes, which are not included in the TAR equation (Grimalt et al., 1985; Nishimura and Baker, 1986; Wang et al., 2010). For the stations visited in this study, the TAR values calculated the traditional way using the odd *n*-alkanes (ranging from 3.43 ± 0.16 to 7.99 ± 0.05) do not adequately reflect the input of OM in this complex coastal system where sediments accumulate OM of both marine and terrestrial origins at varying ratios, especially at stations 25, 23, 21. However, if calculating the TAR values using the even *n*-alkanes in the denominator as shown in equation (2.1), the decreasing TAR values better reflects the water system in this study as seen in Fig. 2.7. There is a more apparent decreasing trend of TAR values towards the Gulf when utilizing the modified equation.

$$\text{Eq. (2.1)} \quad TAR_{(mod)} = \frac{nC_{27} + nC_{29} + nC_{31}}{nC_{16} + nC_{18} + nC_{20}}$$

The more marine character of OM at station 25 is also better highlighted using this alternative equation (Fig. 2.7). Additionally, the $TAR_{(mod)}$ values are better correlated with the bulk sediment $\delta^{13}C$ values than the TAR values calculated using Bourbonniere and Meyer's equation (0.62 vs. 0.37, respectively; Supplemental Material). These findings suggest that the TAR proxy developed and used widely in biomarker analysis may not be fitting for all systems. For the St. Lawrence Estuary and Gulf, a better approximation for terrestrial or aquatic inputs of OM may be to use the proposed alternative equation which is better correlated with other measurements taken at these stations. Although using the even *n*-alkanes appears to better estimate the relative proportions of the two sources than the original equation, it is still far from perfect, and it does not imply that it can be applied to any other system without further work. Moreover, as for any other proxy, it should not be used alone without corroboration from other molecular or isotopic proxies.

Another proxy typically used to estimate the contribution of *n*-alkanes in sediments, proposed by Ficken et al. (2000), is the P_{aq} , which is designed to calculate the proportion of aquatic submerged plants and terrestrial plant inputs (Table 2.2). This ratio again does not account for inputs other than those of aquatic and terrestrial plants for the specific *n*-alkanes used in the equation. Based on their findings, Ficken et al. determined that values in sediment extracts ranging from 0.1 to 0.4 possibly indicated a mixture of terrestrial plants and emerged and submerged aquatic macrophytes. Unsurprisingly, the P_{aq} values calculated in this study ranged from 0.295 to 0.377. This ratio does not reveal much useful information for the sediments in our dynamic system, aside from the fact that the contribution from emerged and submerged plants is not negligible and constant at all stations with the exception of station 16 in the Gulf, where the ratio is significantly lower ($p < 0.05$).

The results obtained in this study show the need for caution when applying diagnostic ratios developed for specific water ecosystems to sediments sampled elsewhere. Although they can provide an estimation of OM inputs and sources in certain situations, they often overestimate terrestrial sources, or can lead to false conclusions. The fact that some ratios seem to accurately reflect the characteristics of the system under study, while others do not, is problematic as a natural reflex is to only present proxy data that supports our understanding of a system, omitting those that don't corroborate the interpretations. Not only should multiple proxy ratios be used, but these ratios should be accompanied by more sensitive methods to determine OM sources

such as bulk sediment $\delta^{13}\text{C}$ values, which have been confirmed to work well for bulk OM origins and subtler, site specific characteristics, using more advanced techniques such as compound specific isotope analysis.

2.5.4 $\delta^{13}\text{C}$ and $\delta^2\text{H}$ of individual *n*-alkanes in surface sediments

For a more sensitive analysis of the origins of the *n*-alkanes, compound specific isotope analysis of both carbon and hydrogen was employed. Due to the more complex nature of this method, it is not applied as universally as are molecular proxies. Furthermore, because of the low abundance of even *n*-alkanes, there are far fewer instances where isotope data are available for both the even and odd *n*-alkanes extracted from sediments. To the best of our knowledge, both $\delta^{13}\text{C}$ and $\delta^2\text{H}$ data for even and odd *n*-alkanes in the same samples have not been reported previously. This is of particular interest, as our data indicate that data for the even *n*-alkanes show more variation at the different stations than those for the odd *n*-alkanes. At all stations, with the exception of $\delta^{13}\text{C}$ for stations DE and G, the weighted average (WA) value of the odd *n*-alkanes was significantly different from the WA value of the even *n*-alkanes (Table 2.5). Owing to these differences, it is possible to exclude petrogenic inputs as a main source of these *n*-alkanes as petrogenic *n*-alkanes do not exhibit this characteristic difference of odd and even *n*-alkane values (Li et al., 2001; Odden et al., 2002; Li and Xiong, 2009). Contrary to the interpretation derived from the NAR and CPI proxies, which indicated possible petroleum inputs at the more marine stations, the differences between the odd and even *n*-alkane $\delta^{13}\text{C}$ WA values increase offshore and are greatest at the marine stations. Stations DE and G, which are closest to Quebec City and are the most severely affected by anthropogenic inputs, are characterized by the lowest differences between the odd and even *n*-alkanes $\delta^{13}\text{C}$, especially in the $n\text{C}_{23}$ to $n\text{C}_{29}$ range (Fig. 2.8). Again, the proxies based on *n*-alkane relative abundances strongly indicate a terrestrial origin. It is possible that at these stations there are small inputs of petrogenic *n*-alkanes that could be influencing the $\delta^{13}\text{C}$ values, information that would not be possible to extract using only the proxies discussed above. Indeed, a series of crude oil-derived *n*-alkanes analyzed in our laboratory consistently had $\delta^{13}\text{C}$ values for both odd and even alkanes in the -32 to -30 ‰ range,

with no saw tooth pattern, as well as maximum *n*-alkane relative abundances below *n*C₂₉ (unpublished data).

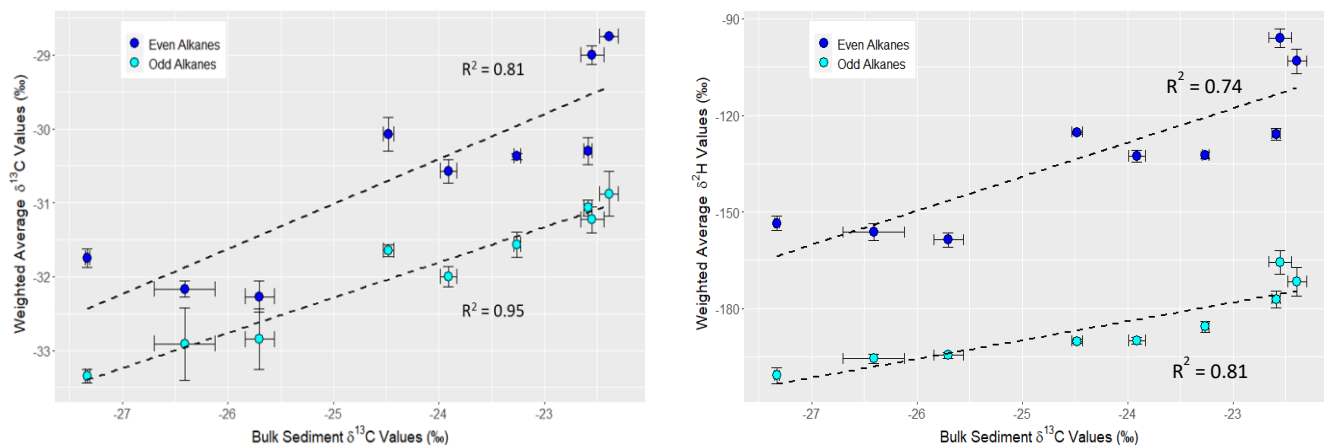


Figure 2.8 Relationship between bulk sediment $\delta^{13}\text{C}$ values and a) weighted average $\delta^{13}\text{C}$ values of odd and even *n*-alkanes and b) weighted average $\delta^2\text{H}$ values of odd and even *n*-alkanes.

The WA $\delta^{13}\text{C}$ and $\delta^2\text{H}$ values for odd numbered *n*-alkanes for each station correlated strongly with the bulk OM $\delta^{13}\text{C}$ values, with coefficients of 0.95 and 0.81, respectively (Fig. 2.8), confirming the use of bulk sediment isotope values as a reliable proxy for overall OM input. The correlations between bulk OM $\delta^{13}\text{C}$ values and WA $\delta^{13}\text{C}$ or WA $\delta^2\text{H}$ values for even numbered *n*-alkanes were slightly weaker, with coefficients of 0.81 and 0.74, respectively. Notably, using the WA values for both $\delta^{13}\text{C}$ and $\delta^2\text{H}$ of the even numbered alkanes in these graphs resulted in the grouping of certain stations when plotted against the bulk sediment $\delta^{13}\text{C}$, the more terrestrial stations (Sag05, DE and G) of the Saguenay Fjord and the Upper St. Lawrence Estuary, with WA $\delta^{13}\text{C}$ values around -32 ‰; then stations 25, 23, 21 and 18.5 with mixed terrestrial and marine OM inputs in the Lower St. Lawrence Estuary and values around -30.5 to -30 ‰; and finally the most marine stations 18 and 16 (located in the Gulf; values of about -29 ‰). Similar compound specific values were noted within each group, but with differences of between 1 and 1.5 ‰ for carbon, and between 20 and 30 ‰ for hydrogen, between each group. These results suggest that the *n*-alkanes found in these three groups of stations originate from multiple sources mixed at different ratios, with the even *n*-alkanes better reflecting the major stepwise changes across the St. Lawrence Estuary and Gulf continuum (Fig. 2.8). In addition to these WA trends, the $\delta^{13}\text{C}$ values for each individual *n*-alkane becomes progressively more depleted by about 1.5 to 3 ‰ between *n*C₂₃ and *n*C₃₁ at all stations, followed by a progressive enrichment by 2 to 3 ‰ between *n*C₃₁ and *n*C₃₆ (Fig. 2.4a), suggesting that these changes in value are linked to a common

biosynthetic and/or degradation pathway. However, the offset between the $\delta^{13}\text{C}$ values profile for each *n*-alkane further support the idea of contrasting ratios of OM sources between the three groups of stations.

As shown in Fig. 2.4a and b, there is a clear sawtooth pattern of $\delta^{13}\text{C}$ and $\delta^2\text{H}$ values from $n\text{C}_{23}$ to $n\text{C}_{36}$, similar to patterns found in other sediments (C. Li et al., 2009; Ahad et al., 2011). Plant material, such as certain C3 angiosperms and gymnosperms, have been shown to significantly contribute to the *n*-alkane pool found in sediments and have the potential to affect their carbon isotope values (Diefendorf et al., 2011, 2015a, b; Bush and McInerney, 2013; Freimuth et al., 2019; Schlanser et al., 2020). These plants contribute significantly to the pool of longer chain *n*-alkanes ($n\text{C}_{27}$ to $n\text{C}_{35}$) and isotopically, gymnosperms have been shown to be more enriched in ^{13}C than their angiosperm counterparts (Chikaraishi and Naraoka, 2003; Diefendorf et al., 2015b; Schlanser et al., 2020). Studies have also shown ^{13}C enrichment of the even numbered *n*-alkanes versus their neighbouring odd *n*-alkane for certain C3 plants, though the opposite was found for hydrogen isotope values (Chikaraishi and Naraoka, 2007). Contrarily, Duan et al. report ^2H enrichment of the even numbered *n*-alkanes versus their neighbouring odd *n*-alkanes in terrestrial herbaceous plants and tree leaf extracts, in agreement with our results (Duan et al., 2011). The tree leaf *n*-alkanes were also more enriched overall compared to the herbaceous plants. Based on the change of vegetation along the St. Lawrence seaway and the rivers that feed into this waterway, the forests gradually change from a mixed hardwood forest (predominantly angiosperm) in the St. Lawrence Valley near the more terrestrial stations, to boreal forest (predominantly gymnosperms) being most prominent in the areas surrounding the gulf and on the closest land to these stations, Anticosti Island, where white spruce, balsam fir, and black spruce are the most abundant tree species. This gradual change is confirmed by the analysis of sedimentary lignin oxidation products that shows decreasing syringyl phenols over vanillyl phenols ratios going seaward, indicative of an increasing proportion of gymnosperm over angiosperm plant OM (unpublished results).

Additionally, sediment age in the Gulf is higher than that of the more terrestrial stations, which could lead to more degraded OM resulting in enriched values at these stations (Brittingham et al., 2017). However, Brittingham et al. reported an increase in $\delta^2\text{H}$ values over a 3-year period, but a decrease in $\delta^{13}\text{C}$. With this in mind, the general enrichment of ^{13}C and ^2H along the continuum, from terrestrial to more marine stations likely results from variations in the

type of terrestrial OM inputs originating from these forests, especially for the higher chain lengths *n*-alkanes ($>nC_{27}$), where there appears to be more variation between stations, as well as the age of the sediments and an increase in marine sourced OM.

Higher (less negative) δ^2H values have also been found in leaf wax *n*-alkanes (nC_{27} , nC_{29} , Cn_{31}) from trees, relative to grasses and herbs (trees -190 to -121 ‰, grasses -227 to -182 ‰; Hou et al., 2007). This could be due to the differences in water uptake or physiological differences of the plant, and not likely due to a change in the isotopic value of the source water (Hou et al., 2007; Pedentchouk and Turich, 2018). Pedentchouk et al. present leaf wax *n*-alkane (nC_{27}) data for angiosperm and gymnosperm species in a similar environment which show differences in both carbon and hydrogen isotope values, with gymnosperms being enriched in ^{13}C but depleted in 2H relative to the angiosperm plants. While there are published data supporting the hypothesis of changes in the isotope values across the continuum owing to change in forest vegetation, there are also data contradicting this hypothesis. Due to the limited amount of data published on carbon and hydrogen isotopic values of individual alkanes in sediments, and even less for both odd and even chain length *n*-alkanes, it is difficult to come to a conclusive explanation for the differences of isotope values along the continuum and between the odd and even *n*-alkanes. While compound specific isotope analysis is a very powerful tool for identifying the possible origins of individual *n*-alkanes, there is much work that still needs to be done to fully understand the patterns in values found in samples such as these. However, the similarity in patterns between the compound specific $\delta^{13}C$ and δ^2H values (saw tooth distribution, gradual enrichment of the value between nC_{30} or nC_{29} and nC_{36} , grouping of stations among three isotopically distinct clusters) suggest that the variations in δ^2H values are caused by the same factors as those for the $\delta^{13}C$ values.

When coupled with other proxies, the grouping of stations is further revealed by the results of principal component analysis (PCA) performed using the following variables: CPI, ACL, TAR values calculated with even *n*-alkanes (equation 1), bulk sediment $\delta^{13}C$, concentration of individual *n*-alkanes (nC_{23} to nC_{36}), $\delta^{13}C$ and δ^2H values of each *n*-alkane (nC_{23} to nC_{36}), and weighted average $\delta^{13}C$ and δ^2H differences between odd and even *n*-alkanes (Fig. 2.9). $\delta^{15}N$ and C/N ratios were not included, as the main goal of this study was to investigate the use of carbon and hydrogen isotope ratios, and *n*-alkanes in source apportionment along the St. Lawrence waterway. Since *n*-alkanes do not include any nitrogen atoms, the plot would not be

representative of the hydrocarbons if those variables were added. Close to 82% of the variability between stations is explained by the first two components of the PCA. The three more terrestrial stations (Sag05, DE and G) group together, while the two stations located in the Gulf, stations 16 and 18 overlap at the other end of the loading plot. The intermediate stations with inputs of OM from both terrestrial and marine origin (stations 25, 23, 21 and 18.5) group in between, with stations 18.5 and 25 slightly separated from stations 21 and 23 in the coordinate space (Fig. 2.9). Together, the isotopic and molecular characterization of sediments and their *n*-alkanes can differentiate stations along a transect with varying OM inputs. The loading plot shown in Fig. 2.9 highlights $\delta^2\text{H}$ as an important variable in the first two dimensions, as it is the most positive loading, followed by $\delta^{13}\text{C}$ of individual *n*-alkanes. The loading plot also shows bulk sediment $\delta^{13}\text{C}$ values as positively correlated with ACL, but negatively correlated to CPI, TAR, and the weighted average $\delta^{13}\text{C}$ and $\delta^2\text{H}$ differences between the odd and even *n*-alkanes.

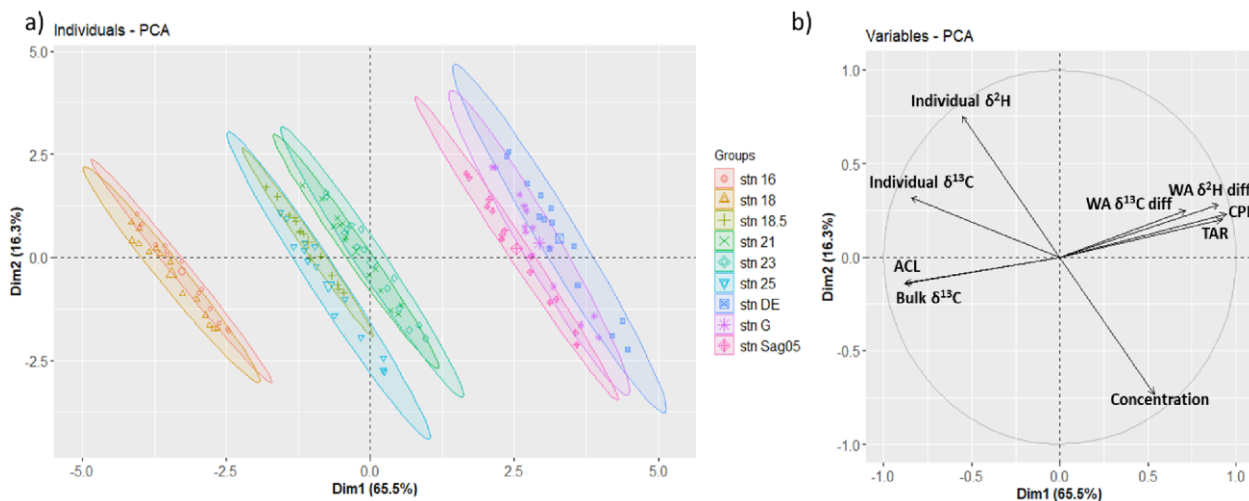


Figure 2.9 Principal component analysis of all stations: a) scores with 95% confidence ellipses. Individual data points are individual *n*-alkanes at each station, and the larger symbol within each group represents the average for all the individual *n*-alkanes; b) loadings. Note that the TAR variable used in the PCA is the modified TAR index as presented in the discussion.

These data present a comprehensive study of the molecular abundances, distributions, and isotopic characterization of sediments along a terrestrial to marine gradient and confirm the need for multiple variables when analyzing OM inputs in sediments. Carbon and hydrogen isotope values of both odd and even numbered *n*-alkanes are shown to be an extremely valuable tool in discriminating between locations having varying OM input from different sources. Notably, molecular data alone, including any of the molecular ratio proxies, and bulk sediment stable

isotope values ($\delta^{13}\text{C}$ and $\delta^{15}\text{N}$) do not allow separation of the stations into these three distinct groups.

2.6 Conclusions

OM source apportionment based solely on proxies using relative abundances of *n*-alkanes should be used with caution and ideally in conjunction with other more sensitive measurements, such as compound specific stable isotope values. Although proxies such as CPI, ACL, TAR, NAR and P_{aq} are more accessible measurements, not requiring any specialized instrumentation, they are prone to under- or overestimation of OM inputs and do not hold up well when multiple OM sources are present. With the addition of isotopic values, whether bulk sediment or compound specific, our data show that the *n*-alkanes along the St. Lawrence waterways are predominantly derived from natural, rather than anthropogenic sources, with variations being driven by changes in the type of vegetation and differing ratios of terrestrial and marine OM inputs along the waterway. In a complex system such as this one, it is imperative to sample at multiple locations as we have shown that local variations caused by river discharge, or deep-water upwelling driven primary productivity contribute to the changes seen between terrestrial and marine stations. Additionally, significant differences were found between the values of the odd and even chain *n*-alkanes, which are less frequently reported in the literature as it can be more difficult to obtain sedimentary *n*-alkane concentrations high enough for accurate isotopic analysis. Our study indicates the even-numbered *n*-alkanes may prove to be more sensitive to OM sources than the odd *n*-alkanes and they should be considered when determining OM origins in sediments.

These LMW and HMW even numbered *n*-alkanes appear to be linked in part to marine sources of organic matter, either planktonic or bacterial, but more work should be carried out to pinpoint their exact origins, in addition to the commonly assumed terrestrial plants. Additional work is also needed to characterize the vegetation along the transect to confirm the exact origins of the odd and even *n*-alkanes found in the sediments, along with studies of how and if the organic matter, including *n*-alkanes, is isotopically fractionated during the processes of transport long-term burial in the sediments. The application of isotopes alongside traditional diagnostic ratios could be a powerful tool in determining variations in OM sources in sediments, temporally. More importantly, compound specific isotope analysis of the even numbered *n*-alkanes would allow identifying and tracking of petroleum-derived contaminants, as molecular data alone are

ineffective owing to the similarity in CPI values for petroleum-derived contaminants and highly degraded OM being discharged by the St. Lawrence River.

2.7 Acknowledgments

The authors would like to thank the captain and crew of the *R/V Coriolis II* for help in sample collection, Thi Hao Bui for assisting with the $\delta^2\text{H}$ measurements, as well as Associate Editor A. Revill and an anonymous reviewer for their insightful comments on an earlier version of the manuscript. This research was made possible thanks to financial support provided by Natural Science and Engineering Research Council of Canada (Grant Number RGPIN-2018-05080), the Canadian Foundation for Innovation (Grant Number 7548), the maritime strategy of the government of Quebec (20152020 action plan), as well as Concordia University.

Chapter 3: Tracking changes in dissolved organic matter along the St. Lawrence River, Estuary and Gulf using PARAFAC analysis, and distinguishing natural organic matter from oil-derived compounds

Anic Imfeld, Lindsay Hounjet, Céline Guéguen, Gwénaëlle Chaillou, Alexandre Ouellet, Yves Gélinas

Corresponding author:
Yves Gélinas
Department of Chemistry and Biochemistry
Concordia University
7141 Sherbrooke Street West,
Montreal, Quebec, Canada, H4B 1R6
Email: yves.gelinas@concordia.ca

3.1 Abstract

The St. Lawrence River, Estuary and Gulf are an integral part of commercial shipping including the transportation of crude oil along the St. Lawrence Seaway and comes with an inevitable risk for minor and major oil spills into this aquatic system. Methods should thus be developed and optimised to allow for the detection of oil-derived contamination in the water column and in the sediment of the Seaway. In this work, fluorescence excitation and emission matrices (EEM) and parallel factor analysis (PARAFAC) modeling was used to characterize the OM along the freshwater-saltwater continuum to determine the applicability of using these methods to tease out oil contamination. Our study included water samples collected from various depths along the St. Lawrence Seaway, as well as samples exposed to oil and subsequently photo oxidised. With this sample set, we found that the OM could be characterized using 4 fluorescent components (C1, C2, C3 and C6) associated with natural OM and identified 2 additional components (C4 and C5) linked to oil-derived compounds. C1, C2 and C3 were found to contain OM coming from terrestrial sources while C6 was marine OM in origin. PARAFAC analysis, specific ultraviolet absorbance (SUVA) and spectral slope (SR) allowed for the characterization of OM along the St. Lawrence River, Estuary and Gulf and provided insight into the molecular size and aromaticity of the OM present as well. With these results, a C4 to C1 total fluorescence ratio was determined to adequately differentiate oil contribution from natural OM in the St. Lawrence waterway, with values over 2.0 being indicative of oil contamination. These fluorescence measurements and proxies could allow for the detection of minor and major oil spill events in the St. Lawrence River, Estuary and Gulf, as well as in the Saguenay Fjord.

3.2 Introduction

The St. Lawrence River, Estuary and Gulf make up a large portion of the St. Lawrence Seaway system (Fig. 3.1). This aquatic highway spans over 3700 km between Canada and the United States and is utilized commercially to ship grain, ore, steel products as well as petroleum products including crude oil (The St. Lawrence Seaway Management Corporation, 2021). The transport of petroleum products by tankers increases the risk for oil spills and oil leaks from the transport vessels themselves. Currently estimated at about 70 MT, the volume of oil transported through the Seaway is likely to escalate in the next decades (D'Arcy, 2004), increasing the concerns surrounding the potential for oil spills along this transect.

The St. Lawrence system is one of the largest coastal estuaries in the world, where physico-chemical characteristics of both fresh and salty waters meet, and where inputs of organic matter (OM) from both terrestrial and marine sources vary in proportions along the freshwater-seawater continuum. The St. Lawrence is also a haven of biodiversity, being home to countless living species, such as birds, marine mammals, fish, and flora. It is thus of extreme importance to preserve the health of this environment to prevent negative detrimental effects on these species and degradation of its physico-chemical properties. Specifically, it is essential to protect this ecosystem from anthropogenic sources of contaminants such as polycyclic aromatic hydrocarbons (PAH) found in petroleum and petroleum products (Wakeham et al., 1980; Corminboeuf et al., 2022). Anthropogenic PAHs are attributed to one of two groups of polyaromatic compounds, either pyrolytic (from wood combustion), or petrogenic (from fuel combustion, oil spills and urban runoffs; Simpson et al., 1996; Abdel-Shafy and Mansour, 2016). The well-known toxic, mutagenic and carcinogenic properties of this group of compounds pose a significant threat to organisms exposed to PAHs in their environment (Menzie et al., 1992; Ikenaka et al., 2013). While parent PAH compounds are of environmental concern, so are their oxidized alteration products (Perera et al., 1998; Knecht et al., 2013). Oxygenated PAHs are produced by the incomplete combustion, chemical oxidation, photooxidation or biological transformation of the parent PAHs (Yu, 2002; Shen et al., 2011), and due to the addition of hydroxyl and carbonyl groups, oxygenated PAHs become more polar, and therefore more soluble in water (Lundstedt et al., 2007).

Although chromatography is the most commonly used technique for the detection of PAHs and oxygenated PAHs in the water column (Pham and Proulx, 1997; Pham et al., 1999;

Luo et al., 2004; Liu et al., 2021), fluorescence spectroscopy has also been employed as a viable approach for their quantitative and qualitative analysis, as well as for other chromophoric compounds present in water samples and petroleum contaminated waters (Coble, 1996; Zhou and Guo, 2012; Zhou et al., 2013; de Bruyn et al., 2018). Excitation emission matrices (EEM), produced by combining emission scans over a range of excitation wavelengths to create a 3D representation of a sample's fluorescence (Stedmon and Bro, 2008), have been successfully exploited to identify different components of dissolved OM, going as far back as 1996 (Coble, 1996). Dissolved OM is a complex mixture of largely uncharacterized organic molecules, making it difficult to identify individual compounds using traditional analytical techniques (Leenheer and Croué, 2003). Methods such as fluorescence and their corresponding EEMs can however provide information about distinct groups of compounds that share common fluorescence characteristics (Stedmon and Markager, 2005).

With the addition of parallel factor analysis (PARAFAC), a multi way data decomposition method, the various groups of fluorophores in a water sample can be discerned, which allows the sources of dissolved OM to be inferred (Coble, 2007; Murphy et al., 2008; Stedmon and Bro, 2008; Tfaily et al., 2015). With PARAFAC, the EEMs can be decomposed into 3-8 main components (EEMs), which are correlated to specific OM chromophore groups (Murphy et al., 2013).

In this study, we utilize PARAFAC analyses of EEMs from a set of water column samples collected along the St. Lawrence River, Estuary and Gulf, as well as the Saguenay Fjord, to track changes in chromophoric dissolved OM composition, along with water samples containing UV irradiated petroleum products to determine its efficiency at teasing out components indicative of oil contamination along a terrestrial-marine continuum. We also test whether its efficiency at confirming the presence of oil-derived components changes along the continuum. The resulting PARAFAC components and dissolved organic carbon (DOC) measurements are compared to further our understanding of OM sources along the St. Lawrence system, and the changes in DOC concentration and EEMs as a result of an oil spill event.

3.3 Materials and methods

3.3.1 Sampling location and collection

Water samples were collected in June 2017 and June 2018 aboard the R/V Lampsilis and R/V Coriolis II using a CTD Rosette fitted with 12.5 L Niskin bottles (estuary and gulf), or a single 12.5 L Niskin bottle mounted on a wire (river). Samples were collected at various stations along the St. Lawrence River, Estuary, Gulf, as well as in the Saguenay Fjord, as shown in Fig. 3.1. Surface water of depths 2-3 m was collected at all stations. Additional depths were sampled between 10-400 m for stations with a stratified water column. The water samples were filtered through combusted 0.7- μm glass fiber filters into combusted 40-mL EPA borosilicate vials with PTFE lined caps for DOC analysis and 60-mL USP Type III soda-lime amber Boston round bottles with PTFE lined caps for absorbance and fluorescence analysis. Surface water samples collected for use in the photooxidation experiment were filtered through 0.7- μm glass fiber filters followed by filtration through 0.2- μm filters and stored in a 1-L USP Type III soda-lime amber Boston round bottle with PTFE lined caps. Samples for DOC analysis were acidified to pH 2 using clean concentrated HCl and all samples were stored at 4°C in the dark until the time of their analysis. Ancillary data for each sampling station is listed in Table B.1 (Supplementary Material).

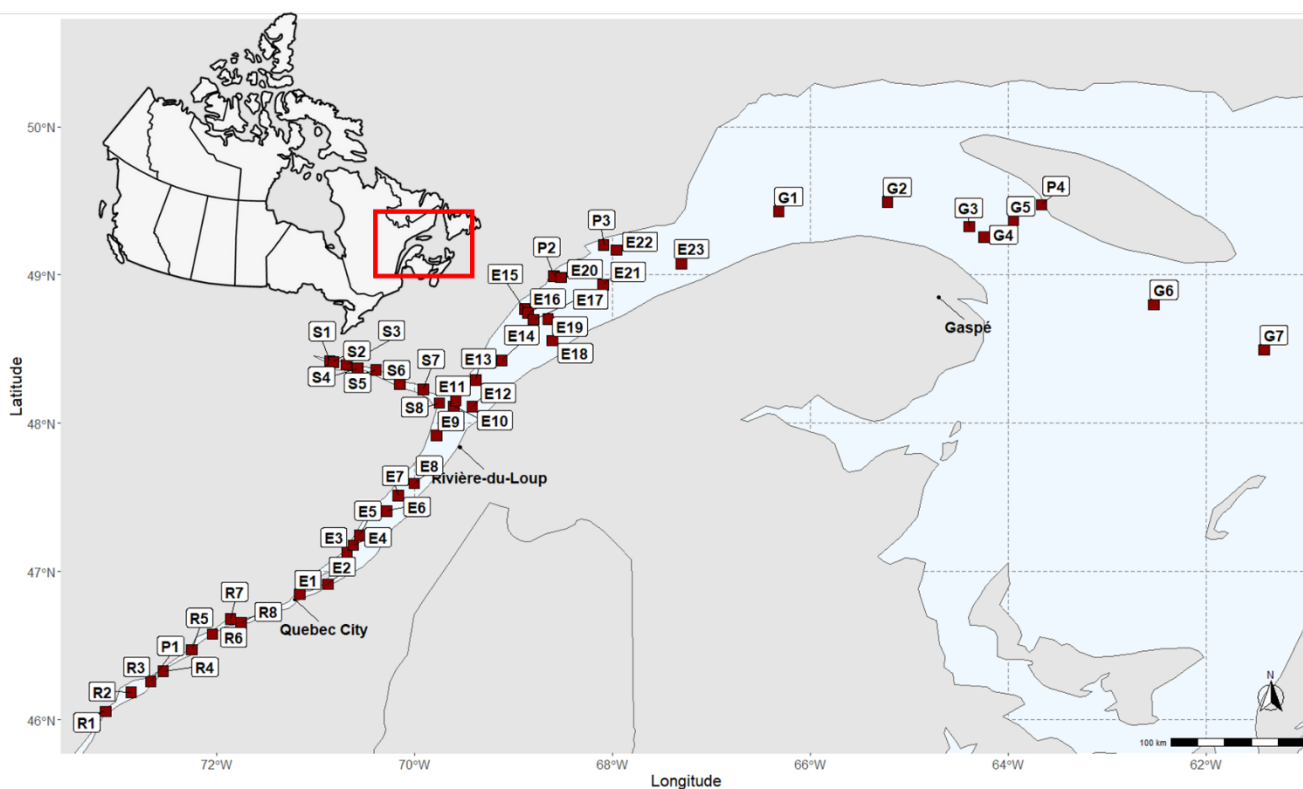


Figure 3.1 Map showing study sites across the St. Lawrence River, Estuary and Gulf, as well as the Saguenay Fjord in Quebec, Canada.

3.3.2 Photooxidation set-up

Approximately 1 g of conventional crude oil (mixed sweet blend, abbreviated MSW) was added to 20 g of filtered surface water from station E1 in a 50-mL beaker. The uncapped beaker was placed under a beam of light produced by a Newport Xe arc lamp passed through a 5-cm long deionized water filter and an Air Mass 1.5 global filter to approximate the solar spectrum (Shankar 2015). The beam of light was turned at a 90° angle using a full spectrum mirror resulting in a vertical projection of the light onto the oil's surface (Hounjet AMOP 2018). Using the Solar Electricity Handbook (Solar Irradiance Calculator), the average annual solar irradiance in Montreal, Canada, is 0.145 kW/m², whereas the irradiance of the Xe Arc lamp reaching the surface of the oil corresponds to 2.39 kW/m², or a 16.5-fold amplification of irradiance. The irradiation time periods were 0.5, 4.5, 18, 30 and 96 hours, with the amplification corresponding to 8.25, 74.25, 297, 495, and 1584 hrs (or approximately 0.35, 3, 12, 21, and 66 days) of continuous light. Each time point was carried out in duplicate with a control sample treated identically but kept in the dark. Post irradiation, the samples were weighed and transferred into a separatory funnel to isolate the aqueous fraction from the oil. The aqueous fraction was collected

in 40-mL EPA borosilicate vials with PTFE lined caps, wrapped in aluminum foil and kept at 4°C prior to analysis.

3.3.3 DOC measurements

DOC concentrations for all 154 samples were measured on a Shimadzu TOC- V_{CSH} organic carbon analyzer. Natural filtered water (pre-combusted glass fiber filters, porosity 0.7 μm) collected at the different stations was acidified to pH <2 with concentrated HCl upon collection, while samples collected at different time points (UV-irradiation experiment) were acidified to pH <2 with concentrated HCl right after the separation of the aqueous and oil phases.

3.3.4 Absorption and fluorescence spectroscopy

Water samples were allowed to reach room temperature prior to analysis. Absorption spectra were collected between 190 nm and 750 nm at 1-nm intervals on an Agilent 8453 UV-Visible Spectrophotometer with a 1-cm path-length quartz cuvette. The samples were treated similarly for fluorescence analysis. The excitation emission matrices (EEM) were generated using a Varian Cary Eclipse Fluorescence Spectrophotometer. EEMs were recorded at 5-nm intervals for excitation spectra between 240 and 450 nm and emission spectra from 245 to 600 nm at an integration time of 0.1 s. Ultrapure water blank spectra were measured in the same way and used to eliminate water Raman peaks.

3.3.5 Indices

Typical indices used to evaluate the OM sources using EEMs include the specific ultraviolet absorbance at 254 nm ($SUVA_{254}$), slope ratio (SR), humification index (HIX), biological index (BIX), and the fluorescence index (FI). $SUVA_{254}$ was calculated by dividing the UV absorption measured at 254 nm by the sample's DOC concentration and was used to assess the aromatic content (Weishaar et al., 2003) and average molecular weight (MW) of DOM, whereas the SR is the spectral slope between 275 nm and 295 nm divided by the slope between 350 nm and 400 nm. SR is inversely correlated with DOM average molecular weight, with higher values indicating lower MW distribution (Helms et al., 2008).

The FI is the ratio of fluorescence at emission wavelengths 450 nm and 500 nm at a fixed excitation of 370 nm and is described as an indicator of aromaticity of DOM in freshwaters (McKnight et al., 2001). HIX is calculated as the ratio of the sum of fluorescence between 435 nm and 480 nm at an excitation wavelength of 254 nm to that between 300 to 345 nm at the same

excitation wavelength and allows to gauge the degree of humification and aromaticity in samples (Zsolnay et al., 1999; Ohno, 2002). Finally, BIX is used to characterize biological production of DOM and is a ratio of the fluorescence measured at an excitation of 310 nm and emitted at 380 nm over the fluorescence measured at excitation 310 nm and emitted at 430 nm (Huguet et al., 2009).

3.3.6 PARAFAC analysis

PARAFAC pre-processing was done using the eemR package in R (Massicotte, 2019). This package allowed for the removal of water blanks from the EEMs as well as the removal of both Raman and Rayleigh scattering. Additionally, the samples were corrected for inner-filter effect and normalisation of EEM fluorescence intensities. The PARAFAC analysis was performed using the staRdom package, also in R (Pucher et al., 2019). The PARAFAC model was validated using split-half analysis and Tucker's congruence coefficients as well as examining residuals. The leverage of each sample and wavelength were examined and 27 samples were removed as outliers. Excitation wavelengths below 250 nm and emission wavelengths below 300 nm were also removed based on previous literature (Stedmon and Markager, 2005). After numerous iterations, the PARAFAC analysis resulted in a robust model consisting of 6 components describing the different fractions of total DOC in the sample set.

3.4 Results

3.4.1 DOC and indices of surface waters along the St. Lawrence River, Estuary, and Gulf, as well as the Saguenay Fjord

The surface DOC concentrations in the Saguenay Fjord, which drains Lake St. Jean in the Laurentian highlands, range from 3.90 to 6.39 mg/L with minimal variation between the two years. A decrease in DOC concentrations can be seen from station S1, the inner most station in the Fjord, towards the St. Lawrence River, as shown in Fig. 3.2A. Fig. 3.2B shows the DOC concentrations for the remaining stations from the river (furthest left) to the Gulf (furthest right), for both 2017 and 2018. The DOC concentrations generally decrease from the freshwater to the marine stations, with some higher values close to the various north shore river plumes (stations P1, P2, and P3). The reason for the higher concentrations in 2018 at stations E3, E4 and E5 is unknown.

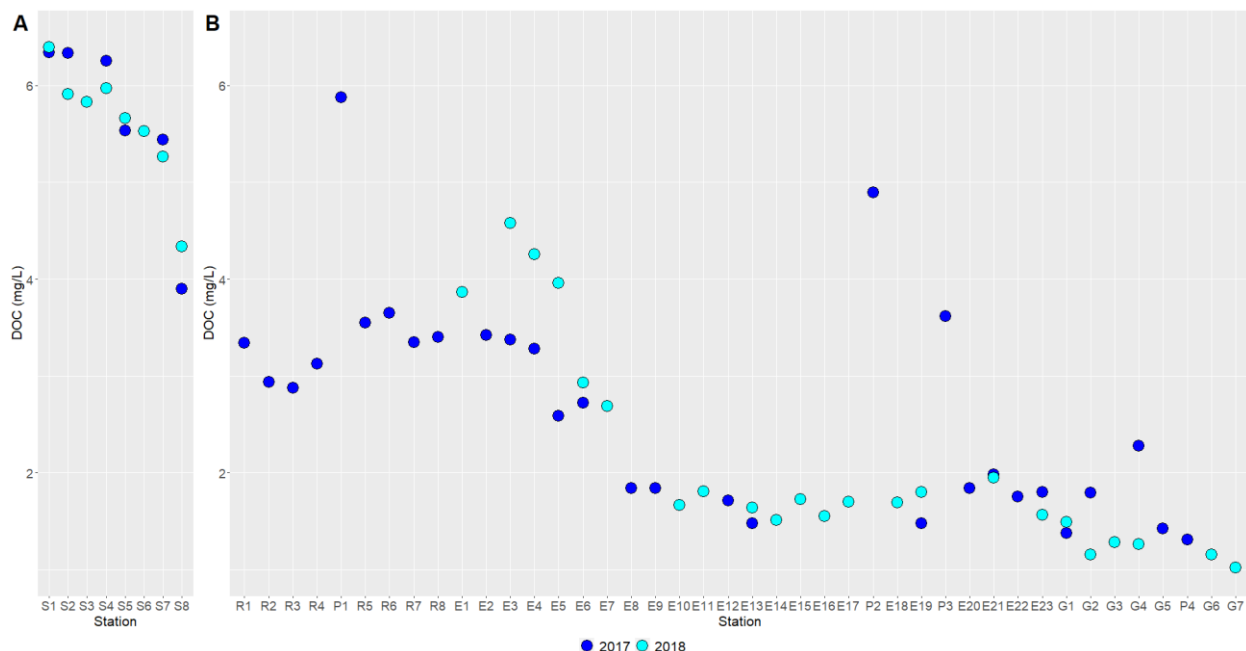


Figure 3.2 DOC concentrations in the surface waters of A) the Saguenay Fjord and B) the St. Lawrence River, Estuary and Gulf for both 2017 and 2018 samples

The $SUVA_{254}$ and SR values for the surface waters of the Saguenay Fjord, as well as the St. Lawrence River, Estuary and Gulf can be found in Fig. 3.3. The $SUVA_{254}$ values show a slight increase from the most upstream freshwater stations (Station R1) towards the Estuary and a decrease from the Estuary to the Gulf. There is also a slight decrease from the inner most station of the Saguenay Fjord towards the river mouth. The SR values in the Saguenay range from 0.77 to 0.91 with no apparent trend along the Fjord. Similarly, the SR values along the River, Estuary and Gulf show little variation until Station 20, where the SR values show differences for the 2 different years sampled. The 2017 samples show a slight increase in SR values towards the marine stations, whereas the 2018 samples have scattered values in this same region.

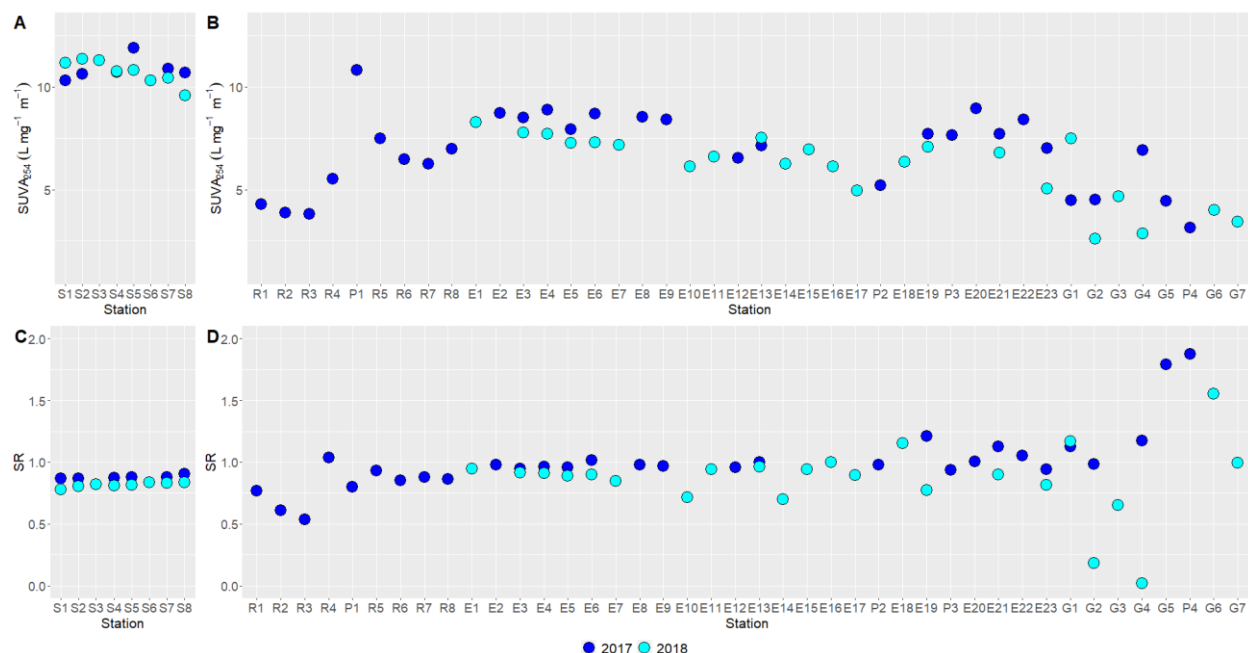


Figure 3.3 SUVA₂₅₄ and SR values for surface waters along the Saguenay Fjord (A and C) and the St. Lawrence River, Estuary and Gulf (B and D) for both 2017 and 2018 samples.

Fig. 3.4 shows the changes in BIX, HIX and FI in the surface of the freshwater stations along the St. Lawrence River and the freshwater portion or the Estuary, as well as in the Saguenay Fjord. Both BIX and FI values show a general decrease in values as the stations near the transition zone at station E4 (in the maximum turbidity zone), while HIX values increase slightly. The BIX, FI and HIX values in the surface waters of the Saguenay Fjord range from 0.35 to 0.44, 1.17 to 1.24, and 0.95 to 0.97 respectively.

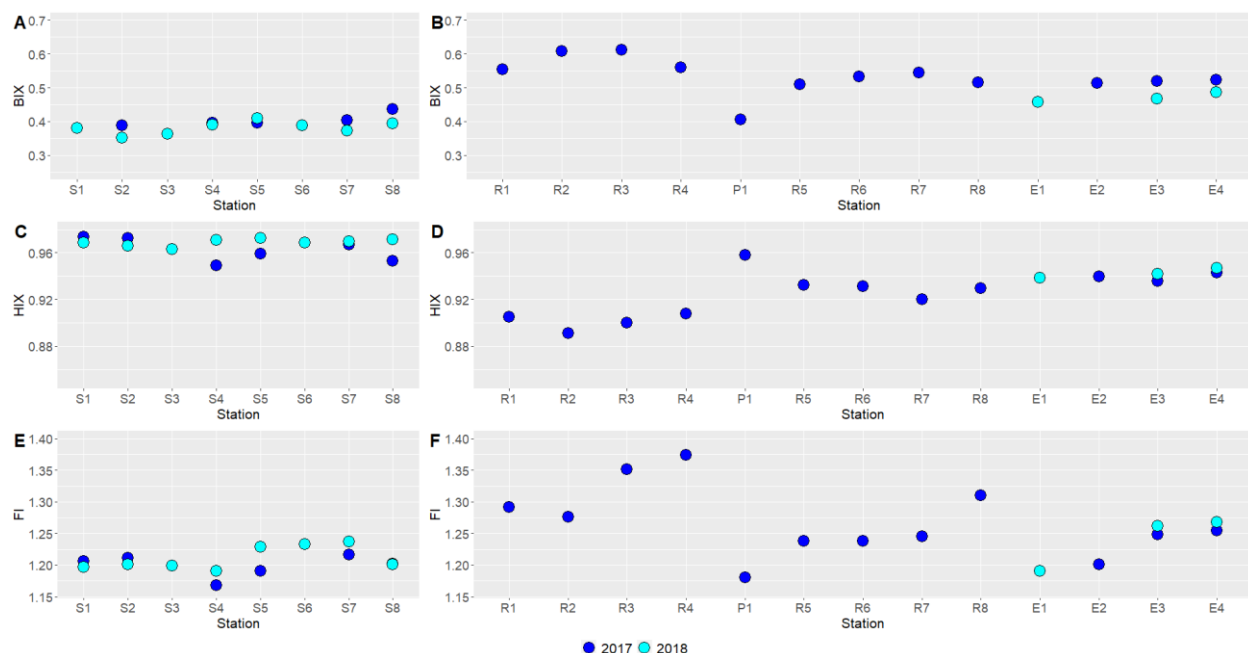


Figure 3.4 BIX, HIX and FI values calculated in surface waters of the Saguenay Fjord (A, C, E) and the freshwater stations along the St. Lawrence River and Estuary until the maximum turbidity zone at station E4 (B, D, F) for both 2017 and 2018 samples.

3.4.2 Photooxidation effects on DOC and EEMs of oil

The measured DOC concentration of the underlying water collected during the photooxidation study increased from 8.45 to 84.32 mg/L as irradiation time increased, while control samples ranged from 7.91 to 14.55 mg/L across the various time points, indicating a production and transfer of the more hydrophilic components of the oil sample to the water subphase occurring mostly during the first few hours (Fig. 3.5).

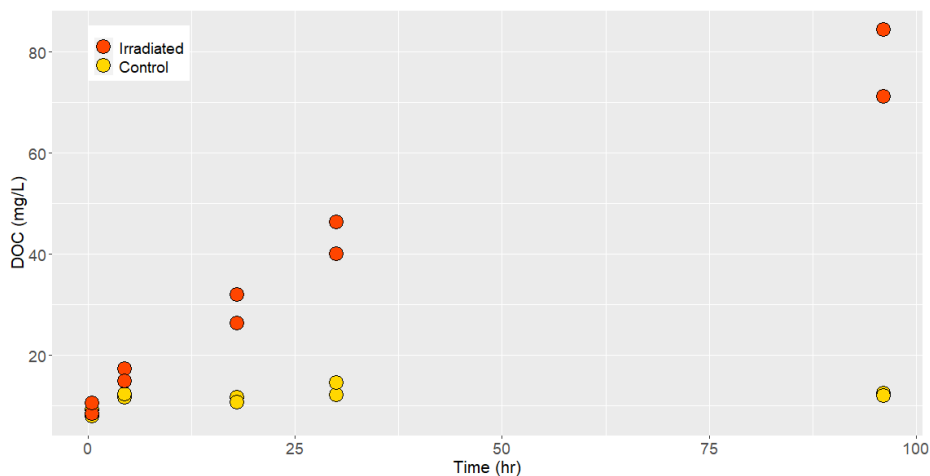


Figure 3.5 DOC concentrations in the water subphase for both irradiated and control samples at varying timepoints.

The excitation and emission wavelengths for the major and minor peaks were determined from the EEMs of the control and post irradiation samples and are reported in Table 3.1. The control samples had excitation/emission values ranging from <245/358 nm to <245/363 nm for the major peak and from 275/335 nm to 290/357 nm for the minor peak. The location of the major peak did not vary much among the different time periods in the control sample while the minor peak shifted to a slightly higher wavelength as irradiation time progressed. Both the major and minor peaks shifted to higher emission wavelengths in the post irradiation samples as irradiation time increased.

Table 3.1 Excitation and emission wavelengths for the major and minor peaks determined from the EEMs of the control and irradiated samples

Sample	Control		Post-Irradiation	
	Max peak	Minor Peak	Max peak	Minor Peak
0.5hrs - 1	<245/358*	275/338	<245/356	275/335
0.5hrs - 2	<245/357	275/338	<245/356	275/335
4.5hrs - 1	<245/359	275/338	<245/367	280/337
4.5hrs - 2	<245/358	275/336	<245/365	275/339
18hrs - 1	<245/361	275/335	<245/378	280/339
18hrs - 2	<245/358	280/340	<245/370	280/344
30hrs - 1	<245/359	280/338	<245/371	285/345
30hrs - 2	<245/363	285/343	<245/378	285/357
96hrs - 1	<245/362	285/343	<245/377	285/357
96hrs - 2	<245/360	290/357	<245/380	280/363

* Measured fluorescence $\lambda_{Ex}/\lambda_{Em}$

SUVA₂₅₄ and SR values are shown for both controls and irradiated samples in Fig. 3.6. Interestingly, there is a significant decrease in the SUVA₂₅₄ values between the controls and irradiated samples at the 30- and 96-hour mark. Irradiated values generally show lower SR values than the controls, as well as a generally decreasing trend for both controls and irradiated samples with time, contrary to other studies in which the SR of CDOM generally increased with irradiation time (Helms et al., 2008).

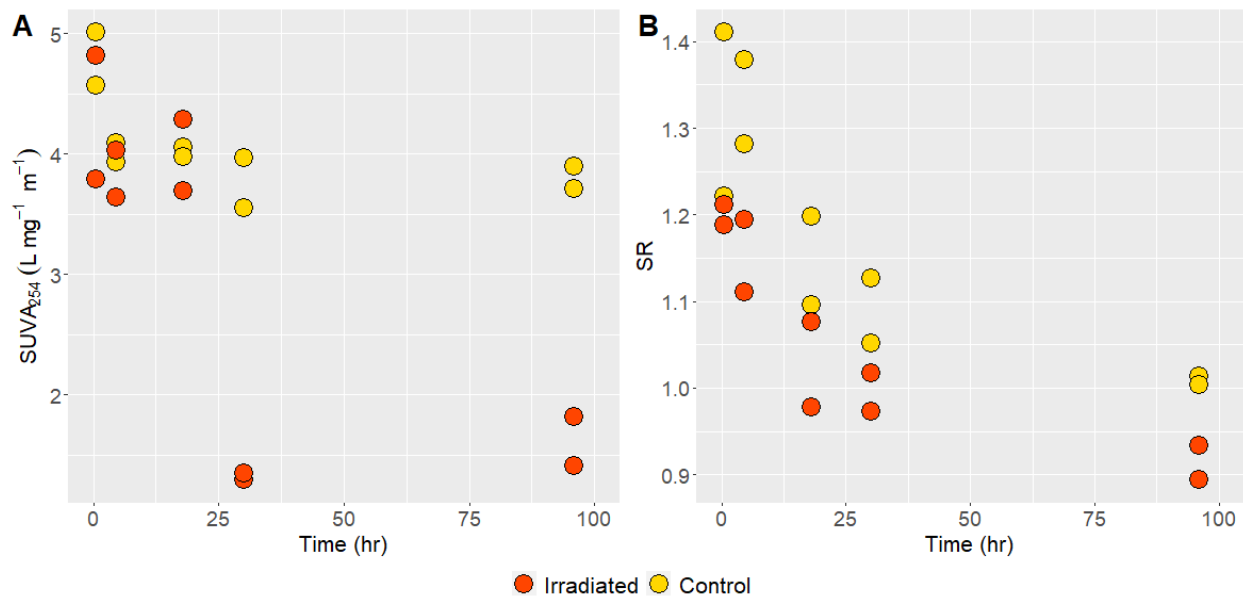


Figure 3.6 SUVA₂₅₄ and SR values, A and B respectively, for both the irradiated and control samples as irradiation time progressed.

Finally, the BIX, HIX and FI were calculated and are presented in Supplementary Table B.2. BIX values for the control samples ranged from 0.92 to 1.51 and generally increased with time, whereas the irradiated samples had values ranging from 0.94 to 1.38 and were generally lower than the control values for irradiation times of 18 hrs and more. Conversely, HIX values for the irradiated samples were consistently higher than the corresponding control samples and increased with irradiation time. FI values ranged from 1.14 to 1.29 for both controls and irradiated samples with no clear trend for either group.

3.4.3 PARAFAC model results

PARAFAC results indicate four main components making up the CDOM in the waters along the St. Lawrence River, Estuary, Gulf and the Saguenay Fjord, together with two additional components attributed to oil derived compounds. The spectral characteristics of the six components identified by the PARAFAC modelling of EEMs are shown in Fig. 3.7A with the light blue and dark blue lines representing the excitation and emission wavelengths, respectively. The contour plots describing the intensities as a function of emission and excitation wavelengths are found in Fig. 3.7B. Table 3.2 describes the classification of each component based on previous literature results.

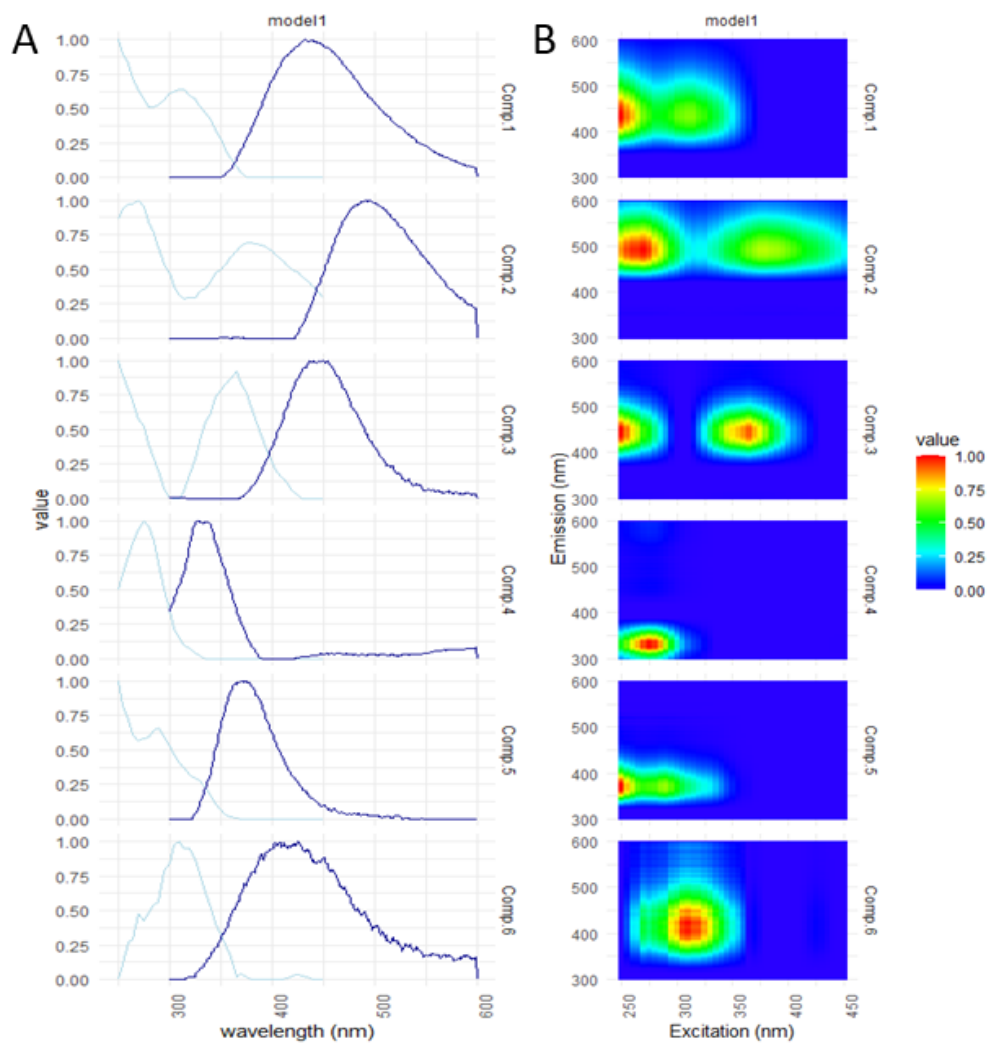


Figure 3.7 Excitation and emission wavelengths of the 6 components (A) and contour plots describing the intensities as a function of their spectral characteristics (B) identified by the PARAFAC model.

Table 3.2 Classification of the six components identified by PARAFAC analysis based on previous literature results.

Component	Excitation/ Emission Maxima	Classification	Reference
1	Ex: <250 (315) Em: 431	Terrestrial/autochthonous, Fulvic acid fluorophore group A peak (260/380–460)	Stedmon and Markager, 2005 Walker et al., 2009
2	Ex: 270 (380) Em: 490	A peak (260/380–460) C peak (350/420–480)	Coble, 1996
3	Ex: <250 (365) Em: 443	A peak (260/380–460) C peak (350/420–480)	Tfaily et al., 2015
4	Ex: 275 Em: 330	Naphthalene like, Oil related	Zhou et al., 2015 Araujo et al., 2021
5	Ex: <250 Em: 370	Oil related, degradation product	Zhou et al., 2013
6	Ex: 310 Em: 408	Marine humic-like M peak (312/380–420)	Coble, 1996

3.5 Discussion

3.5.1 DOC and indices along the St. Lawrence River, Estuary, and Gulf, as well as the Saguenay Fjord

The DOC concentrations for samples collected in both 2017 and 2018 along the St. Lawrence Estuary and Gulf, as well as the Saguenay Fjord, are comparable to those previously reported in the literature for this region (Barber et al., 2017). The surface DOC concentrations decrease from the inland stations towards the more marine stations in the Gulf with increases in DOC near the river plumes where fresh terrestrial OM is introduced to the St. Lawrence, as shown in Fig. 3.8A. The Saguenay Fjord is where the highest concentrations of DOC were found, again in agreement with the findings of Barber et al. (2017). The Saguenay Fjord's high DOC concentrations are caused by terrestrial OM runoff from the surrounding boreal forest and carried by the Saguenay River. It is an important section of the St. Lawrence waterway as it discharges a large amount of terrestrial OM into the Estuary, mostly in the dissolved phase. A series of north shore rivers also discharge terrestrial DOC into the Estuary, as can be seen for samples collected at stations located near the mouth of the Des Outardes and Manicouagan Rivers (Stations P2 and

P3), where DOC concentrations are higher than in the main channel of the Estuary (Thomas, 2014).

The $SUVA_{254}$ values, and therefore the aromaticity of the DOC, increased from the River towards the Estuary, with the highest values found in the Saguenay Fjord (Fig. 3.8B). These high $SUVA_{254}$ values along the Saguenay Fjord and towards the mouth of the Fjord are due again to the contribution of terrestrial OM originating from the boreal forest, which contains high proportions of aromatic-rich lignin and tannin, as well as their degradation products. Conversely, the more marine stations show lower $SUVA_{254}$ values, again in agreement with the less aromatic and more labile marine OM found at those locations. Interestingly, the $SUVA_{254}$ values along the freshwater stations of the St. Lawrence River (Station R1 to E1) were characterized by $SUVA_{254}$ values similar to those measured at the marine stations and lower than those found at the estuarine stations. The main water source feeding the river is discharged from the Great Lakes and is influenced by several riverine lakes along its course. These lakes have a lower water flow compared to the river, leading to clearer surface waters owing to the sedimentation of particulate matter and greater sunlight penetration. DOC in these lakes is therefore more efficiently exposed to UV radiation, which results in better degradation of the aromatics and thus lower $SUVA_{254}$ values.

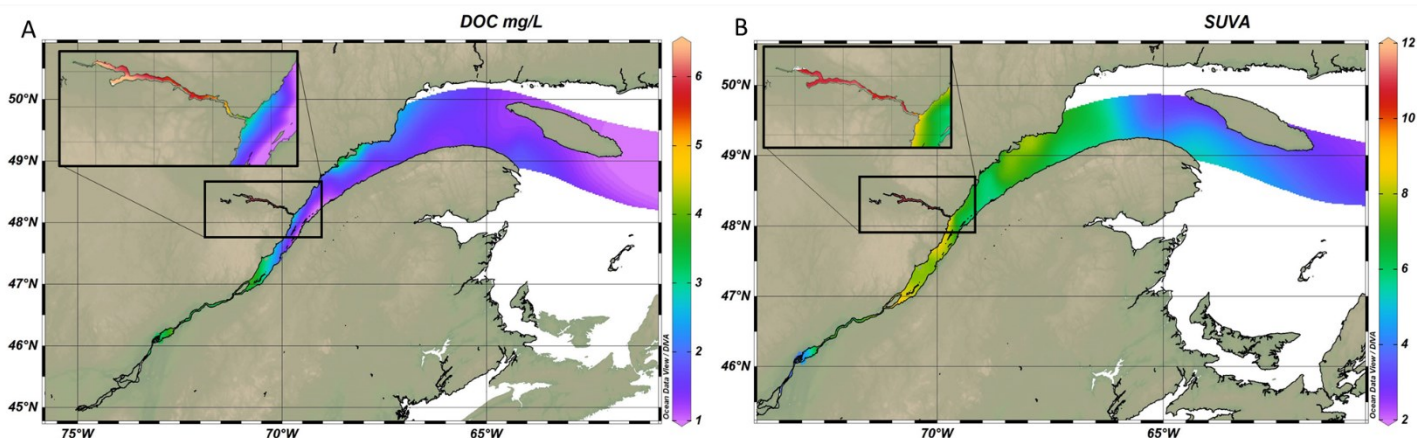


Figure 3.8 DOC concentrations (A) and $SUVA_{254}$ (B) trends along the St. Lawrence waterway from the river to the gulf.

While DOC and $SUVA_{254}$ values showed little to no variance between the two sampling years, SR values varied broadly from station to station and for the different years in a way that is difficult to explain at the marine stations of the Gulf (Fig. 3.3D). SR values have been reported as diagnostic for photodegradation (positive correlation) and for microbial processing and average

molecular weight of the DOC (negative correlation), but this index might be inapplicable in our system.

Lastly, the BIX and HIX values of the surface waters for the freshwater stations (stations R1 to E4) can be found in Fig. 3.9. Low BIX values, such as those found in the St. Lawrence River, indicate that the CDOM in these samples comprises a low contribution from autochthonous OM components. BIX values are usually lower where the CDOM is mainly derived from terrestrial inputs and higher where the CDOM is dominated by biological sources such as plankton-derived DOC and bacteria metabolic products (Huguet et al., 2009; Singh et al., 2010; Li et al., 2022). The highest BIX values in the St. Lawrence River were found in Lake St. Pierre where the water flow rate is low compared to the river, allowing for increased UV penetration and increased productivity and bacterial activity, likely leading to a high BIX index.

The HIX index showed an increasing trend from Lac St. Pierre at station R2 towards the maximum turbidity zone at station E4, indicating a higher degree of CDOM humification closer to the estuary and lower values in Lake St. Pierre, again suggesting a biological origin for CDOM. Finally, there was no obvious trend in the FI values measured along the St. Lawrence River. However, all the FI values were below 1.4 indicating a mainly terrestrial origin of humic substances (McKnight et al., 2001), which disagrees with the findings derived from the other ratios. However, the BIX and HIX indices are interpreted relative to the rest of the stations; while the FI suggests mainly terrestrial origins, the other indices provide further information on the source of OM relative to one another.

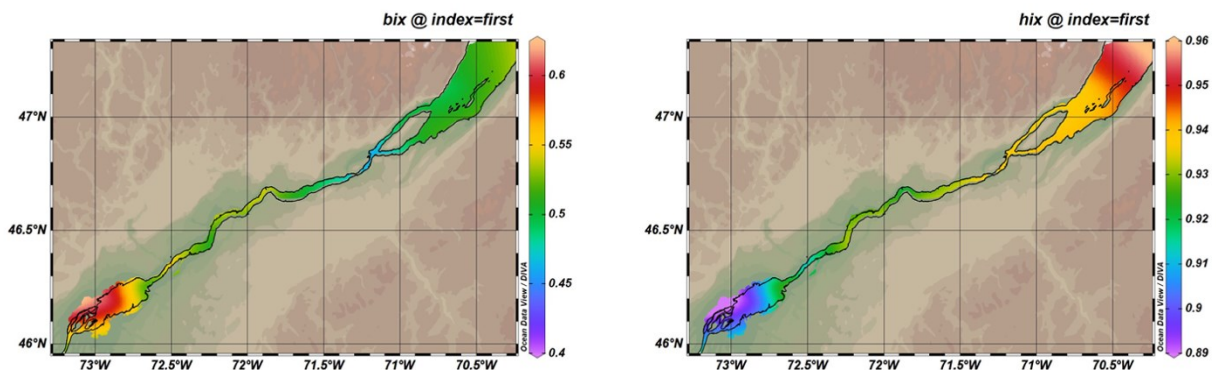


Figure 3.9 BIX and HIX trends along the freshwaters of the St. Lawrence River and Estuary, from station R1 to station E4.

3.5.2 Photooxidation effects on DOC and EEMs of oil

The water used for the photooxidation experiments was collected from the surface (3m) of station E1 in 2018. Station A has a salinity level of 0.098 p.s.u and the DOC concentration at this station prior to the addition of the oil was 3.69 mg/L. Following the deposition of the oil on the surface of the water, the DOC concentrations of the water ranged from 7.91 mg/L to 14.55 mg/L, averaging a 3-fold increase in DOC concentration. This increase suggests a quick transfer of the more polar compounds from the oil layer to the underlying water in the first few hours, prior to any external manipulations. This water-amendable fraction of oils has been found to contain benzene, toluene, ethylbenzene and xylene (BTEX) compounds as well as other compounds such as naphthalenes and naphthalic acids (Faksness and Brandvik, 2008; Jaggi et al., 2017). Additionally, when exposed to UV light, aromatic components of oil are photo-modified to more water-soluble compounds such as phenols and epoxides, further increasing the DOC concentration as irradiation progresses to a concentration as high as 84 mg/L after 96 hours (Fig. 3.5). $SUVA_{254}$ values (Fig. 3.6), which have been shown to be strongly correlated to DOC aromaticity (Traina et al., 1990; Weishaar et al., 2003), are also distinctly different between the control and irradiation samples after about 20 hours of irradiation, suggesting that the aromatic compounds in the oil are being effectively degraded. These results agree with many studies showing the role of photooxidation in the long-term weathering of oils (Dutta and Harayama, 2000; Prince et al., 2003). The shift of the major peak of the EEMs of the irradiated samples to higher emission wavelengths relative to those of the control samples (Table 3.1) also suggests that there are changes in chemical composition due to photooxidation. This shift to longer emission wavelengths again likely reflects the partial oxidation of the aromatic components of the oil.

The SR has been found to be inversely correlated with DOM average molecular weight (MW), with higher values indicating lower molecular weight distribution (Helms et al., 2008). Interestingly, the spectral slope for both control and irradiated samples decreased as irradiation time progressed. Contrary to the trends seen for natural samples free of oil, the apparent MW of the DOM in the water samples with an oil slick increased as irradiation progressed. Typically, photodegradation of natural OM would result in a decrease in MW (Helms et al., 2008; Du et al., 2016) whereas with our samples, the apparent MW of DOM increased as the components in the oil were amended to become more water soluble. The controls shielded from irradiation also

showed a decrease between 0.5 to 90 hrs, but to a lesser extent than the irradiated samples. These results suggest that the more water amenable components in the oil slowly diffuse into the underlying aqueous subphase in both the controls and the samples, but that this process was enhanced with photooxidation as components with increasingly higher MW were transferred from the oil to the aqueous subphase.

While the FI and BIX do not add any supplementary information as there are no obvious differences between the control and the irradiated samples, as well as no trends as time progressed (Supplementary Table B.2), the HIX results reiterate that the irradiated samples allowed for the alteration of compounds in the oil to become more water soluble and move from the oil slick to the underlying water as irradiation advances. The HIX values increased from 0.36 to 0.66 as irradiation time progressed from 0.5 to 90 hrs, respectively, indicating the partial oxidation of humic-like compounds in the oil, followed by their transfer to the subphase.

3.5.3 Component interpretation and variations along the freshwater-seawater continuum

Six individual fluorescent components were identified in the oil-amended samples using PARAFAC analysis (Fig. 3.7). The first three components in our model (C1, C2 and C3) have two excitation peaks and one emission peak, which according to previous studies correlate with terrestrial OM peak A in the ultraviolet region and C peak in the visible region (Table 3.2). These regions are associated with terrestrial, humic, allochthonous sources for peak A, and terrestrial, anthropogenic, agriculture sources for peak C (Coble, 2007). Components 4 and 5 appear to be oil related based on a study by Zhou et al 2013. The contribution of the components to total fluorescence in the oil samples (Fig. 3.10) corroborate this assumption as these 2 components make up the majority of the total fluorescence. The final component, C6 resembles the M peak identified by Coble (2007), which corresponds to marine humic-like sources and are mostly derived from plankton. They are predominantly aliphatic in composition, with a low aromatic content (Harvey et al., 1983; Coble, 1996; Whitby et al., 2020).

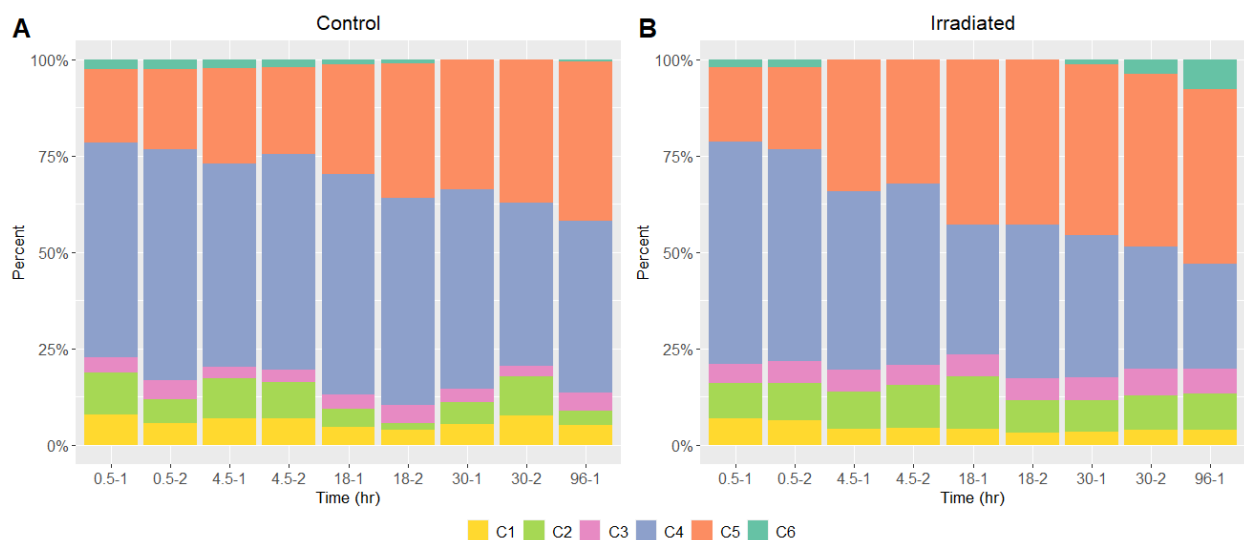


Figure 3.10 Relative contribution of each component to total fluorescence for the control (A) and irradiated (B) samples at all time points.

While C1, C2 and C3 all correspond to terrestrial OM sources, there is additional information that can be teased out from the variations in the excitation and emission wavelengths of the major peaks. Because C2 absorbs at longer excitation and emission wavelengths than C1 and C3, the expectation is that it consists of high MW, hydrophobic compounds, according to a critical review of reoccurring PARAFAC components (Ishii and Boyer, 2012). Conversely, C1 corresponds to shorter excitation wavelengths and is therefore more likely to consist of low MW compounds. C3 falls between C1 and C2 in terms of excitation wavelengths and thus is expected to contain compounds that are intermediate in MW relative to C1 and C2.

Interestingly, there is a strong correlation in the relative contribution of C1 and C3 for the majority of surface waters along the St. Lawrence River, Estuary and Gulf (both years included). However as shown in Fig. 3.11, the surface waters of the Saguenay Fjord and the river mouth stations (Stations P1, P2 and P3) do not fall on the same trend line. The relative contribution of C1 to total fluorescence for these stations averages around 29 to 30% with stations P1 and P2 having slightly lower percent contributions, whereas C3 varied much more along these stations. These findings indicate the OM sources for C1 is similar at every station of the Saguenay Fjord, with the same sources contributing to DOC discharged from the north shore rivers. Terrestrial OM sources at these stations is greatly influenced by relatively fresh terrestrial OM from the forested watersheds of the boreal forest, as also suggested from alkane-specific stable isotope ratios ($\delta^{13}\text{C}$ and $\delta^2\text{H}$) in another study (Imfeld et al., 2022).

marine OM compared to terrestrial OM, would make up a larger percentage of the total fluorescence.

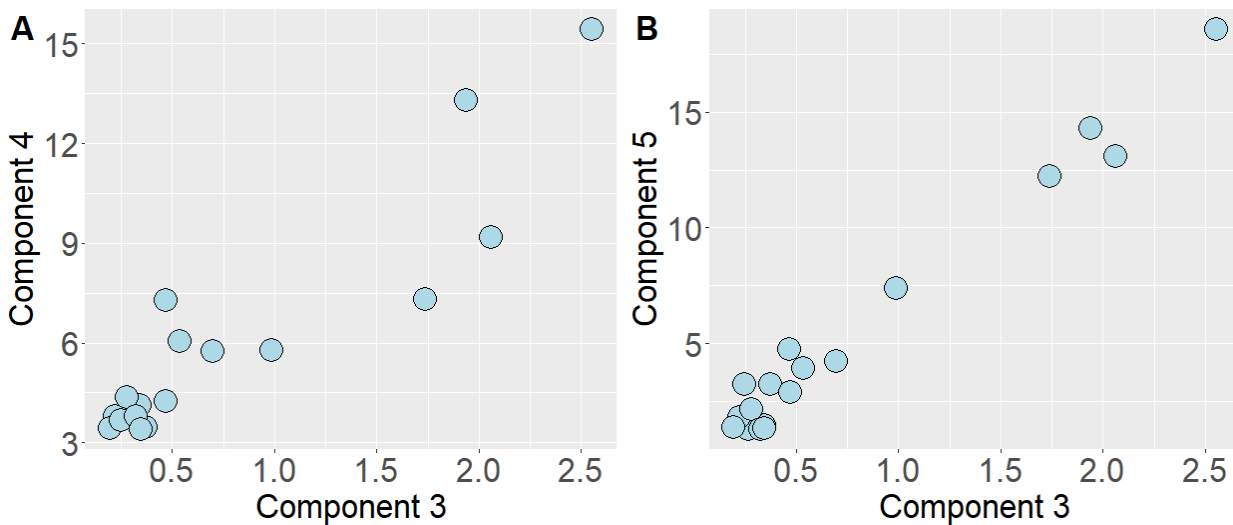


Figure 3.12 Relationship between C4 and C5 with C3 in all samples in contact with oil (control and irradiated samples).

Fig. 3.13 also shows the more than 10-fold decrease in total fluorescence along the terrestrial to marine continuum, which linearly correlates with the changes in DOC concentrations measured in the surface waters at the same stations (Appendix Fig. B.1). However, changes in the total fluorescence intensity and in the relative contributions of the different components identified using PARAFAC were not limited to surface waters as large variations with depth were measured in the water column for both sampling years (Fig. 3.14). There is a large decrease in total fluorescence at all stations from surface to the deep waters, due to primary production reworking the majority of DOM in the surface waters.

Interestingly, C6 shows a generally higher relative contribution to the total fluorescence in the 2018 sampling year compared to the 2017 sampling year. Component 6 is associated to marine-humic substances, which could be a result of reworked planktonic OM. It is possible that during the 2018 sampling mission, the annual algal bloom occurred shortly before the sampling mission, and thus the higher plankton-derived DOC concentration associated with blooms is reflected in the relative contribution to total fluorescence of C6 compared to samples from 2017. This hypothesis could be corroborated with chlorophyll data, which unfortunately was not collected in 2018.

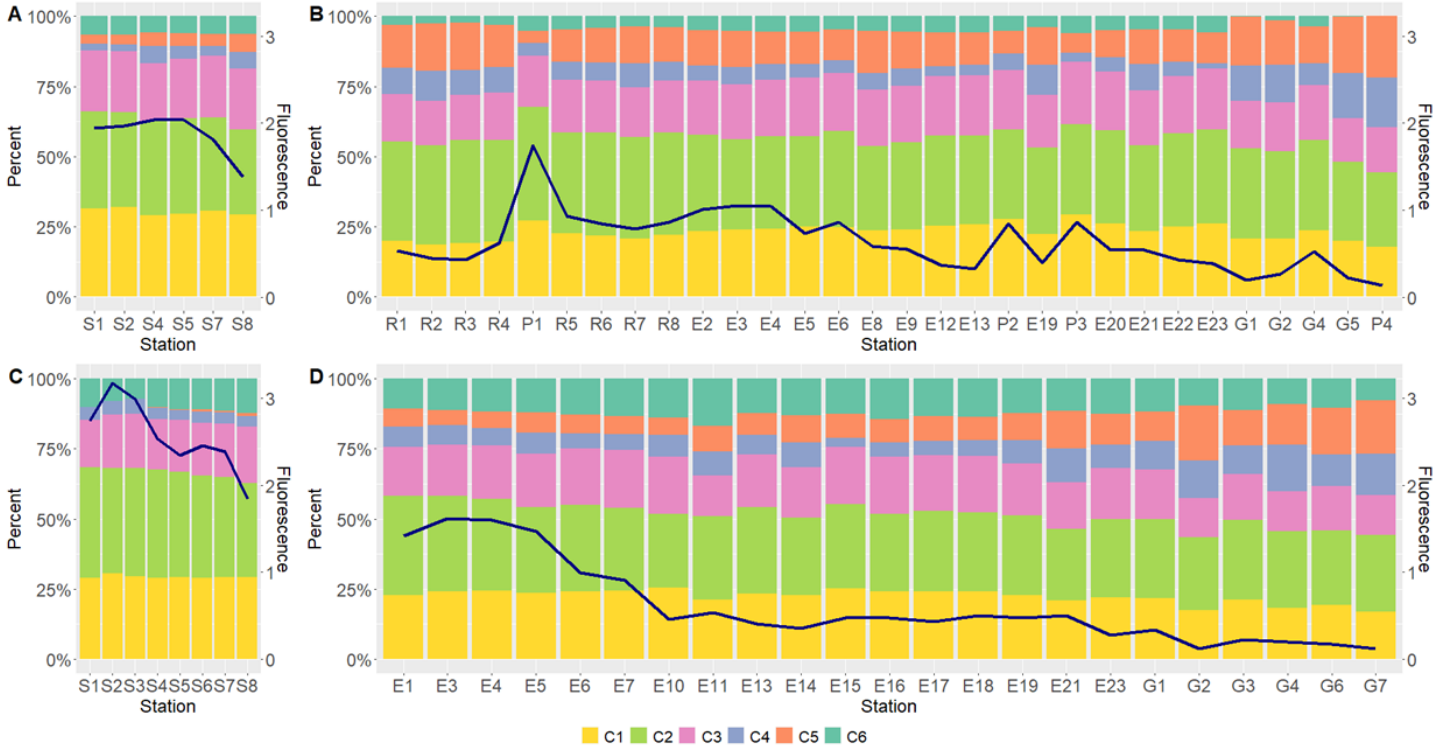


Figure 3.13 Relative contribution of each component to total fluorescence for surface waters collected along the Saguenay Fjord in 2017 (A) and 2018 (C) and along the St. Lawrence River, Estuary and Gulf in 2017 (B) and 2018 (D). The stations labelled P (2017 only) correspond to water sampled in the plume of north shore rivers.

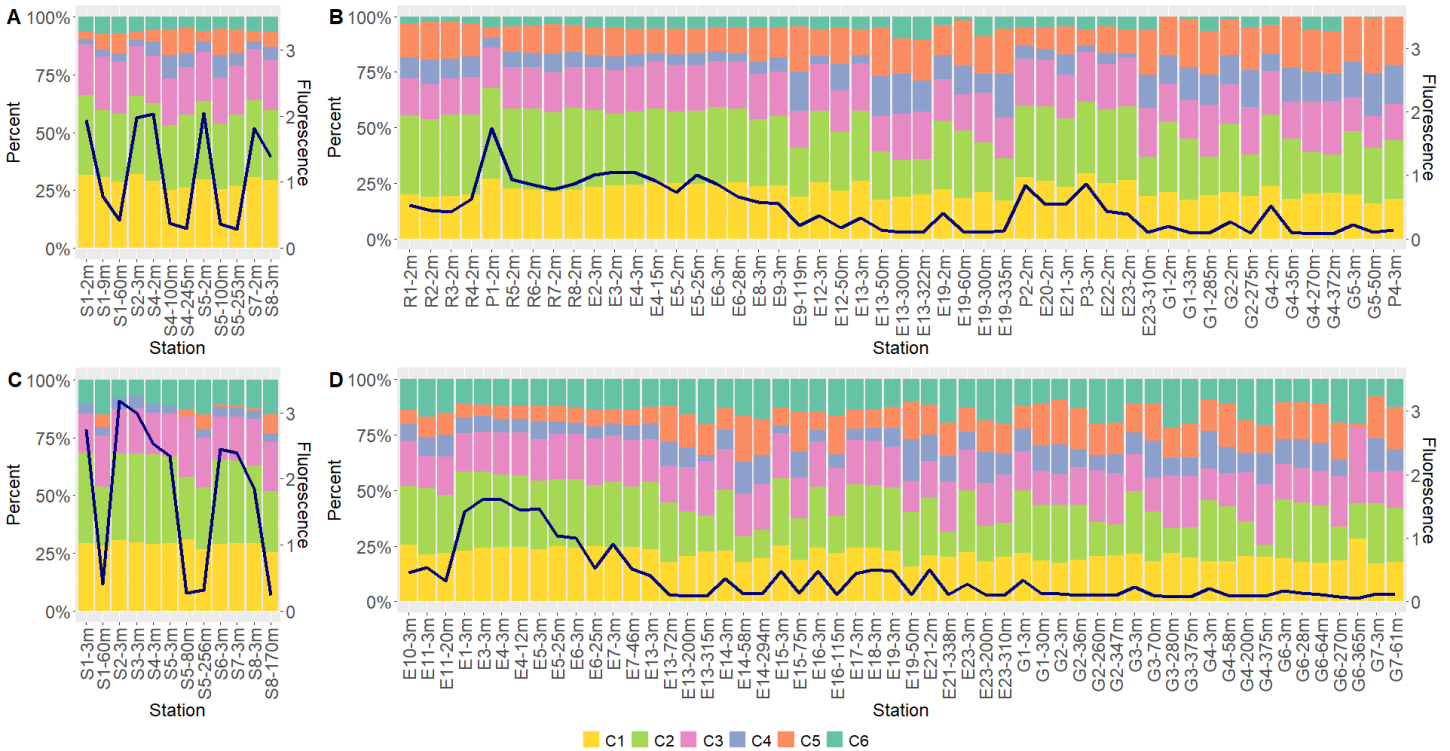


Figure 3.14 Relative contribution of each component to total fluorescence for waters at all depths collected along the Saguenay Fjord in 2017 (A) and 2018 (C) and along the St. Lawrence River, Estuary and Gulf in 2017 (B) and 2018 (D)

3.5.4 Proposed ratio for distinguishing natural OM from petroleum OM

The water samples containing UV irradiated petroleum products show variations in the contribution of C4 and C5 between the control samples and those exposed to irradiation, particularly at longer exposure times (Fig. 3.15). C5 is likely correlated to some degree to photodegraded oil components as the differences between the control and the irradiated samples are greater than those of C4. Using the knowledge gained from the irradiation of oil on water samples, C4 and C5, which are strongly correlated to the oil compounds, can be exploited to define a proxy ratio allowing the detection of oil in the St. Lawrence waterways.

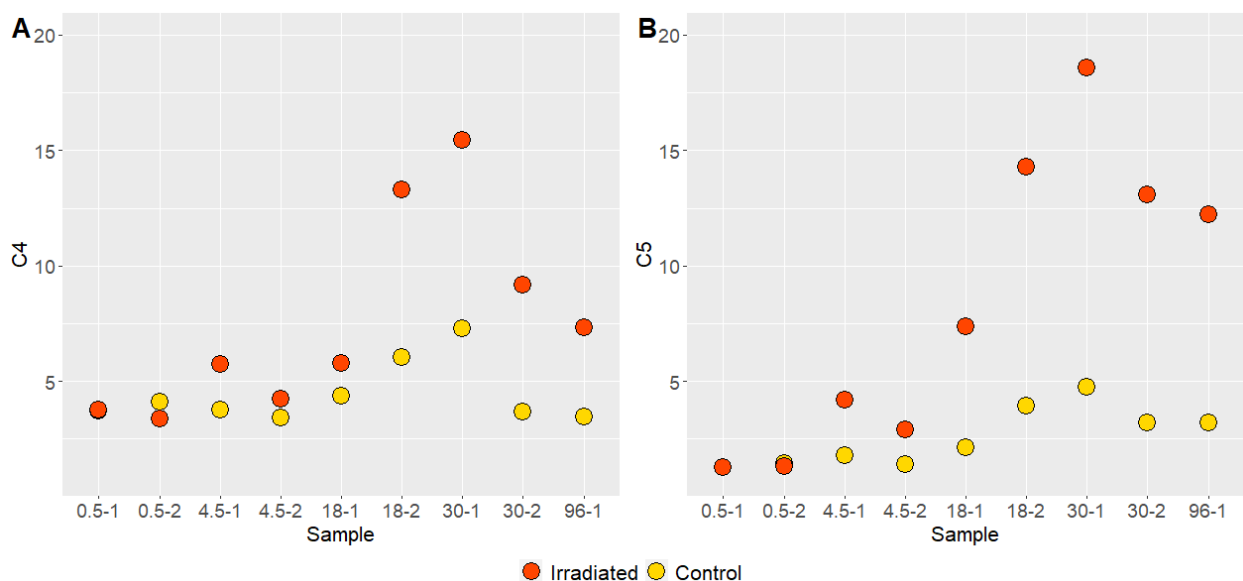


Figure 3.15 Comparison of the absolute fluorescence value of C4 (A) and C5 (B) between the irradiated and control samples at all time points.

Intuitively, C4 should be considered in such proxy because it is associated only to oil derived products while C5 is affected by aromatic amino acids in proteins and peptides. Fig. 3.16 shows the calculated fluorescence intensity ratio between C4 and that of the most prominent terrestrial component, C1. There are large differences between samples contaminated with irradiated oil products versus natural water samples, at any depth and location along the St. Lawrence River, Estuary and Gulf, as well as in the Saguenay Fjord. Not only are there large differences, but additionally both the oil-contaminated, non-irradiated control samples and oil-contaminated samples that underwent irradiation for varying durations clearly stand out from the natural water samples, showing the potential sensitivity of this ratio for the detection of oil contamination in the St. Lawrence water system. The C4/C1 values for the natural water samples

collected along the St. Lawrence and Saguenay continuum ranged from 0 to 1.22, while those for water samples contaminated with oil and oil degradation products ranged between 5.50 and 12.21 respectively. These results indicate that any samples with C4/C1 values over 2.0 would have some degree of oil contamination in this environment. This threshold value of 2.0 represents a 6-sigma process, where the set limit is 6 standard deviations above the average fluorescence of all the natural samples analyzed. It allows for a threshold to be established along the St. Lawrence River, Estuary and Gulf, as well as the Saguenay Fjord, and future samples could be compared to the values in this paper if a spill event occurred. Noteworthy, the fluorescence intensity ratio between C5 and C1, which shows an increase in ratio value with UV exposure time (data not shown), could also possibly be used to assess the degree of photodegradation of the oil contaminants, but would require a lot more work to better understand the potential and limitations of such proxy.

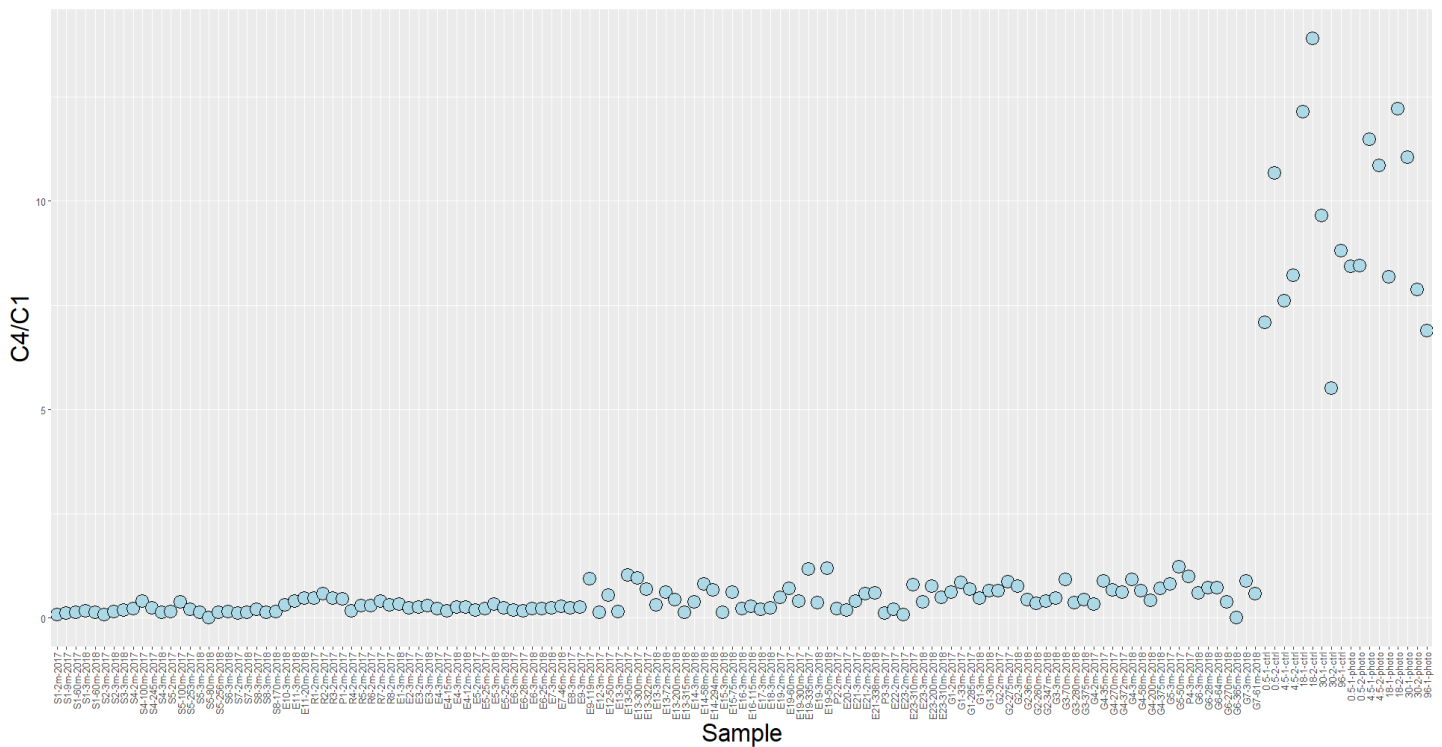


Figure 3.16 Ratio of C4 to C1 for all waterway samples at all depth (2017 and 2018), alongside the samples exposed to oil.

3.6 Conclusion

Compared to other heavily industrialised coastal systems, the St. Lawrence Estuary and Gulf is considered to be in relatively good ecosystem health. The deep waters of the Estuary are however affected by permanent hypoxia, with dissolved O₂ levels that have decreased in a

stepwise fashion since the beginning of the last century (Gilbert et al., 2005), reaching critically low levels ($<40 \mu\text{M}$) in the past few years. This system is thus already under stress from anthropogenic activities taking place in its large watershed, which results in a discharge of nutrients, dissolved and particulate organic matter, as well as organic and inorganic pollutants. The threat associated with the continuous and increasing oil transit through this important ecosystem is thus of great concern and should lead to the characterization of the baseline hydrocarbon levels in the sediment (Corminboeuf et al., 2022; Imfeld et al., 2022) and in the water column, as well as to the development of methods allowing rapid and efficient detection of petroleum-derived contaminants (this work; Imfeld et al., 2022).

PARAFAC analysis was used in this work to tease out 6 components from a set of water samples that included samples containing water soluble oil compounds and photooxidized oil products. Four components, C1, C2, C3 and C6, were found to originate from natural OM including terrestrial humic-like and marine humic-like compounds. The other two components, C4 and C5, were correlated with the presence of oil and oil degradation products in the water samples. With these 6 components, we were able to infer information not only about the origin of the chromophoric dissolved OM present at the various stations along the St. Lawrence River, Estuary and Gulf, but more specifically about its aromaticity and apparent molecular size. While C1, C2 and C3 were associated with terrestrial humic-like compounds, the subtle differences between them were likely linked to contrasting freshness and/or origin of the dissolved OM, as shown by the results obtained for the Saguenay Fjord samples in Fig. 3.11.

Our data shows that EEMs and PARAFAC are powerful tools to characterize the chromophoric OM along a terrestrial to marine continuum, but also that it is possible to identify the presence of oil products and their degradation products in these water samples. Although a lot more work is needed to evaluate its robustness, we propose a new proxy for the St. Lawrence Waterway, based on the ratio of the fluorescence intensity of C4 over that of C1, to determine if oil-derived contamination is present. In particular, additional experiments are needed to test the effect of the concentration of oil-derived products on this proxy. Furthermore, a second fluorescence intensity ratio, between C5 and C1, appears related to the degree of degradation of the oil and could possibly be used following a more rigorous analysis. The changes in chemical composition of oil-derived compounds caused by photooxidation can potentially result in more toxic soluble compounds that should be monitored in aquatic environments. These fluorescence

measurements and proxies could allow for the detection of minor and major oil spill events in the St. Lawrence River, Estuary and Gulf, as well as in the Saguenay Fjord.

Chapter 4: Conclusions, Perspectives and Future Work

The overall goal of this research was to characterize the OM along the St. Lawrence Waterway and determine if the techniques used could aid in differentiating natural OM from oil-derived contaminants. While both methods, spectroscopic and biomarker analysis, are useful in characterizing OM, a series of limitations and caution must be considered when these techniques are exploited for OM source identification. Spectroscopic techniques, such as the application of indices and PARAFAC analysis, have the benefit of being rapid, simple and cost-effective while still having the capability to differentiate bulk OM changes along the waterway. Additionally, for the detection of oil-derived compounds, we found that EEMs and PARAFAC analysis showed promises at teasing out the photo oxidized oil derived OM from naturally occurring OM in the water column. We were able to establish a new ratio proxy that would allow to detect an eventual spill and follow its dispersion and degradation if it were to occur in the future in the water column of the St. Lawrence Waterway. However, spectroscopic analysis only allows for the detection of fluorescent dissolved OM and for the general grouping of compounds, not the characterization of individual compounds.

Contrarily, biomarker analysis, while requiring extensive work up prior to analysis, and an important mass of sample for CSIA, allows for more in-depth data to be collected. Unlike spectroscopic analysis, specific compounds can be detected and quantified instead of groups of compounds bearing similar fluorescent functional groups. In our study, the selected biomarkers were *n*-alkanes, which were analysed both molecularly and isotopically. Compared to EEM and PARAFAC, these analyses gave better insights to the origin of the compounds and specifically with stable carbon and hydrogen stable isotopes analysis, relative changes in OM sources along the St. Lawrence Waterway. With molecular characterization and diagnostic ratios alone, we found that the interpretation of the OM source was not always accurate, especially when there was more than one source input. Diagnostic ratios also could not always distinguish between marine OM and petroleum-derived OM as results for both look similar, and therefore without prior knowledge of the sample, the source could be misinterpreted. With the addition of isotopic analysis, we could further probe the source and origin of the *n*-alkanes. Specifically, we found that the even *n*-alkanes showed greater differences in both hydrogen and carbon stable isotopes values between the stations analyzed compared to the more abundant odd *n*-alkanes. Even carbon chain length *n*-alkanes can thus be more efficiently used to identify subtle changes in the source of the OM at specific stations such as Station 25 for example. To the best of our knowledge, our

research resulted in the first complete set of molecular and isotopic data along a terrestrial-marine continuum with both hydrogen and carbon analysis of individual *n*-alkanes, both odd and even chain lengths. Because the odd *n*-alkanes are more abundant, they are the easier compounds to analysis for stable isotope values, and therefore, the more challenging analysis of the even *n*-alkanes is often missing in the literature. Unfortunately, it means that an abundance of information is then being missed as well, including the sawtooth pattern that is seen between the isotope values of odd and even *n*-alkanes, as well as the absolute difference in concentrations between the neighbouring *n*-alkanes. Just like the spectroscopic analyses of samples from the water column, the baseline abundance and compound specific stable isotopes values that have been measured in the sediment along the St. Lawrence Waterway as part of this research will allow for the tracking and detection of an oil spill should one occur in the future. Specifically, stable carbon and hydrogen isotope analysis of both even and odd *n*-alkanes will be vital to assess any contamination as it is the difference between the stable isotope carbon and hydrogen values of the even and odd *n*-alkanes that provides the most powerful approach to distinguish between the natural and petroleum-derived OM.

It is important for researchers who are applying these techniques to other natural systems to be aware that not all diagnostic ratios can be used interchangeably from one system to the next, for both spectroscopic and biomarker analysis, and some ratios may not be useful at all for tracking changes in their systems. It would be beneficial to systematically determine the extent to which these ratios can be applied in a system, and to determine at what degree contamination starts to alter the diagnostic ratio from being perceived as natural vs. anthropogenic. This could be achieved by measuring the terrestrial and marine end members within in a system as well the contaminant end member (i.e. various petroleum samples). Furthermore, systematically determining the limits that carbon and hydrogen isotopes of individual *n*-alkanes can differentiate between sources when the input of anthropogenic petroleum source increases.

Through our research, we presented spectroscopic, molecular, and isotopic analyses for water and sediments of the St. Lawrence Waterway and how these characterizations could be applied to differentiate natural OM from petroleum-derived OM. We hope that the approaches used here will promote the use of stable isotope analysis on both odd and even chain length *n*-alkanes in biogeochemical analyses, especially in terrestrial OM to better understand the changes in isotopic values we found along the terrestrial-marine continuum. While our research has

highlighted the changes in molecular and isotopic values in the surface sediments across a continuum (spatial variations), it could be further applied to sediments at depth to evaluate the changes in molecular and isotopic values with depth (temporal variations). This would allow for a historic record to be established to probe changes in the environment through time. It would also be interesting to see PARAFAC analysis coupled with carbon isotope analysis of the dissolved organic carbon along the St. Lawrence continuum to tease out further information from OM pool in the surface and deep water samples. These techniques are so versatile, when applied in conjunction with traditional methods, that there seems to be a plethora of information still available to assess the various OM source inputs along a dynamic system such as the St. Lawrence Waterway.

References:

- Abdel-Shafy H. I. and Mansour M. S. M. (2016) A review on polycyclic aromatic hydrocarbons: Source, environmental impact, effect on human health and remediation. *Egyptian Journal of Petroleum* **25**, 107–123.
- Ahad J. M. E., Ganeshram R. S., Bryant C. L., Cisneros-Dozal L. M., Ascough P. L., Fallick A. E. and Slater G. F. (2011) Sources of n-alkanes in an urbanized estuary: Insights from molecular distributions and compound-specific stable and radiocarbon isotopes. *Marine Chemistry* **126**, 239–249.
- Aichner B., Ott F., Słowiński M., Noryskiewicz A. M., Brauer A. and Sachse D. (2018) Leaf wax n-alkane distributions record ecological changes during the Younger Dryas at Trzechowskie paleolake (northern Poland) without temporal delay. *Climate of the Past* **14**, 1607–1624.
- Aloulou F., Kallel M., Dammak M., Elleuch B. and Saliot A. (2010) Even-numbered n-alkanes/n-alkenes predominance in surface sediments of Gabes Gulf in Tunisia. *Environmental Earth Science* **61**, 1–10.
- Andersson M., Klug M., Eggen O. A. and Ottesen R. T. (2014) Polycyclic aromatic hydrocarbons (PAHs) in sediments from lake Lille Lungegårdsvannet in Bergen, western Norway; appraising pollution sources from the urban history. *Science of The Total Environment* **470–471**, 1160–1172.
- Ankit Y., Mishra P. K., Kumar P., Jha D. K., Kumar V. V., Ambili V. and Anoop A. (2017) Molecular distribution and carbon isotope of n-alkanes from Ashtamudi Estuary, South India: Assessment of organic matter sources and paleoclimatic implications. *Marine Chemistry* **196**, 62–70.
- Barber A., Sirois M., Chaillou G. and Gélinas Y. (2017) Stable isotope analysis of dissolved organic carbon in Canada's eastern coastal waters. *Limnology and Oceanography* **62**, S71–S84.
- Bayona J. M., Domínguez C. and Albaigés J. (2015) Analytical developments for oil spill fingerprinting. *Trends in Environmental Analytical Chemistry* **5**, 26–34.
- Bourbonniere R. A. and Meyers P. A. (1996) Sedimentary geolipid records of historical changes in the watersheds and productivities of Lakes Ontario and Erie. *Limnology and Oceanography* **41**, 352–359.
- Brittingham A., Hren M. T. and Hartman G. (2017) Microbial alteration of the hydrogen and carbon isotopic composition of n-alkanes in sediments. *Organic Geochemistry* **107**, 1–8.
- de Bruyn W., Chang D., Bui T., Hok S. and Clark C. (2018) Photochemical degradation of oil products in seawater monitored by 3D excitation emission matrix (EEM) fluorescence spectroscopy: implications for coloured dissolved organic matter (CDOM) studies. *Environmental Science and Pollution Research* **25**, 34777–34787.

- Bush R. T. and McNerney F. A. (2013) Leaf wax n-alkane distributions in and across modern plants: Implications for paleoecology and chemotaxonomy. *Geochimica et Cosmochimica Acta* **117**, 161–179.
- Chen F. X., Fang N. F., Wang Y. X., Tong L. S. and Shi Z. H. (2017) Biomarkers in sedimentary sequences: Indicators to track sediment sources over decadal timescales. *Geomorphology* **278**, 1–11.
- Chen W., Westerhoff P., Leenheer J. A. and Booksh K. (2003) Fluorescence Excitation–Emission Matrix Regional Integration to Quantify Spectra for Dissolved Organic Matter. *Environ. Sci. Technol.* **37**, 5701–5710.
- Chen Y., Cao J., Zhao J., Xu H., Arimoto R., Wang G., Han Y., Shen Z. and Li G. (2014) n-Alkanes and polycyclic aromatic hydrocarbons in total suspended particulates from the southeastern Tibetan Plateau: Concentrations, seasonal variations, and sources. *Science of The Total Environment* **470–471**, 9–18.
- Chikaraishi Y. and Naraoka H. (2003) Compound-specific δD – $\delta^{13}C$ analyses of n-alkanes extracted from terrestrial and aquatic plants. *Phytochemistry* **63**, 361–371.
- Chikaraishi Y. and Naraoka H. (2007) $\delta^{13}C$ and δD relationships among three n-alkyl compound classes (n-alkanoic acid, n-alkane and n-alkanol) of terrestrial higher plants. *Organic Geochemistry* **38**, 198–215.
- Clear Seas (2022) Clear Seas Centre for Responsible Marine Shipping. *Clear Seas*.
- Coble P. G. (1996) Characterization of marine and terrestrial DOM in seawater using excitation-emission matrix spectroscopy. *Marine Chemistry* **51**, 325–346.
- Coble P. G. (2007) Marine Optical Biogeochemistry: The Chemistry of Ocean Color. *Chemical Review* **107**, 402–418.
- Corminboeuf A., Montero-Serrano J.-C., St-Louis R., Dalpé A. and Gélinas Y. (2022) Pre- and post-industrial levels of polycyclic aromatic hydrocarbons in sediments from the Estuary and Gulf of St. Lawrence (eastern Canada). *Marine Pollution Bulletin* **174**, 113219.
- Cranwell P. A. (1984) Lipid geochemistry of sediments from Upton Broad, a small productive lake. *Organic Geochemistry* **7**, 25–37.
- D’Arcy P. (2004) *Sustainable navigation strategy for the St. Lawrence : Stratégie de navigation durable pour le Saint-Laurent.*, desLibris.
- Deines P. (1980) Chapter 9 - THE ISOTOPIC COMPOSITION OF REDUCED ORGANIC CARBON. In *The Terrestrial Environment, A* (eds. P. Fritz and J. Ch. Fontes). Handbook of Environmental Isotope Geochemistry. Elsevier, Amsterdam. pp. 329–406.

- Derrien M., Yang L. and Hur J. (2017) Lipid biomarkers and spectroscopic indices for identifying organic matter sources in aquatic environments: A review. *Water Research* **112**, 58–71.
- Diefendorf A. F., Freeman K. H., Wing S. L., Currano E. D. and Mueller K. E. (2015a) Paleogene plants fractionated carbon isotopes similar to modern plants. *Earth and Planetary Science Letters* **429**, 33–44.
- Diefendorf A. F., Freeman K. H., Wing S. L. and Graham H. V. (2011) Production of n-alkyl lipids in living plants and implications for the geologic past. *Geochimica et Cosmochimica Acta* **75**, 7472–7485.
- Diefendorf A. F., Leslie A. B. and Wing S. L. (2015b) Leaf wax composition and carbon isotopes vary among major conifer groups. *Geochimica et Cosmochimica Acta* **170**, 145–156.
- Du Y., Zhang Y., Chen F., Chang Y. and Liu Z. (2016) Photochemical reactivities of dissolved organic matter (DOM) in a sub-alpine lake revealed by EEM-PARAFAC: An insight into the fate of allochthonous DOM in alpine lakes affected by climate change. *Science of The Total Environment* **568**, 216–225.
- Duan Y., Wu B., Xu L., He J. and Sun T. (2011) Characterisation of n-alkanes and their hydrogen isotopic composition in sediments from Lake Qinghai, China. *Organic Geochemistry* **42**, 720–726.
- Dutta T. K. and Harayama S. (2000) Fate of Crude Oil by the Combination of Photooxidation and Biodegradation. *Environmental Science and Technology* **34**, 1500–1505.
- Faksness L.-G. and Brandvik P. J. (2008) Distribution of water soluble components from Arctic marine oil spills — A combined laboratory and field study. *Cold Regions Science and Technology* **54**, 97–105.
- Ficken K. J., Li B., Swain D. L. and Eglinton G. (2000) An n-alkane proxy for the sedimentary input of submerged/floating freshwater aquatic macrophytes. *Organic Geochemistry* **31**, 745–749.
- Freimuth E. J., Diefendorf A. F., Lowell T. V. and Wiles G. C. (2019) Sedimentary n-alkanes and n-alkanoic acids in a temperate bog are biased toward woody plants. *Organic Geochemistry* **128**, 94–107.
- Gearing J. N., Gearing P. J., Rudnick D. T., Requejo A. G. and Hutchins M. J. (1984) Isotopic variability of organic carbon in a phytoplankton-based, temperate estuary. *Geochimica et Cosmochimica Acta* **48**, 1089–1098.
- Gilbert D., Sundby B., Gobeil C., Mucci A. and Tremblay G.-H. (2005) A seventy-two-year record of diminishing deep-water oxygen in the St. Lawrence estuary: The northwest Atlantic connection. *Limnology and Oceanography* **50**, 1654–1666.

- Grimalt J., Albaigés J., Al-Saad H. T. and Douabul A. A. Z. (1985) n-Alkane distributions in surface sediments from the Arabian Gulf. *Naturwissenschaften* **72**, 35–37.
- Han J. and Calvin M. (1969) Hydrocarbon Distribution of Algae and Bacteria, and Microbiological Activity in Sediments. *Proceedings of the National Academy of Sciences* **64**, 436–443.
- Harvey G. R., Boran D. A., Chesal L. A. and Tokar J. M. (1983) The structure of marine fulvic and humic acids. *Marine Chemistry* **12**, 119–132.
- Hayes J. M. (1993) Factors controlling ^{13}C contents of sedimentary organic compounds: Principles and evidence. *Marine Geology* **113**, 111–125.
- He D., Nemiah Ladd S., Saunders C. J., Mead R. N. and Jaffé R. (2020) Distribution of n-alkanes and their $\delta^2\text{H}$ and $\delta^{13}\text{C}$ values in typical plants along a terrestrial-coastal-oceanic gradient. *Geochimica et Cosmochimica Acta* **281**, 31–52.
- Hedges J. I., Keil R. G. and Benner R. (1997) What happens to terrestrial organic matter in the ocean? *Organic Geochemistry* **27**, 195–212.
- Hélie J.-F. and Hillaire-Marcel C. (2006) Sources of particulate and dissolved organic carbon in the St Lawrence River: isotopic approach. *Hydrological Processes* **20**, 1945–1959.
- Helms J. R., Stubbins A., Ritchie J. D., Minor E. C., Kieber D. J. and Mopper K. (2008) Absorption spectral slopes and slope ratios as indicators of molecular weight, source, and photobleaching of chromophoric dissolved organic matter. *Limnology and Oceanography* **53**, 955–969.
- Herman P. H. J., Middelburg J. J. and Koppel J. van de (1999) Ecology of estuarine macrobenthos. *Advances in Ecological Research* **29**, 195–240.
- Hou J., D'Andrea W. J., MacDonald D. and Huang Y. (2007) Hydrogen isotopic variability in leaf waxes among terrestrial and aquatic plants around Blood Pond, Massachusetts (USA). *Organic Geochemistry* **38**, 977–984.
- Hu L., Guo Z., Feng J., Yang Z. and Fang M. (2009) Distributions and sources of bulk organic matter and aliphatic hydrocarbons in surface sediments of the Bohai Sea, China. *Marine Chemistry* **113**, 197–211.
- Huang Y., Shuman B., Wang Y. and Webb T. (2004) Hydrogen isotope ratios of individual lipids in lake sediments as novel tracers of climatic and environmental change: a surface sediment test. *J Paleolimnol* **31**, 363–375.
- Huguet A., Vacher L., Relexans S., Saubusse S., Froidefond J. M. and Parlanti E. (2009) Properties of fluorescent dissolved organic matter in the Gironde Estuary. *Organic Geochemistry* **40**, 706–719.

- Ikenaka Y., Sakamoto M., Nagata T., Takahashi H., Miyabara Y., Hanazato T., Ishizuka M., Isobe T., Kim J.-W. and Chang K.-H. (2013) Effects of polycyclic aromatic hydrocarbons (PAHs) on an aquatic ecosystem: acute toxicity and community-level toxic impact tests of benzo[a]pyrene using lake zooplankton community. *Journal of Toxicological Sciences* **38**, 131–136.
- Imfeld A., Ouellet A., Douglas P. M. J., Kos G. and Gélinas Y. (2022) Molecular and stable isotope analysis ($\delta^{13}\text{C}$, $\delta^2\text{H}$) of sedimentary n-alkanes in the St. Lawrence Estuary and Gulf, Quebec, Canada: Importance of even numbered n-alkanes in coastal systems. *Organic Geochemistry* **164**, 104367.
- Ishii S. K. L. and Boyer T. H. (2012) Behavior of Reoccurring PARAFAC Components in Fluorescent Dissolved Organic Matter in Natural and Engineered Systems: A Critical Review. *Environmental Science and Technology* **46**, 2006–2017.
- Ishiwatari R., Fujino N., Brincat D., Yamamoto S., Takahara H., Shichi K. and Krivonogov S. K. (2009) A 35kyr record of organic matter composition and $\delta^{13}\text{C}$ of n-alkanes in bog sediments close to Lake Baikal: Implications for paleoenvironmental studies. *Organic Geochemistry* **40**, 51–60.
- ITOPF (2018) Data & Statistics - ITOPF.
- Jaggi A., Snowdon R. W., Stopford A., Radović J. R., Oldenburg T. B. P. and Larter S. R. (2017) Experimental simulation of crude oil-water partitioning behavior of BTEX compounds during a deep submarine oil spill. *Organic Geochemistry* **108**, 1–8.
- Katrantsiotis C., Kylander M. E., Smittenberg R., Yamoah K. K. A., Hättestrand M., Avramidis P., Strandberg N. A. and Norström E. (2018) Eastern Mediterranean hydroclimate reconstruction over the last 3600 years based on sedimentary n-alkanes, their carbon and hydrogen isotope composition and XRF data from the Gialova Lagoon, SW Greece. *Quaternary Science Reviews* **194**, 77–93.
- Kennicutt M. C., Barker C., Brooks J. M., DeFreitas D. A. and Zhu G. H. (1987) Selected organic matter source indicators in the Orinoco, Nile and Changjiang deltas. *Organic Geochemistry* **11**, 41–51.
- Killops V. J. and Killops S. D. (2013) *Introduction to Organic Geochemistry.*, John Wiley & Sons.
- Knecht A. L., Goodale B. C., Truong L., Simonich M. T., Swanson A. J., Matzke M. M., Anderson K. A., Waters K. M. and Tanguay R. L. (2013) Comparative developmental toxicity of environmentally relevant oxygenated PAHs. *Toxicology and Applied Pharmacology* **271**, 266–275.
- Lamb A. L., Wilson G. P. and Leng M. J. (2006) A review of coastal palaeoclimate and relative sea-level reconstructions using $\delta^{13}\text{C}$ and C/N ratios in organic material. *Earth-Science Reviews* **75**, 29–57.

- Leenheer J. A. and Croué J.-P. (2003) Peer Reviewed: Characterizing Aquatic Dissolved Organic Matter. *Environmental Science and Technology* **37**, 18A-26A.
- Li C., Sessions A. L., Kinnaman F. S. and Valentine D. L. (2009) Hydrogen-isotopic variability in lipids from Santa Barbara Basin sediments. *Geochimica et Cosmochimica Acta* **73**, 4803–4823.
- Li M., Huang Y., Obermajer M., Jiang C., Snowdon L. R. and Fowler M. G. (2001) Hydrogen isotopic compositions of individual alkanes as a new approach to petroleum correlation: case studies from the Western Canada Sedimentary Basin. *Organic Geochemistry* **32**, 1387–1399.
- Li Y. and Xiong Y. (2009) Identification and quantification of mixed sources of oil spills based on distributions and isotope profiles of long-chain n-alkanes. *Marine Pollution Bulletin* **58**, 1868–1873.
- Li Y., Xiong Y., Yang W., Xie Y., Li S. and Sun Y. (2009) Compound-specific stable carbon isotopic composition of petroleum hydrocarbons as a tool for tracing the source of oil spills. *Marine Pollution Bulletin* **58**, 114–117.
- Li Y., Zhang Y., Li Z., Wan J., Dang C. and Fu J. (2022) Characterization of colored dissolved organic matter in the northeastern South China Sea using EEMs-PARAFAC and absorption spectroscopy. *Journal of Sea Research* **180**, 102159.
- Lichtfouse É., Derenne S., Mariotti A. and Largeau C. (1994) Possible algal origin of long chain odd n-alkanes in immature sediments as revealed by distributions and carbon isotope ratios. *Organic Geochemistry* **22**, 1023–1027.
- Liu M., Hu J., Lin Y., Ke H., Lian J., Xu Y., Chen K., Zheng H., Chen M. and Cai M. (2021) Full-depth profiles of PAHs in the Western South China Sea: Influence of Upwelling and Mesoscale Eddy. *Chemosphere* **263**, 127933.
- Lundstedt S., White P. A., Lemieux C. L., Lynes K. D., Lambert I. B., Öberg L., Haglund P. and Tysklind M. (2007) Sources, Fate, and Toxic Hazards of Oxygenated Polycyclic Aromatic Hydrocarbons (PAHs) at PAH- contaminated Sites. *Ambio* **36**, 475–486.
- Luo X., Mai B., Yang Q., Fu J., Sheng G. and Wang Z. (2004) Polycyclic aromatic hydrocarbons (PAHs) and organochlorine pesticides in water columns from the Pearl River and the Macao harbor in the Pearl River Delta in South China. *Marine Pollution Bulletin* **48**, 1102–1115.
- Magid J., Luxhøi J. and Lyshede O. B. (2004) Decomposition of plant residues at low temperatures separates turnover of nitrogen and energy rich tissue components in time. *Plant and Soil* **258**, 351–365.
- Marzi R., Torkelson B. E. and Olson R. K. (1993) A revised carbon preference index. *Organic Geochemistry* **20**, 1303–1306.

- Massicotte P. (2019) eemR: Tools for Pre-Processing Emission-Excitation-Matrix (EEM) Fluorescence Data. <https://github.com/PMassicotte/eemR>
- McKnight D. M., Boyer E. W., Westerhoff P. K., Doran P. T., Kulbe T. and Andersen D. T. (2001) Spectrofluorometric characterization of dissolved organic matter for indication of precursor organic material and aromaticity. *Limnology and Oceanography* **46**, 38–48.
- Menzie C. A., Potocki B. B. and Santodonato J. (1992) Exposure to carcinogenic PAHs in the environment. *Environmental Science and Technology* **26**, 1278–1284.
- Mille G., Asia L., Guiliano M., Malleret L. and Doumenq P. (2007) Hydrocarbons in coastal sediments from the Mediterranean sea (Gulf of Fos area, France). *Marine Pollution Bulletin* **54**, 566–575.
- Murphy K. R., Stedmon C. A., Graeber D. and Bro R. (2013) Fluorescence spectroscopy and multi-way techniques. PARAFAC. *Analytical Methods* **5**, 6557–6566.
- Murphy K. R., Stedmon C. A., Waite T. D. and Ruiz G. M. (2008) Distinguishing between terrestrial and autochthonous organic matter sources in marine environments using fluorescence spectroscopy. *Marine Chemistry* **108**, 40–58.
- Murray A. P., Edwards D., Hope J. M., Boreham C. J., Booth W. E., Alexander R. A. and Summons R. E. (1998) Carbon isotope biogeochemistry of plant resins and derived hydrocarbons. *Organic Geochemistry* **29**, 1199–1214.
- Nishimura M. and Baker E. W. (1986) Possible origin of n-alkanes with a remarkable even-to-odd predominance in recent marine sediments. *Geochimica et Cosmochimica Acta* **50**, 299–305.
- Odden W., Barth T. and Talbot M. R. (2002) Compound-specific carbon isotope analysis of natural and artificially generated hydrocarbons in source rocks and petroleum fluids from offshore Mid-Norway. *Organic Geochemistry* **33**, 47–65.
- Ohno T. (2002) Fluorescence Inner-Filtering Correction for Determining the Humification Index of Dissolved Organic Matter. *Environmental Science and Technology* **36**, 742–746.
- Packard T., Chen W., Blasco D., Savenkoff C., Vézina A. F., Tian R., St-Amand L., Roy S. O., Lovejoy C., Klein B., Therriault J.-C., Legendre L. and Ingram R. G. (2000) Dissolved organic carbon in the Gulf of St. Lawrence. *Deep Sea Research Part II: Topical Studies in Oceanography* **47**, 435–459.
- Pearson A. and Eglinton T. I. (2000) The origin of n-alkanes in Santa Monica Basin surface sediment: a model based on compound-specific $\Delta^{14}\text{C}$ and d^{13}C data. *Organic Geochemistry*, 14.
- Pearson A., McNichol A. P., Benitez-Nelson B. C., Hayes J. M. and Eglinton T. I. (2001) Origins of lipid biomarkers in Santa Monica Basin surface sediment: a case study using compound-specific $\Delta^{14}\text{C}$ analysis. *Geochimica et Cosmochimica Acta* **65**, 3123–3137.

- Pedentchouk N. and Turich C. (2018) Carbon and hydrogen isotopic compositions of n-alkanes as a tool in petroleum exploration. *Geological Society, London, Special Publications* **468**, 105–125.
- Perera F. P., Whyatt R. M., Jedrychowski W., Rauh V., Manchester D., Santella R. M. and Ottman R. (1998) Recent developments in molecular epidemiology: A study of the effects of environmental polycyclic aromatic hydrocarbons on birth outcomes in Poland. *American Journal of Epidemiology* **147**, 309–314.
- Peters K. E., Sweeney R. E. and Kaplan I. R. (1978) Correlation of carbon and nitrogen stable isotope ratios in sedimentary organic matter 1. *Limnology and Oceanography* **23**, 598–604.
- Peters K. E., Walters C. C. and Moldowan J. M. (2005) *The Biomarker Guide: Biomarkers and isotopes in the environment and human history.*, Cambridge University Press.
- Pham T.-T. and Proulx S. (1997) PCBs and PAHs in the Montreal Urban Community (Quebec, Canada) wastewater treatment plant and in the effluent plume in the St Lawrence River. *Water Research* **31**, 1887–1896.
- Pham T.-T., Proulx S., Brochu C. and Moore S. (1999) Composition of PCBs and PAHs in the Montreal Urban Community Wastewater and in the Surface Water of the St. Lawrence River (Canada). *Water, Air, & Soil Pollution* **111**, 251–270.
- Poynter J. and Eglinton G. (1990) Molecular composition of sediments from ODP Hole 116-717C. *Proceedings of the Ocean Drilling Program, distal Bengal Fan; covering Leg 116 of the cruises of the drilling vessel JOIDES Resolution, Colombo, Sri Lanka, to Colombo, Sri Lanka, sites 717-719, 2 July 1987-19 August 1987.*
- Prince R. C., Garrett R. M., Bare R. E., Grossman M. J., Townsend T., Suflita J. M., Lee K., Owens E. H., Sergy G. A., Braddock J. F., Lindstrom J. E. and Lessard R. R. (2003) The Roles of Photooxidation and Biodegradation in Long-term Weathering of Crude and Heavy Fuel Oils. *Spill Science & Technology Bulletin* **8**, 145–156.
- Pucher M., Wunsch U., Weigelhofer G., Murphy K., Hein T. and Graeber D. (2019) staRdom: Versatile Software for Analyzing Spectroscopic Data of Dissolved Organic Matter in R. *Water* **11**, 2366.
- Sachse D., Billault I., Bowen G. J., Chikaraishi Y., Dawson T. E., Feakins S. J., Freeman K. H., Magill C. R., McInerney F. A., van der Meer M. T. J., Polissar P., Robins R. J., Sachs J. P., Schmidt H.-L., Sessions A. L., White J. W. C., West J. B. and Kahmen A. (2012) Molecular Paleohydrology: Interpreting the Hydrogen-Isotopic Composition of Lipid Biomarkers from Photosynthesizing Organisms. *Annual Review of Earth and Planetary Sciences* **40**, 221–249.
- Sachse D., Radke J. and Gleixner G. (2006) δD values of individual n-alkanes from terrestrial plants along a climatic gradient – Implications for the sedimentary biomarker record. *Organic Geochemistry* **37**, 469–483.

- Schlanser K. M., Diefendorf A. F., West C. K., Greenwood D. R., Basinger J. F., Meyer H. W., Lowe A. J. and Naake H. H. (2020) Conifers are a major source of sedimentary leaf wax n-alkanes when dominant in the landscape: Case studies from the Paleogene. *Organic Geochemistry* **147**, 104069.
- Sessions A. L., Burgoyne T. W., Schimmelmann A. and Hayes J. M. (1999) Fractionation of hydrogen isotopes in lipid biosynthesis. *Organic Geochemistry* **30**, 1193–1200.
- Sessions A. L., Jahnke L. L., Schimmelmann A. and Hayes J. M. (2002) Hydrogen isotope fractionation in lipids of the methane-oxidizing bacterium *Methylococcus capsulatus*. *Geochimica et Cosmochimica Acta* **66**, 3955–3969.
- Shen G., Tao S., Wang Wei, Yang Y., Ding J., Xue M., Min Y., Zhu C., Shen H., Li W., Wang B., Wang R., Wang Wentao, Wang X. and Russell A. G. (2011) Emission of Oxygenated Polycyclic Aromatic Hydrocarbons from Indoor Solid Fuel Combustion. *Environmental Science and Technology* **45**, 3459–3465.
- Silliman J. E., Meyers P. A., Ostrom P. H., Ostrom N. E. and Eadie B. J. (2000) Insights into the origin of perylene from isotopic analyses of sediments from Saanich Inlet, British Columbia. *Organic Geochemistry* **31**, 1133–1142.
- Silva T. R., Lopes S. R. P., Spörl G., Knoppers B. A. and Azevedo D. A. (2012) Source characterization using molecular distribution and stable carbon isotopic composition of n-alkanes in sediment cores from the tropical Mundaú–Manguaba estuarine–lagoon system, Brazil. *Organic Geochemistry* **53**, 25–33.
- Simpson C. D., Mosi A. A., Cullen W. R. and Reimer K. J. (1996) Composition and distribution of polycyclic aromatic hydrocarbon contamination in surficial marine sediments from Kitimat Harbor, Canada. *Science of The Total Environment* **181**, 265–278.
- Singh S., D'Sa E. J. and Swenson E. M. (2010) Chromophoric dissolved organic matter (CDOM) variability in Barataria Basin using excitation–emission matrix (EEM) fluorescence and parallel factor analysis (PARAFAC). *Science of The Total Environment* **408**, 3211–3222.
- Smith B. N. and Epstein S. (1971) Two categories of c/c ratios for higher plants. *Plant Physiology* **47**, 380–384.
- Smith J. N. and Schafer C. T. (1999) Sedimentation, bioturbation, and Hg uptake in the sediments of the estuary and Gulf of St. Lawrence. *Limnology and Oceanography* **44**, 207–219.
- Sojinu S. O., Sonibare O. O., Ekundayo O. and Zeng E. Y. (2012) Assessing anthropogenic contamination in surface sediments of Niger Delta, Nigeria with fecal sterols and n-alkanes as indicators. *Science of The Total Environment* **441**, 89–96.
- Stedmon C. A. and Bro R. (2008) Characterizing dissolved organic matter fluorescence with parallel factor analysis: a tutorial. *Limnology and Oceanography: Methods* **6**, 572–579.

- Stedmon C. A. and Markager S. (2005) Resolving the variability in dissolved organic matter fluorescence in a temperate estuary and its catchment using PARAFAC analysis. *Limnology and Oceanography* **50**, 686–697.
- Stedmon C. A., Markager S. and Bro R. (2003) Tracing dissolved organic matter in aquatic environments using a new approach to fluorescence spectroscopy. *Marine Chemistry* **82**, 239–254.
- Stedmon C. A., Thomas D. N., Granskog M., Kaartokallio H., Papadimitriou S. and Kuosa H. (2007) Characteristics of Dissolved Organic Matter in Baltic Coastal Sea Ice: Allochthonous or Autochthonous Origins? *Environmental Science & Technology* **41**, 7273–7279.
- Strobel P., Haberzettl T., Bliedtner M., Struck J., Glaser B., Zech M. and Zech R. (2020) The potential of $\delta^2\text{H}$ n-alkanes and $\delta^{18}\text{O}$ sugar for paleoclimate reconstruction - A regional calibration study for South Africa. *Science of the Total Environment* **716**, 137045.
- Tan F. C. and Strain P. M. (1979) Organic carbon isotope ratios in recent sediments in the St Lawrence Estuary and the Gulf of St Lawrence. *Estuarine and Coastal Marine Science* **8**, 213–225.
- Tan F. C. and Strain P. M. (1983) Sources, sinks and distribution of organic carbon in the St. Lawrence Estuary, Canada. *Geochimica et Cosmochimica Acta* **47**, 125–132.
- Tfaily M. M., Corbett J. E., Wilson R., Chanton J. P., Glaser P. H., Cawley K. M., Jaffé R. and Cooper W. T. (2015) Utilization of PARAFAC-Modeled Excitation-Emission Matrix (EEM) Fluorescence Spectroscopy to Identify Biogeochemical Processing of Dissolved Organic Matter in a Northern Peatland. *Photochemistry and Photobiology* **91**, 684–695.
- The St. Lawrence Seaway Management Corporation (2021) About Hwy H₂O. <https://hwyh2o.com/about-hwy-h2o/>
- Thomas J. (2014) Variabilité spatiale et temporelle des propriétés optiques et chimiques de la matière organique dissoute dans les rivières de la Côte-Nord, Québec, Canada. Masters, Université du Québec à Rimouski.
- Thornton S. F. and McManus J. (1994) Application of Organic Carbon and Nitrogen Stable Isotope and C/N Ratios as Source Indicators of Organic Matter Provenance in Estuarine Systems: Evidence from the Tay Estuary, Scotland. *Estuarine, Coastal and Shelf Science* **38**, 219–233.
- Tissot B. P. and Welte D. H. (1984) Diagenesis, Catagenesis and Metagenesis of Organic Matter. In *Petroleum Formation and Occurrence* (eds. B. P. Tissot and D. H. Welte). Springer, Berlin, Heidelberg. pp. 69–73.
- Traina S. J., Novak J. and Smeck N. E. (1990) An Ultraviolet Absorbance Method of Estimating the Percent Aromatic Carbon Content of Humic Acids. *Journal of Environmental Quality* **19**, 151–153.

- Twichell S. C., Meyers P. A. and Diester-Haass L. (2002) Significance of high C/N ratios in organic-carbon-rich Neogene sediments under the Benguela Current upwelling system. *Organic Geochemistry* **33**, 715–722.
- Volkman J. K., Farrington J. W. and Gagosian R. B. (1987) Marine and terrigenous lipids in coastal sediments from the Peru upwelling region at 15°S: Sterols and triterpene alcohols. *Organic Geochemistry* **11**, 463–477.
- Wakeham S. G., Forrest J., Masiello C. A., Gélinas Y., Alexander C. R. and Leavitt P. R. (2004) Hydrocarbons in Lake Washington Sediments. A 25-Year Retrospective in an Urban Lake. *Environmental Science and Technology* **38**, 431–439.
- Wakeham S. G., Lee C., Hedges J. I., Hernes P. J. and Peterson M. J. (1997) Molecular indicators of diagenetic status in marine organic matter. *Geochimica et Cosmochimica Acta* **61**, 5363–5369.
- Wakeham S. G., Schaffner C. and Giger W. (1980) Poly cyclic aromatic hydrocarbons in Recent lake sediments—II. Compounds derived from biogenic precursors during early diagenesis. *Geochimica et Cosmochimica Acta* **44**, 415–429.
- Wang J.-Z., Yang Z.-Y. and Chen T.-H. (2012) Source apportionment of sediment-associated aliphatic hydrocarbon in a eutrophicated shallow lake, China. *Environmental Science and Pollution Research* **19**, 4006–4015.
- Wang S., Liu G., Yuan Z. and Da C. (2018) n-Alkanes in sediments from the Yellow River Estuary, China: Occurrence, sources and historical sedimentary record. *Ecotoxicology and Environmental Safety* **150**, 199–206.
- Wang Yongli, Fang X., Zhang T., Li Y., Wu Y., He D. and Wang Youxiao (2010) Predominance of even carbon-numbered n-alkanes from lacustrine sediments in Linxia Basin, NE Tibetan Plateau: Implications for climate change. *Applied Geochemistry* **25**, 1478–1486.
- Weishaar J. L., Aiken G. R., Bergamaschi B. A., Fram M. S., Fujii R. and Mopper K. (2003) Evaluation of Specific Ultraviolet Absorbance as an Indicator of the Chemical Composition and Reactivity of Dissolved Organic Carbon. *Environmental Science and Technology* **37**, 4702–4708.
- Whitby H., Planquette H., Cassar N., Bucciarelli E., Osburn C. L., Janssen D. J., Cullen J. T., González A. G., Völker C. and Sarthou G. (2020) A call for refining the role of humic-like substances in the oceanic iron cycle. *Scientific Reports* **10**, 6144.
- Yamamoto S., Kawamura K., Seki O., Meyers P. A., Zheng Y. and Zhou W. (2010) Paleoenvironmental significance of compound-specific $\delta^{13}\text{C}$ variations in n-alkanes in the Hongyuan peat sequence from southwest China over the last 13ka. *Organic Geochemistry* **41**, 491–497.

- Yu H. (2002) Environmental carcinogenic polycyclic aromatic hydrocarbons: photochemistry and phototoxicity. *Journal of environmental science and health. Part C, Environmental carcinogenesis & ecotoxicology reviews* **20**, 149–183.
- Zhang X., Gillespie A. L. and Sessions A. L. (2009) Large D/H variations in bacterial lipids reflect central metabolic pathways. *Proceedings of the National Academy of Sciences* **106**, 12580–12586.
- Zhang Z. and Sachs J. P. (2007) Hydrogen isotope fractionation in freshwater algae: I. Variations among lipids and species. *Organic Geochemistry* **38**, 582–608.
- Zhou Z. and Guo L. (2012) Evolution of the optical properties of seawater influenced by the Deepwater Horizon oil spill in the Gulf of Mexico. *Environmental Research Letters* **7**, 025301.
- Zhou Z., Guo L., Shiller A. M., Lohrenz S. E., Asper V. L. and Osburn C. L. (2013) Characterization of oil components from the Deepwater Horizon oil spill in the Gulf of Mexico using fluorescence EEM and PARAFAC techniques. *Marine Chemistry* **148**, 10–21.
- Zsolnay A., Baigar E., Jimenez M., Steinweg B. and Saccomandi F. (1999) Differentiating with fluorescence spectroscopy the sources of dissolved organic matter in soils subjected to drying. *Chemosphere* **38**, 45–50.

Appendix A

Supplemental Material for:

Complete molecular and stable isotope analysis ($\delta^{13}\text{C}$, $\delta^2\text{H}$) of sedimentary *n*-alkanes in coastal systems: the importance of even numbered *n*-alkanes in the St. Lawrence Estuary and Gulf, Quebec, Canada

(A. Imfeld, A. Ouellet, P. Douglas, G. Kos, and Y. G  linas)

This section presents the individual concentrations for the *n*-alkanes ($n\text{C}_{17}$ to $n\text{C}_{36}$) extracted at each station, Table A.1, as well as the individual $\delta^{13}\text{C}$ and $\delta^2\text{H}$ of $n\text{C}_{23}$ to $n\text{C}_{36}$ in Table A.2 and A.3 respectively. Additional visual graphics are included to show the relationship of the TAR values calculated using the two different methods and the bulk $\delta^{13}\text{C}$ values in Figure A.1, as well as the relationship between the bulk $\delta^{13}\text{C}$ and bulk $\delta^{15}\text{N}$, Figure A.2.

Table A.1 Concentration ($\mu\text{g/gOC}$) and standard deviation of individual n -alkanes at each station ($n=3$)

n -alkane	Station								
	Sag05	DE	G	25	23	21	18.5	18	16
$n\text{C}_{17}$	8.84 ± 1.1	11.36 ± 1.9	10.34 ± 0.87	9.21 ± 0.13	5.90 ± 0.36	4.82 ± 0.44	4.20 ± 0.41	4.31 ± 0.03	3.00 ± 0.24
$n\text{C}_{18}$	6.94 ± 0.96	7.90 ± 1.18	7.09 ± 0.57	9.61 ± 0.08	5.36 ± 0.32	4.45 ± 0.35	3.72 ± 0.34	5.06 ± 0.07	4.17 ± 0.23
$n\text{C}_{19}$	7.47 ± 0.93	8.03 ± 1.32	7.30 ± 0.54	7.60 ± 0.13	4.83 ± 0.23	3.98 ± 0.36	3.23 ± 0.27	3.31 ± 0.07	2.34 ± 0.13
$n\text{C}_{20}$	6.95 ± 0.93	7.92 ± 1.44	6.88 ± 0.54	10.86 ± 0.32	5.72 ± 0.20	4.84 ± 0.51	3.64 ± 0.25	5.53 ± 0.12	4.84 ± 0.33
$n\text{C}_{21}$	11.58 ± 1.18	13.47 ± 2.17	12.86 ± 0.88	12.65 ± 0.20	8.66 ± 0.40	7.02 ± 0.60	4.44 ± 0.31	4.30 ± 0.09	3.68 ± 0.28
$n\text{C}_{22}$	8.83 ± 1.01	12.59 ± 3.57	11.27 ± 0.63	15.72 ± 0.42	9.03 ± 0.40	7.31 ± 0.55	4.79 ± 0.35	7.18 ± 0.04	6.36 ± 0.43
$n\text{C}_{23}$	17.43 ± 2.20	27.90 ± 4.77	28.60 ± 2.46	25.95 ± 0.54	17.66 ± 0.64	13.67 ± 1.23	7.41 ± 0.57	5.88 ± 0.10	5.80 ± 0.47
$n\text{C}_{24}$	8.74 ± 1.33	12.41 ± 2.29	12.70 ± 1.18	17.21 ± 0.22	10.10 ± 0.52	7.91 ± 0.83	5.07 ± 0.35	7.04 ± 0.03	6.70 ± 0.48
$n\text{C}_{25}$	29.37 ± 3.95	42.65 ± 7.23	40.43 ± 3.46	33.64 ± 0.97	24.67 ± 1.24	18.21 ± 1.75	9.76 ± 0.95	7.24 ± 0.14	8.01 ± 0.70
$n\text{C}_{26}$	9.12 ± 1.15	13.48 ± 2.64	13.95 ± 1.12	17.88 ± 0.22	11.34 ± 0.37	8.87 ± 0.80	5.50 ± 0.40	6.85 ± 0.09	6.86 ± 0.51
$n\text{C}_{27}$	54.49 ± 7.05	69.29 ± 11.01	59.98 ± 4.88	51.58 ± 1.42	37.87 ± 1.57	29.22 ± 2.72	15.62 ± 1.31	11.22 ± 0.29	13.36 ± 1.10
$n\text{C}_{28}$	8.93 ± 1.14	13.35 ± 2.25	13.73 ± 0.85	17.73 ± 0.28	10.85 ± 0.57	8.22 ± 0.99	5.22 ± 0.34	5.92 ± 0.12	6.18 ± 0.47
$n\text{C}_{29}$	46.43 ± 6.22	73.90 ± 12.09	63.31 ± 4.94	52.86 ± 0.95	38.61 ± 1.44	30.04 ± 2.96	17.82 ± 1.48	13.48 ± 0.34	17.45 ± 1.21
$n\text{C}_{30}$	6.49 ± 0.71	9.55 ± 1.59	9.96 ± 0.60	14.82 ± 0.92	9.21 ± 0.31	7.28 ± 0.61	4.51 ± 0.28	4.71 ± 0.14	4.88 ± 0.48
$n\text{C}_{31}$	31.42 ± 3.67	55.86 ± 8.61	51.35 ± 3.69	45.52 ± 0.88	33.00 ± 2.00	25.40 ± 2.96	15.60 ± 1.09	11.94 ± 0.32	15.54 ± 1.14
$n\text{C}_{32}$	5.95 ± 0.58	7.32 ± 1.30	8.00 ± 0.63	12.20 ± 0.70	7.41 ± 0.57	6.18 ± 0.78	4.16 ± 0.16	3.53 ± 0.10	4.07 ± 0.31
$n\text{C}_{33}$	12.82 ± 1.24	19.29 ± 2.93	18.38 ± 0.84	18.91 ± 0.42	13.83 ± 0.42	11.31 ± 1.16	7.16 ± 0.47	5.20 ± 0.14	6.48 ± 0.49
$n\text{C}_{34}$	3.64 ± 0.30	3.74 ± 0.83	4.24 ± 0.53	7.58 ± 0.13	4.32 ± 0.31	3.57 ± 0.59	2.08 ± 0.11	1.91 ± 0.16	1.95 ± 0.13
$n\text{C}_{35}$	4.56 ± 0.38	6.16 ± 0.97	6.41 ± 0.66	7.44 ± 0.41	5.10 ± 0.21	3.98 ± 0.43	2.40 ± 0.14	1.48 ± 0.12	1.68 ± 0.13
$n\text{C}_{36}$	3.03 ± 0.35	2.46 ± 0.40	3.50 ± 0.79	6.22 ± 0.12	3.07 ± 0.53	2.30 ± 0.23	1.33 ± 0.15	1.03 ± 0.10	1.04 ± 0.04

Table A.2 $\delta^{13}\text{C}$ value (‰) and standard deviation of individual *n*-alkanes at each station (n=3)

<i>n</i> -alkane	Station								
	Sag05	DE	G	25	23	21	18.5	18	16
<i>n</i> C ₂₃	-32.53 ± 0.45	-31.01 ± 0.08	-31.25 ± 0.44	-30.57 ± 0.08	-31.39 ± 0.22	-30.87 ± 0.22	-29.99 ± 0.62	-30.22 ± 0.96	-30.62 ± 1.50
<i>n</i> C ₂₄	-31.49 ± 0.19	-31.51 ± 0.09	-31.78 ± 0.22	-29.40 ± 0.17	-30.08 ± 0.44	-30.02 ± 0.19	-30.22 ± 0.22	-28.09 ± 0.40	-27.95 ± 0.41
<i>n</i> C ₂₅	-32.93 ± 0.28	-31.87 ± 0.33	-31.76 ± 0.28	-31.25 ± 0.20	-31.51 ± 0.23	-31.24 ± 0.43	-31.12 ± 0.30	-31.31 ± 0.13	-30.60 ± 0.22
<i>n</i> C ₂₆	-31.73 ± 0.20	-31.87 ± 0.12	-31.91 ± 0.22	-29.97 ± 0.17	-30.58 ± 0.36	-30.36 ± 0.18	-30.41 ± 0.21	-28.56 ± 0.20	-28.55 ± 0.22
<i>n</i> C ₂₇	-33.37 ± 0.12	-32.66 ± 0.86	-32.47 ± 0.60	-31.73 ± 0.25	-31.42 ± 0.10	-31.25 ± 0.35	-31.13 ± 0.33	-31.13 ± 0.23	-30.75 ± 0.12
<i>n</i> C ₂₈	-32.16 ± 0.19	-32.47 ± 0.30	-32.58 ± 0.34	-30.48 ± 0.38	-31.06 ± 0.35	-30.57 ± 0.51	-30.52 ± 0.40	-29.13 ± 0.38	-29.19 ± 0.07
<i>n</i> C ₂₉	-33.83 ± 0.21	-33.40 ± 0.94	-33.50 ± 1.07	-31.80 ± 0.10	-32.53 ± 0.66	-31.71 ± 0.40	-31.43 ± 0.48	-31.36 ± 0.27	-31.20 ± 0.76
<i>n</i> C ₃₀	-31.95 ± 0.30	-33.02 ± 0.16	-32.82 ± 0.04	-30.20 ± 0.50	-30.46 ± 0.67	-30.58 ± 0.49	-30.42 ± 0.52	-29.99 ± 0.24	-29.29 ± 0.36
<i>n</i> C ₃₁	-33.63 ± 0.17	-34.28 ± 0.71	-34.08 ± 0.20	-32.35 ± 0.42	-32.56 ± 0.16	-32.44 ± 0.19	-31.26 ± 0.41	-31.71 ± 0.29	-31.20 ± 0.43
<i>n</i> C ₃₂	-31.71 ± 0.05	-32.71 ± 0.31	-32.83 ± 0.27	-30.58 ± 0.68	-31.06 ± 0.31	-30.90 ± 0.32	-30.41 ± 0.48	-29.91 ± 0.21	-29.37 ± 0.08
<i>n</i> C ₃₃	-33.29 ± 0.49	-33.33 ± 0.27	-33.24 ± 0.37	-31.62 ± 0.28	-32.47 ± 0.53	-31.76 ± 0.36	-31.02 ± 0.25	-31.26 ± 0.20	-30.28 ± 0.31
<i>n</i> C ₃₄	-31.38 ± 0.64	-31.41 ± 0.11	-31.74 ± 0.21	-30.09 ± 0.13	-30.10 ± 0.17	-30.17 ± 0.59	-29.87 ± 0.89	-29.33 ± 0.51	-28.36 ± 0.31
<i>n</i> C ₃₅	-32.22 ± 0.52	-32.02 ± 0.28	-32.94 ± 0.66	-31.28 ± 0.48	-31.77 ± 0.69	-30.69 ± 0.68	-30.06 ± 0.85	-30.59 ± 0.96	-30.24 ± 0.69
<i>n</i> C ₃₆	-31.35 ± 0.53	-31.75 ± 0.28	-32.05 ± 0.80	-29.76 ± 1.12	-30.30 ± 0.37	-29.02 ± 1.68	-29.30 ± 0.31	-28.95 ± 0.94	-28.37 ± 0.38

Table A.3 $\delta^2\text{H}$ value (‰) and standard deviation of individual *n*-alkanes at each station (n=3)

<i>n</i> -alkane	Station								
	Sag05	DE	G	25	23	21	18.5	18	16
<i>n</i> C ₂₃	-198.78 ± 6.58	-189.51 ± 1.01	-187.74 ± 3.61	-188.85 ± 4.44	-184.91 ± 4.10	-183.07 ± 1.71	-174.08 ± 9.81	-151.12 ± 6.11	-150.25 ± 19.94
<i>n</i> C ₂₄	-182.38 ± 1.20	-172.66 ± 5.74	-183.71 ± 2.70	-124.58 ± 0.68	-136.88 ± 3.14	-135.14 ± 2.16	-137.85 ± 3.16	-96.64 ± 6.51	-89.06 ± 9.74
<i>n</i> C ₂₅	-210.47 ± 2.00	-198.94 ± 1.04	-200.10 ± 2.11	-197.62 ± 0.44	-196.82 ± 3.32	-190.79 ± 1.58	-180.10 ± 4.53	-166.42 ± 2.19	-172.08 ± 5.61
<i>n</i> C ₂₆	-172.57 ± 2.79	-169.93 ± 1.19	-172.16 ± 2.06	-138.02 ± 0.69	-148.81 ± 1.46	-148.21 ± 0.73	-133.23 ± 2.55	-96.20 ± 2.16	-106.99 ± 3.44
<i>n</i> C ₂₇	-209.26 ± 1.44	-202.23 ± 1.09	-202.43 ± 1.11	-198.36 ± 0.59	-199.10 ± 1.55	-194.93 ± 1.72	-186.36 ± 2.23	-175.00 ± 2.54	-179.43 ± 2.46
<i>n</i> C ₂₈	-161.76 ± 2.44	-167.17 ± 1.70	-166.35 ± 1.70	-140.22 ± 0.95	-148.42 ± 1.28	-143.87 ± 3.52	-136.57 ± 1.12	-103.97 ± 3.27	-115.67 ± 1.80
<i>n</i> C ₂₉	-204.80 ± 1.88	-202.47 ± 1.46	-201.17 ± 0.78	-197.07 ± 0.18	-196.41 ± 1.75	-192.92 ± 1.48	-182.65 ± 1.86	-172.22 ± 2.89	-177.02 ± 1.08
<i>n</i> C ₃₀	-141.13 ± 2.74	-148.29 ± 0.44	-147.22 ± 1.51	-125.56 ± 3.65	-129.45 ± 2.00	-128.33 ± 1.41	-121.56 ± 1.04	-99.19 ± 3.25	-111.42 ± 0.45
<i>n</i> C ₃₁	-192.89 ± 1.00	-191.81 ± 2.58	-190.76 ± 0.61	-186.76 ± 0.72	-189.89 ± 4.78	-181.04 ± 2.06	-177.89 ± 2.75	-170.20 ± 6.18	-177.92 ± 6.75
<i>n</i> C ₃₂	-138.64 ± 3.08	-139.34 ± 3.07	-144.74 ± 9.38	-117.59 ± 0.45	-120.50 ± 3.64	-124.52 ± 0.58	-117.42 ± 3.59	-94.73 ± 2.77	-104.53 ± 1.87
<i>n</i> C ₃₃	-177.78 ± 5.06	-177.89 ± 2.73	-176.96 ± 3.29	-170.91 ± 2.29	-166.55 ± 3.39	-169.20 ± 5.32	-159.26 ± 3.21	-148.07 ± 3.84	-157.96 ± 1.85
<i>n</i> C ₃₄	-106.51 ± 4.79	-105.90 ± 2.93	-109.44 ± 1.79	-97.82 ± 4.01	-98.16 ± 3.29	-103.22 ± 2.15	-97.85 ± 7.13	-75.20 ± 3.87	-89.50 ± 7.64
<i>n</i> C ₃₅	-125.67 ± 6.69	-132.83 ± 2.18	-130.55 ± 0.33	-125.34 ± 0.61	-123.31 ± 3.22	-124.19 ± 3.28	-121.56 ± 2.57	-110.92 ± 2.78	-122.07 ± 2.42
<i>n</i> C ₃₆	-102.21 ± 3.65	-98.37 ± 11.21	-107.82 ± 2.58	-96.20 ± 2.63	-91.97 ± 5.22	-100.38 ± 3.67	-92.03 ± 5.75	-72.63 ± 3.78	-76.91 ± 6.34

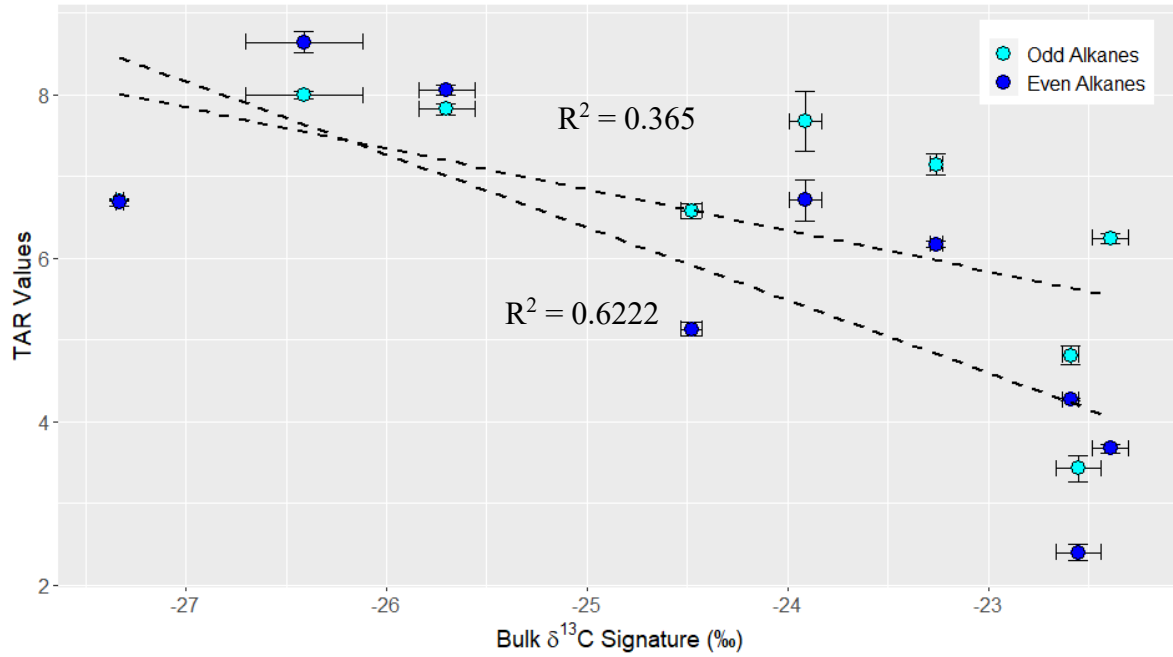


Figure A.1 Regression of TAR values vs bulk carbon isotope values, R^2 values shown for TAR values calculated with odd n -alkanes compared to even n -alkanes in the denominator. Error bars represent standard deviations.

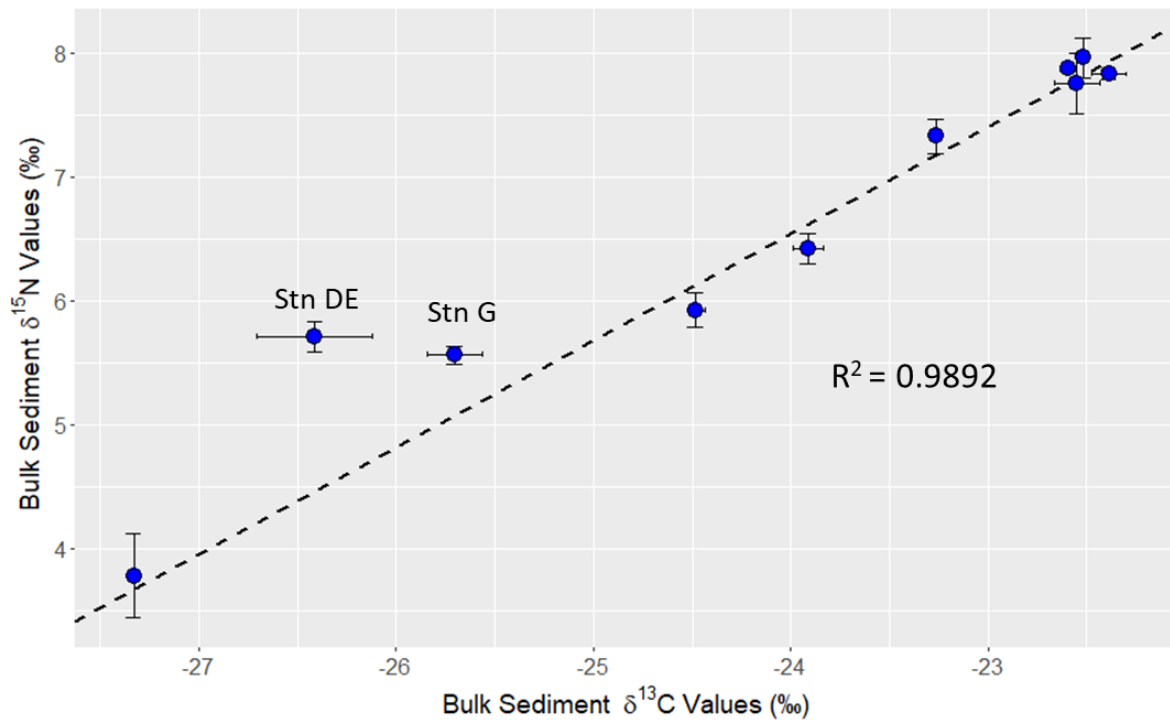


Figure A.0.2 Relationship between bulk nitrogen and carbon isotope values with regression not including stations DE and G. Error bars represent standard deviations.

Appendix B

Supplemental Material for:

Tracking changes in dissolved organic matter along the St. Lawrence River, Estuary and Gulf using PARAFAC analysis, and distinguishing natural organic matter from oil-derived compounds

(A. Imfeld, L. Hounjet, C. Guéguen, G. Chaillou, A. Ouellet, and Y. Gélinas)

Table B.1 Traditional nomenclature for stations samples, along with the name assigned for the purpose of this paper, as well as longitude, latitude, depth, bottom depth, salinity, DOC, temperature, dissolved oxygen transmissivity and density for each sample collected

Traditional Name	Name in this Paper	Year	Latitude (degree)	Longitude (degree)	Depth (m)	Water Column Depth (m)	Salinity (p.s.u)	DOC (mg/L)	Temp. (°C)	Dissolved Oxygen (µM)	Transmissivity (%)	Density
Stn St-Fulgence	S1	2017	48.4211	-70.8577	2	69	6.2	6.4	12.2	302.3	69.4	4.3
Stn St-Fulgence	S1	2017	48.4211	-70.8577	9	69	21.5	2.6	2.6	312.5	90.1	16.7
Stn St-Fulgence	S1	2017	48.4211	-70.8577	60	69	27.4	2.2	1.0	286.0	95.1	21.9
Stn Sag 05	S2	2017	48.4125	-70.8210	3	89	5.8	6.3	12.3	300.3	68.9	3.9
Stn Sag 20	S4	2017	48.3703	-70.5763	2	259	6.1	6.3	12.6	319.1	73.0	4.1
Stn Sag 20	S4	2017	48.3703	-70.5763	100	259	28.1	1.9	1.5	282.5	95.8	22.5
Stn Sag 20	S4	2017	48.3703	-70.5763	245	259	29.8	1.6	2.5	237.7	93.2	23.8
Stn Sag 30	S5	2017	48.3593	-70.3899	2	268	5.7	5.5	12.8	311.3	73.2	3.9
Stn Sag 30	S5	2017	48.3593	-70.3899	100	268	28.3	1.4	1.9	278.2	95.7	22.6
Stn Sag 30	S5	2017	48.3593	-70.3899	253	268	29.9	1.2	2.5	237.7	92.8	23.8
Stn Sag 42	S7	2017	48.2288	-69.9133	2	157	7.9	5.4	11.7	310.1	81.1	5.6
Stn Sag 48	S8	2017	48.1357	-69.7479	3	184	16.2	3.9	8.2	305.9	85.3	11.8
Stn St-Ignace	R1	2017	46.0553	-73.1225	2	12.5	0.1	3.3				
Stn Lac St-Pierre	R2	2017	46.1848	-72.8640	2	12.5	0.1	2.9				
Stn Nicolet	R3	2017	46.2587	-72.6657	2	12.5	0.1	2.9	23.3			
Stn R. St-Maurice	P1	2017	46.2587	-72.6657	2	12.5	0.1	5.9	22.9			
Stn Trois-Rivières	R4	2017	46.3277	-72.5408	2	12.5	0.1	3.1	22.7			
Stn Lac St-Pierre-les-Becquets	R5	2017	46.4725	-72.2508	2	12.5	0.1	3.6	22.9			
Stn Grondines	R6	2017	46.5768	-72.0427	2	12.5	0.1	3.7	22.8			
Stn Porneuf	R7	2017	46.6800	-71.8617	2	12.5	0.1	3.4	22.8			
Stn Plage Maurice	R8	2017	46.6530	-71.7550	2	12.5	0.1	3.4	22.8			
Stn B	E2	2017	46.9138	-70.8754	3	22	0.1	3.4	17.9	278.1	49.5	0.0
Stn D	E3	2017	47.1294	-70.6843	2	10	4.8	3.4	14.7	272.2	0.4	2.8

Stn DE	E4	2017	47.1794	-70.6199	3	17	3.0	3.3	15.7	275.4	0.6	1.5
Stn DE	E4	2017	47.1794	-70.6199	15	17	7.9	2.9	13.4	276.7	1.4	5.4
Stn E	E5	2017	47.2437	-70.5562	2	29	4.6	2.6	15.5	275.1	0.7	2.9
Stn E	E5	2017	47.2437	-70.5562	25	29	13.3	3.2	10.6	283.6	10.2	10.1
Stn F1	E6	2017	47.4080	-70.2822	3	47	8.5	2.7	13.0	284.7	8.9	6.0
Stn F1	E6	2017	47.4080	-70.2822	28	47	14.6	2.2	10.0	287.1	4.5	11.1
Stn H	E8	2017	47.5952	-70.0016	3	62	19.1	1.8	7.8	293.1	48.0	14.7
Stn J	E9	2017	47.9176	-69.7769	3	128	18.6	1.8	9.1	293.2	56.0	14.3
Stn J	E9	2017	47.9176	-69.7769	119	128	30.4	0.8	1.3	290.5	87.6	24.4
Stn K	E12	2017	48.1136	-69.4174	3	104	24.2	1.7	5.2	288.5	72.2	19.2
Stn K	E12	2017	48.1136	-69.4174	50	104	30.8	0.9	1.5	273.9	89.3	24.6
Stn 25	E13	2017	48.2923	-69.3817	3	325	26.7	1.5	4.7	297.7	90.0	21.1
Stn 25	E13	2017	48.2923	-69.3817	50	325	31.3	0.9	0.3	315.0	95.7	25.1
Stn 25	E13	2017	48.2923	-69.3817	300	325	34.4	0.5	5.3	52.8	80.5	27.1
Stn 25	E13	2017	48.2923	-69.3817	322	325	34.4	0.6	5.3	52.6	78.6	27.1
Stn 23	E19	2017	48.7013	-68.6514	2	345	25.2	1.5	6.7	296.3	81.4	19.7
Stn 23	E19	2017	48.7013	-68.6514	60	345	31.9	0.6	0.0	294.4	96.1	25.6
Stn 23	E19	2017	48.7013	-68.6514	300	345	34.4	0.5	5.5	46.3	95.2	27.2
Stn 23	E19	2017	48.7013	-68.6514	335	345	34.5	0.5	5.5	45.1	89.5	27.2
Stn Panache R. Outardes	P2	2017	48.9918	-68.5900	2		16.7	4.9	9.6	321.9	85.0	12.8
Stn 22.5N	E20	2017	48.9830	-68.5215	2		23.2	1.8	7.2	324.9	81.5	18.0
Stn 22	E21	2017	48.9340	-68.0923	3	352	22.4	2.0	9.5	380.1	68.0	17.2
Stn Panache R. Manicouagan	P3	2017	49.2012	-68.0870	3		18.7	3.6	8.2	322.1	85.5	14.6
Stn 21.5N	E22	2017	49.1689	-67.9574	2		23.3	1.8	9.5	378.9	74.1	17.9
Stn 21	E23	2017	49.0769	-67.3011	2	325	22.1	1.8	9.8	384.2	71.7	16.9
Stn 21	E23	2017	49.0769	-67.3011	310	325	34.6	0.8	5.9	59.4	91.6	27.3
Stn 20	G1	2017	49.4285	-66.3169	2	332	28.2	1.4	11.8	288.6	91.5	21.7
Stn 20	G1	2017	49.4285	-66.3169	33	332	33.5	1.0	-0.3	300.3	95.6	25.7
Stn 20	G1	2017	49.4285	-66.3169	285	332	34.6	0.7		62.2	98.1	27.2
Stn 19	G2	2017	49.4917	-65.2198	2	362	27.6	1.8		308.2	90.2	20.9

Stn 19	G2	2017	49.4917	-65.2198	275	362	34.6	0.6		63.3	97.9	27.2
Stn 18	G4	2017	49.2551	-64.2416	2	364	22.7	2.3		379.2	71.8	16.8
Stn 18	G4	2017	49.2551	-64.2416	35	364	31.7	1.0		322.2	97.9	25.4
Stn 18	G4	2017	49.2551	-64.2416	270	364	34.5	0.8		72.1	98.4	27.2
Stn 18	G4	2017	49.2551	-64.2416	372	364	34.8	0.6		87.3	95.0	27.4
Stn Anticosti	G5	2017	49.3674	-63.9454	3		28.1	1.4		293.5	90.4	21.6
Stn Anticosti	G5	2017	49.3674	-63.9454	50		32.0	1.0		321.9	97.9	25.7
Stn Jupiter	P4	2017	49.4744	-63.6605	3		30.4	1.3		317.1	91.8	23.8
Stn St-Fulgence	S1	2018	48.4211	-70.8577	3	69	0.3	6.4	5.1	366.1	53.2	0.2
Stn St-Fulgence	S1	2018	48.4211	-70.8577	60	69	28.9	1.7	0.9	248.2	95.9	23.2
Stn Sag 05	S2	2018	48.4125	-70.8210	3	89	0.9	5.9	4.9	365.9	55.9	0.7
Stn Sag 15	S3	2018	48.3952	-70.6892	3	234	3.1	5.8	4.5	362.8	59.9	2.7
Stn Sag 20	S4	2018	48.3703	-70.5763	3	259	3.0	6.0	4.5	365.8	60.8	2.0
Stn Sag 30	S5	2018	48.3593	-70.3899	3	268	3.0	5.7	4.5	368.9	62.0	2.3
Stn Sag 30	S5	2018	48.3593	-70.3899	80	268	29.1	1.3	0.6	268.6	95.8	23.3
Stn Sag 30	S5	2018	48.3593	-70.3899	256	268	30.6	1.2	1.5	219.1	93.9	24.5
Stn Sag 36	S6	2018	48.2628	-70.1474	3	228	3.4	5.5	5.8	363.0	64.1	2.6
Stn Sag 42	S7	2018	48.2288	-69.9133	3	157	5.1	5.3	5.7	354.6	63.7	4.0
Stn Sag 48	S8	2018	48.1357	-69.7479	3	184	13.6	4.3	4.7	330.5	76.2	10.7
Stn Sag 48	S8	2018	48.1357	-69.7479	170	184	29.9	1.1	1.3	280.0	90.5	24.0
Stn Sag EXT1	E10	2018	48.1147	-69.6030	3	34	26.2	1.7	2.9	292.1	85.2	20.8
Stn Sag EXT2	E11	2018	48.1524	-69.5824	3	148	24.9	1.8	5.9	298.5	77.5	19.7
Stn Sag EXT2	E11	2018	48.1524	-69.5824	20	148	27.3	1.3	3.9	292.2	83.9	21.7
Stn A	E1	2018	46.8459	-71.1614	3	26	0.1	3.9	13.5	292.6	46.8	
Stn D	E3	2018	47.1294	-70.6843	3	10	0.6	4.6	12.6	288.8	0.2	
Stn DE	E4	2018	47.1794	-70.6199	3	17	2.9	4.3	11.5	286.1	0.2	1.8
Stn DE	E4	2018	47.1794	-70.6199	12	17	7.2	4.1	9.7	281.3	0.2	5.3
Stn E	E5	2018	47.2437	-70.5562	3	29	6.6	4.0	10.2	284.0	1.6	4.0
Stn E	E5	2018	47.2437	-70.5562	25	29	13.6	3.2	7.3	279.0	0.2	10.6
Stn F1	E6	2018	47.4080	-70.2822	3	47	13.5	2.9	8.4	280.2	10.1	10.3

Stn F1	E6	2018	47.4080	-70.2822	25	47	25.8	1.8	2.6	266.9	2.4	20.6
Stn G	E7	2018	47.5115	-70.1629	3	62	15.8	2.7	6.8	279.5	21.0	13.6
Stn G	E7	2018	47.5115	-70.1629	46	62	25.1	1.8	2.9	267.2	0.6	20.0
Stn 25	E13	2018	48.2923	-69.3817	3	325	25.2	1.6	5.1	303.3	69.2	20.1
Stn 25	E13	2018	48.2923	-69.3817	72	325	31.8	0.9	-0.7	306.1	97.0	25.5
Stn 25	E13	2018	48.2923	-69.3817	200	325	33.5	0.9	3.3	131.3	96.5	26.7
Stn 25	E13	2018	48.2923	-69.3817	315	325	34.4	0.7	5.5	56.9	83.9	27.1
Stn 24	E14	2018	48.4227	-69.1177	3	310	26.9	1.5	3.1	288.4	86.2	22.1
Stn 24	E14	2018	48.4227	-69.1177	58	310	32.2	0.7	-0.1	267.8	96.7	25.8
Stn 24	E14	2018	48.4227	-69.1177	294	310	34.4	0.8	5.6	49.6	82.2	27.2
Stn 23A	E15	2018	48.7713	-68.8864	3	88	25.0	1.7	6.7	351.4	63.6	19.5
Stn 23A	E15	2018	48.7713	-68.8864	75	88	32.3	0.8	0.1	256.9	94.5	25.9
Stn 23B	E16	2018	48.7436	-68.8511	3	123	25.1	1.6	5.9	283.0	71.0	19.7
Stn 23B	E16	2018	48.7436	-68.8511	115	123	33.0	0.7	1.8	193.1	88.8	26.4
Stn 23C	E17	2018	48.6994	-68.7958	3	197	24.9	1.7	5.8	285.8	69.1	19.6
Stn 23E	E18	2018	48.5565	-68.6059	3	45	25.3	1.7	4.8	279.1	68.3	19.9
Stn 23	E19	2018	48.7013	-68.6514	3	345	25.6	1.8	6.3	285.5	69.2	19.3
Stn 23	E19	2018	48.7013	-68.6514	50	345	31.8	1.0	-0.7	306.7	98.1	25.6
Stn 22	E21	2018	48.9340	-68.0923	2	352	23.4	1.9	6.1	397.3	60.7	18.3
Stn 22	E21	2018	48.9340	-68.0923	338	352	34.6	0.7	5.8	54.7	90.0	27.2
Stn 21	E23	2018	49.0769	-67.3011	3	325	27.3	1.6	5.3	393.5	81.3	21.6
Stn 21	E23	2018	49.0769	-67.3011	200	325	34.0	0.7	4.7	80.4	97.1	27.0
Stn 21	E23	2018	49.0769	-67.3011	310	325	34.6	0.7	6.0	60.9	89.6	27.3
Stn 20	G1	2018	49.4285	-66.3169	3	332	27.5	1.5	5.7	392.9	87.9	22.3
Stn 20	G1	2018	49.4285	-66.3169	30	332	31.7	1.1	-0.6	319.4	95.4	25.5
Stn 19	G2	2018	49.4917	-65.2198	3	362	30.9	1.2	5.6	308.6	98.4	24.1
Stn 19	G2	2018	49.4917	-65.2198	36	362	32.0	1.0	0.0	282.4	97.3	25.8
Stn 19	G2	2018	49.4917	-65.2198	260	362	34.6	0.7	6.0	61.5	98.5	27.2
Stn 19	G2	2018	49.4917	-65.2198	347	362	34.8	0.7	6.2	70.5	94.5	27.3
Stn 18.5	G3	2018	49.3253	-64.3934	3	389	28.3	1.3	5.0	349.3	90.1	22.3

Stn 18.5	G3	2018	49.3253	-64.3934	70	389	31.8	0.9	-0.7	309.4	97.7	25.5
Stn 18.5	G3	2018	49.3253	-64.3934	280	389	34.6	0.6	6.0	63.4	98.6	27.2
Stn 18.5	G3	2018	49.3253	-64.3934	375	389	34.8	1.3	6.2	71.3	94.2	27.4
Stn 18	G4	2018	49.2551	-64.2416	3	364	29.0	1.3	5.3	329.9	92.4	22.9
Stn 18	G4	2018	49.2551	-64.2416	58	364	31.8	0.9	-0.8	307.8	98.1	25.5
Stn 18	G4	2018	49.2551	-64.2416	200	364	34.3	0.6	5.4	79.2	98.3	27.0
Stn 18	G4	2018	49.2551	-64.2416	375	364	34.8	0.5	6.3	89.1	96.2	27.4
Stn 17	G6	2018	48.8004	-62.5253	3	379	30.0	1.2	6.1	313.0	97.6	23.6
Stn 17	G6	2018	48.8004	-62.5253	28	379	31.3	1.2	0.2	322.7	90.4	25.1
Stn 17	G6	2018	48.8004	-62.5253	64	379	31.8	0.9	-0.8	311.8	99.1	25.5
Stn 17	G6	2018	48.8004	-62.5253	270	379	34.7	0.7	6.7	94.6	98.8	27.3
Stn 17	G6	2018	48.8004	-62.5253	365	379	34.9	0.7	6.4	103.3	95.0	27.4
Stn 16	G7	2018	48.4944	-61.4124	3	418	30.9	1.0	3.4	110.5	96.4	27.5
Stn 16	G7	2018	48.4944	-61.4124	61	418	31.6	0.9	-0.3	93.9	99.0	27.2

Table B.2 BIX, HIX and FI values calculated at the various time points for both control and irradiated samples.

Sample	BIX		HIX		FI	
	Control	Irradiated	Control	Irradiated	Control	Irradiated
0.5hrs - 1	0.92	0.94	0.39	0.36	1.14	1.20
0.5hrs - 2	1.08	0.97	0.32	0.39	1.18	1.22
4.5hrs - 1	1.02	1.29	0.40	0.49	1.29	1.22
4.5hrs - 2	1.07	1.19	0.38	0.48	1.24	1.20
18hrs - 1	1.35	1.21	0.33	0.62	1.28	1.21
18hrs - 2	1.51	1.38	0.33	0.51	1.25	1.21
30hrs - 1	1.38	1.35	0.37	0.55	1.17	1.24
30hrs - 2	1.21	1.29	0.47	0.61	1.29	1.20
96hrs - 1	1.47	1.19	0.41	0.66	1.26	1.16
96hrs - 2	1.41	1.25	0.48	0.66	1.27	1.23

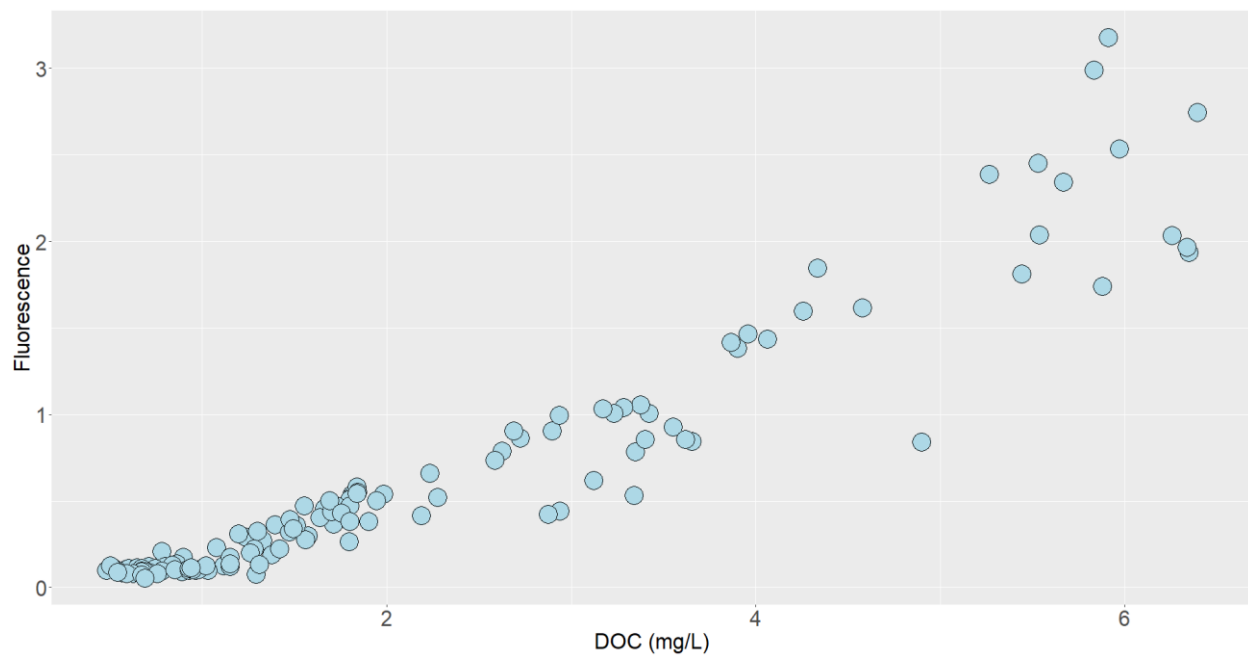


Figure B.0.1 Relationship between DOC concentration and total fluorescence for surface waters along the St. Lawrence River, Estuary and Gulf as well as the Saguenay Fjord

Appendix C

Additional data collected throughout the research presented in this thesis including molecular and/or isotopic characterization of various oil samples. Included in this section are hydrocarbons extracted from a crude oil and a terrestrial sediment (station G). The alkanes and PAH fraction were combined at various levels (10% crude oil, 90% natural, etc.) and measured for concentration and carbon isotope values.

Table C.1 Carbon isotope values (‰) of *n*-alkanes for various oil samples analyzed in triplicate with their standard deviations

	L040457-04 Sweet 4		L35070-01 Petrolia Haldiman #4		L035228-05 Suncor Light Sahara		L035228-05 Suncor Light Troll		L035071-01 Junex		Bakken Shale		L040457-21 Synth 1		L040457-06 Medium Sour 2		L040457-05 Medium Sour 1		L040457-23 Synbit 1		L040457-24 Synbit 2	
chain length	avg	SD	avg	SD	avg	SD	avg	SD	avg	SD	avg	SD	avg	SD	avg	SD	avg	SD	avg	SD	avg	SD
20	-31.36	0.24	-31.80	0.29	-29.88	0.49	-28.93	0.47	-30.86	0.22	-29.96	0.32	-31.72	0.16	-31.32	0.26	-31.74	0.05	-31.82	0.03	-31.33	0.32
21	-31.16	0.23	-31.48	0.24	-30.58	0.17	-29.29	0.15	-30.99	0.23	-30.31	0.06	-31.57	0.21	-31.19	0.05	-31.67	0.08	-31.29	0.26	-31.22	0.22
22	-31.18	0.21	-31.43	0.22	-30.37	0.18	-29.70	0.20	-31.08	0.18	-30.83	0.20	-31.60	0.13	-31.18	0.12	-31.57	0.13	-31.76	0.22	-31.30	0.29
23	-30.73	0.03	-31.30	0.25	-30.25	0.18	-29.31	0.07	-31.10	0.20	-30.47	0.10	-31.47	0.05	-31.10	0.20	-31.55	0.06	-31.38	0.01	-31.18	0.31
24	-30.95	0.12	-31.11	0.58	-30.06	0.11	-29.10	0.05	-30.99	0.20	-30.42	0.14	-31.82	0.08	-31.34	0.10	-31.75	0.13	-31.72	0.05	-31.39	0.23
25	-30.40	0.17	-31.18	0.37	-29.74	0.63	-29.23	0.10	-30.52	0.17	-30.51	0.22	-31.29	0.25	-31.00	0.09	-31.65	0.14	-31.19	0.08	-31.26	0.14
26	-30.48	0.41	-31.10	0.45	-30.02	0.14	-28.94	0.21	-30.84	0.37	-30.03	0.17	-31.25	0.17	-30.68	0.07	-31.41	0.06	-31.60	0.57	-30.97	0.39
27	-30.16	0.17	-31.19	0.24	-30.12	0.18	-28.99	0.20	-30.81	0.25	-30.32	0.18	-31.21	0.58	-30.37	0.26	-31.35	0.40	-31.30	0.40	-30.65	0.19
28	-30.25	0.28	-31.13	0.22	-30.00	0.07	-28.99	0.14	-30.78	0.11	-30.14	0.10	-30.82	0.22	-30.01	0.53	-30.95	0.05	-31.58	0.39	-30.29	0.15
29	-30.35	0.25	-31.10	0.23	-30.00	0.14	-29.45	0.76	-30.89	0.09	-30.11	0.10	-31.28	0.16	-31.18	0.85	-31.59	0.21	-32.32	0.13	-30.75	0.37
30	-30.29	0.03	-31.06	0.30	-30.08	0.14	-29.21	0.78	-31.02	0.81	-30.09	0.10	-30.74	0.47	-31.38	0.80	-31.62	0.17	-31.04	0.86	-30.63	0.36
31	-30.63	0.61			-30.01	0.16	-29.25	0.33	-30.94	0.17			-30.28	0.39	-31.07	0.57	-31.39	0.35			-31.25	1.60
32	-28.92	0.87			-30.15	0.07	-29.31	0.07	-31.04	0.27					-29.92	1.13	-30.83	0.31			-30.76	1.45
33	-29.19	1.94			-30.40	0.22	-29.48	0.21							-30.29	0.82	-32.54	1.93			-29.71	1.71
34					-30.45	0.19	-29.52	0.17							-31.92	0.15	-31.38	0.02				

Table C.2 PAH concentrations (ppm) of mixed hydrocarbon samples

Compound	0% oil		10% oil		20% oil		30% oil		40% oil		50% oil		60% oil		70% oil		80% oil		90% oil		100% oil	
	Avg	SD	Avg	SD	Avg	SD	Avg	SD	Avg	SD	Avg	SD	Avg	SD	Avg	SD	Avg	SD	Avg	SD	Avg	SD
NP	0.01	0.00	0.53	0.04	1.12	0.05	1.71	0.09	2.17	0.05	2.59	0.12	3.06	0.06	3.84	0.05	4.17	0.07	4.86	0.21	5.29	0.08
2-MNP			1.50	0.10	3.14	0.13	4.76	0.22	5.93	0.14	6.85	0.30	8.04	0.11	9.93	0.10	10.84	0.22	12.36	0.45	13.29	0.24
1-MNP			1.05	0.07	2.27	0.10	3.52	0.16	4.45	0.12	5.23	0.31	6.20	0.04	7.65	0.11	8.45	0.16	9.70	0.39	10.48	0.17
FL			0.15	0.01	0.32	0.02	0.44	0.05	0.60	0.02	0.69	0.05	0.83	0.04	1.08	0.01	1.17	0.04	1.39	0.06	1.55	0.04
PHE	1.15	0.05	1.32	0.06	1.46	0.07	1.65	0.08	1.74	0.04	1.77	0.12	1.90	0.04	2.18	0.04	2.23	0.05	2.48	0.11	2.59	0.03
ANT	0.07	0.01	0.07	0.02	0.04	0.01	0.03	0.01	0.01	0.00												
FLA	2.15	0.07	2.02	0.09	1.78	0.09	1.61	0.07	1.34	0.02	1.01	0.07	0.75	0.05	0.51	0.03	0.52	0.02	0.09	0.02		0.00
RET	4.44	0.09	4.16	0.18	3.76	0.17	3.39	0.16	2.88	0.06	2.23	0.17	1.75	0.06	1.40	0.02	0.97	0.05	0.50	0.04		0.01
PYR	1.70	0.05	1.62	0.07	1.47	0.07	1.36	0.08	1.16	0.03	0.93	0.09	0.72	0.04	0.57	0.02	0.56	0.01	0.22	0.02		0.02
BaA	0.75	0.03	0.66	0.05	0.56	0.03	0.45	0.05	0.33	0.01	0.20	0.04	0.09	0.01	0.02	0.01						
CHR	0.98	0.05	0.92	0.05	0.78	0.06	0.70	0.06	0.56	0.01	0.43	0.05	0.28	0.05	0.22	0.01	0.10	0.01				
BbF	1.18	0.04	1.09	0.07	0.93	0.03	0.84	0.05	0.68	0.03	0.47	0.04	0.33	0.02	0.24	0.02	0.08	0.02				
BkF	0.41	0.02	0.35	0.01	0.29	0.01	0.24	0.03	0.16	0.00	0.04	0.02										
BaP	0.83	0.01	0.77	0.03	0.68	0.04	0.59	0.03	0.48	0.01	0.29	0.03	0.18	0.01	0.11	0.01						
PER	7.33	0.17	6.83	0.28	6.16	0.24	5.53	0.23	4.70	0.06	3.83	0.23	3.05	0.08	2.40	0.07	1.52	0.04	0.63	0.05		
IcdP	0.39	0.02	0.37	0.03	0.26	0.03	0.17	0.02	0.07	0.02	0.14	0.03	0.04	0.01								
BghiP	0.41	0.01	0.36	0.03	0.27	0.02	0.20	0.03	0.09	0.01												

Table C.3 Alkane concentrations (ppm) of mixed hydrocarbon samples

chain length	0% oil		10% oil		20% oil		30% oil		40% oil		50% oil		60% oil		70% oil		80% oil		90% oil		100% oil	
	Avg	SD	Avg	SD	Avg	SD	Avg	SD	Avg	SD	Avg	SD	Avg	SD	Avg	SD	Avg	SD	Avg	SD	Avg	SD
12	2.55	0.10	3.26	0.09	3.65	0.15	4.49	0.14	4.75	0.18	5.86	0.10	5.93	0.37	6.85	0.10	7.78	0.56	7.79	0.02	8.75	0.54
13	0.12	0.04	1.00	0.03	1.71	0.09	2.64	0.12	3.21	0.14	4.39	0.06	5.08	0.37	6.26	0.08	7.43	0.53	7.74	0.01	8.89	0.56
14	2.85	0.11	3.52	0.09	3.83	0.18	4.54	0.12	4.77	0.19	5.73	0.09	5.84	0.36	6.64	0.04	7.43	0.56	7.41	0.03	8.20	0.51
15	1.18	0.04	1.94	0.05	2.47	0.10	3.28	0.11	3.69	0.16	4.71	0.06	5.05	0.33	6.01	0.06	6.97	0.51	7.09	0.03	8.06	0.48
16	1.02	0.06	1.78	0.07	2.23	0.16	2.98	0.12	3.36	0.18	4.39	0.08	4.78	0.39	5.66	0.05	6.59	0.59	6.63	0.01	7.57	0.51
17	2.54	0.09	3.10	0.10	3.37	0.12	3.97	0.08	4.13	0.17	4.96	0.06	5.14	0.31	5.82	0.07	6.56	0.52	6.48	0.02	7.28	0.51
18	0.80	0.06	1.42	0.05	1.83	0.11	2.50	0.13	2.81	0.11	3.72	0.04	3.97	0.27	4.77	0.06	5.60	0.51	5.65	0.01	6.52	0.46
19	1.61	0.04	2.06	0.05	2.36	0.10	2.87	0.07	3.11	0.08	3.80	0.05	3.98	0.28	4.63	0.06	5.24	0.46	5.18	0.03	5.85	0.40
20	1.25	0.05	1.72	0.04	1.99	0.09	2.50	0.07	2.73	0.10	3.39	0.05	3.63	0.20	4.17	0.04	4.79	0.41	4.81	0.03	5.47	0.33
21	2.57	0.07	2.91	0.07	2.99	0.08	3.36	0.11	3.35	0.12	3.93	0.09	3.99	0.24	4.40	0.03	4.88	0.46	4.72	0.03	5.15	0.31
22	2.09	0.09	2.52	0.06	2.71	0.14	3.12	0.08	3.23	0.12	3.85	0.07	3.99	0.20	4.48	0.05	5.07	0.40	4.98	0.02	5.53	0.35
23	5.97	0.16	6.03	0.12	5.66	0.20	5.76	0.09	5.33	0.18	5.62	0.13	5.14	0.36	5.23	0.04	5.22	0.48	4.61	0.00	4.54	0.29
24	2.50	0.07	2.74	0.09	2.72	0.12	3.01	0.08	3.01	0.10	3.42	0.11	3.20	0.26	3.67	0.01	3.98	0.37	3.81	0.02	4.10	0.26
25	8.37	0.31	8.22	0.18	7.56	0.24	7.41	0.17	6.79	0.13	6.81	0.16	6.03	0.43	5.83	0.05	5.37	0.54	4.51	0.03	3.81	0.20
26	2.90	0.14	2.96	0.08	2.80	0.11	2.94	0.07	2.72	0.11	3.01	0.06	2.70	0.19	2.86	0.01	2.92	0.27	2.66	0.01	2.69	0.19
27	11.70	0.30	11.44	0.24	10.36	0.21	9.97	0.17	8.74	0.27	8.45	0.19	6.95	0.50	6.19	0.13	5.03	0.54	3.40	0.02	1.76	0.10
28	2.95	0.14	3.00	0.10	2.71	0.08	2.73	0.04	2.43	0.08	2.53	0.06	2.02	0.24	2.01	0.02	1.74	0.20	1.36	0.01	1.17	0.10
29	12.14	0.28	11.86	0.24	10.69	0.29	10.21	0.19	8.80	0.25	8.37	0.23	6.60	0.48	5.64	0.14	4.27	0.53	2.70	0.05	0.91	0.07
30	1.90	0.22	1.93	0.07	1.65	0.06	1.57	0.03	1.34	0.05	1.34	0.03	0.91	0.15	0.92	0.01	0.75	0.09	0.58	0.00	0.38	0.02
31	10.56	0.30	10.31	0.23	9.15	0.23	8.63	0.10	7.25	0.25	6.87	0.16	5.00	0.47	4.38	0.10	3.11	0.39	1.83	0.03	0.68	0.04
32	1.83	0.15	1.91	0.07	1.74	0.07	1.73	0.04	1.50	0.05	1.51	0.03	1.23	0.08	1.19	0.03	1.07	0.04	1.01	0.02	0.84	0.03
33	4.47	0.30	4.57	0.17	3.95	0.14	3.73	0.03	3.09	0.11	3.00	0.05	2.16	0.24	2.09	0.04	1.61	0.11	1.25	0.01	0.90	0.00
34	1.49	0.14	1.59	0.02	1.46	0.04	1.42	0.03	1.29	0.02	1.26	0.04	1.12	0.03	1.14	0.04	1.09	0.03	1.02	0.01	0.97	0.01
35	2.14	0.19	2.18	0.03	1.96	0.05	1.87	0.07	1.64	0.06	1.66	0.06	1.33	0.07	1.33	0.01	1.23	0.02	1.13	0.01	1.08	0.00
36	1.40	0.08	1.52	0.03	1.43	0.04	1.43	0.02	1.29	0.03	1.32	0.02	1.21	0.02	1.21	0.02	1.19	0.02	1.17	0.00		

Table C.4 Carbon isotope values (‰) of *n*-alkanes of mixed hydrocarbon samples

Chain Length	0% oil		10% oil		20% oil		30% oil		40% oil		50% oil		60% oil		70% oil		80% oil		90% oil		100% oil	
	Avg	SD	Avg	SD	Avg	SD	Avg	SD	Avg	SD	Avg	SD	Avg	SD	Avg	SD	Avg	SD	Avg	SD	Avg	SD
20	-31.88	0.32	-31.86	0.32	-31.58	0.12	-31.43	0.54	-31.09	0.32	-30.70	0.62	-31.16	0.05	-31.44	0.12	-31.00	0.55	-31.08	0.12	-31.36	0.24
21	-31.56	0.12	-31.36	0.17	-31.19	0.09	-31.28	0.31	-31.23	0.08	-31.10	0.20	-31.06	0.13	-31.17	0.09	-30.72	0.55	-30.93	0.04	-31.16	0.23
22	-32.23	0.10	-32.04	0.10	-31.88	0.09	-31.67	0.14	-31.22	0.23	-31.05	0.19	-31.32	0.36	-31.37	0.04	-30.89	0.55	-30.90	0.10	-31.18	0.21
23	-31.22	0.03	-31.01	0.12	-30.90	0.08	-30.88	0.14	-30.77	0.10	-30.74	0.05	-30.88	0.32	-30.94	0.07	-30.55	0.57	-30.59	0.09	-30.73	0.03
24	-33.26	0.10	-32.91	0.04	-32.61	0.09	-32.39	0.14	-31.77	0.04	-31.39	0.28	-31.92	0.94	-31.84	0.10	-31.26	0.41	-31.14	0.06	-30.95	0.12
25	-30.97	0.03	-30.79	0.03	-30.52	0.06	-30.60	0.13	-30.53	0.16	-30.63	0.27	-30.96	0.95	-30.70	0.07	-30.83	0.50	-30.29	0.12	-30.40	0.17
26	-34.05	0.04	-33.68	0.23	-31.93	1.13	-31.89	1.13	-30.87	0.07	-30.67	0.10	-30.43	0.02	-30.92	0.14	-30.51	0.48	-30.54	0.14	-30.48	0.41
27	-31.76	0.04	-31.59	0.05	-31.29	0.13	-31.53	0.05	-31.36	0.04	-31.08	0.13	-31.13	0.32	-31.37	0.16	-30.95	0.43	-31.07	0.06	-30.16	0.17
28	-31.66	0.22	-30.78	0.94	-31.62	0.13	-31.35	0.38	-31.12	0.23	-30.86	0.29	-30.96	0.22	-30.98	0.41	-30.72	0.65	-30.50	0.34	-30.25	0.28
29	-32.26	0.02	-32.12	0.03	-31.87	0.06	-32.06	0.05	-31.85	0.03	-31.77	0.09	-31.77	0.19	-31.98	0.04	-31.43	0.46	-31.51	0.11	-30.35	0.25
30	-32.07	0.09	-31.85	0.09	-31.73	0.04	-31.58	0.10	-31.42	0.26	-31.37	0.11	-31.42	0.38	-31.46	0.30	-30.75	0.30	-31.18	0.21	-30.29	0.03
31	-32.79	0.07	-32.68	0.09	-32.46	0.00	-32.51	0.13	-32.34	0.05	-32.40	0.10	-32.42	0.23	-32.58	0.09	-32.02	0.56	-31.73	0.19	-30.63	0.61
32	-30.61	0.02	-29.93	0.79	-31.30	0.25	-30.27	0.41	-30.11	0.44	-30.22	0.56	-30.58	0.16	-30.53	0.74	-30.69	0.05			-28.92	0.87
33	-32.06	0.15	-31.99	0.04	-32.02	0.17	-31.82	0.09	-31.79	0.05	-32.06	0.39	-31.79	0.20	-32.23	0.22	-31.55	0.55			-29.19	1.94
34	-31.96	0.04	-31.03	0.05	-31.27	0.43	-31.12	0.42	-30.98	0.10	-31.32	0.36	-30.77	0.04								
35	-32.03	0.44	-30.62	0.21	-30.44	0.57	-30.93	0.36	-31.14	0.85	-31.93	1.33	-30.09	0.71								